AD_____

Award Number: W81XWH-09-1-0461

TITLE: Tissue Repair and Regeneration Following Orthopedic and Craniofacial Trauma

PRINCIPAL INVESTIGATOR: David A. Puleo, Ph.D.

CONTRACTING ORGANIZATION: University of Kentucky
Lexington, KY 40506

REPORT DATE: July 2012

TYPE OF REPORT: Annual

PREPARED FOR: U.S. Army Medical Research and Materiel Command
Fort Detrick, Maryland 21702-5012

REPORT DOCUMENTATION PAGE

Form Approved
OMB No. 0704-0188

1. REPORT DATE	2. REPORT TYPE	3. DATES COVERED
July 2012	Annual	1 July 2011 - 30 June 2012

4. TITLE AND SUBTITLE

Tissue Repair and Regeneration Following Orthopedic and Craniofacial Trauma

5a. CONTRACT NUMBER

5b. GRANT NUMBER
W81XWH-09-1-0461

5c. PROGRAM ELEMENT NUMBER

6. AUTHOR(S)

David Puleo, Leonidas Bachas, Thomas Dziubla, Todd Milbrandt, Larry Cunningham, J. Zachary Hilt

E-Mail: puleo@uky.edu

5d. PROJECT NUMBER

5e. TASK NUMBER

5f. WORK UNIT NUMBER

7. PERFORMING ORGANIZATION NAME(S) AND ADDRESS(ES)

University of Kentucky
Lexington, KY 40506

8. PERFORMING ORGANIZATION REPORT NUMBER

9. SPONSORING / MONITORING AGENCY NAME(S) AND ADDRESS(ES)
U.S. Army Medical Research and Materiel Command
Fort Detrick, Maryland 21702-5012

10. SPONSOR/MONITOR'S ACRONYM(S)

11. SPONSOR/MONITOR'S REPORT NUMBER(S)

12. DISTRIBUTION / AVAILABILITY STATEMENT
Approved for Public Release; Distribution Unlimited

13. SUPPLEMENTARY NOTES

14. ABSTRACT

The majority of explosion-induced trauma sustained by armed service members results in loss of tissue and contamination with a variety of materials, biological and nonbiological. This project is developing materials to treat bacterially infected osseous injuries, such as those that occur in the long bones, head, and face. More specifically, a moldable bone graft substitute providing localized, controlled, sequential release of antimicrobial and osteogenic agents is being formulated to enable timely and complete healing of large, infected bone defects. Following development and testing of the tunable bone filler system in earlier phases of the project, ongoing efforts are directed at systematically examining the potential for these proactive biomaterials to enhance tissue repair in a rodent model of an infected segmental long bone defect. A dose-dependent increase in bone formation was observed in response to loading of simvastatin in the core of the bone filler system. As expected, a greater amount of mineralized tissue was observed at a longer follow-up time. The effect of localized delivery of antibiotic in enhancing the effect of simvastatin-loaded cores was confirmed. Results thus far have shown that localized delivery of antibiotic outperformed systemic administration through the first month of observation. With the infection at least partially inhibited by sustained release of antibiotics from the implant, simvastatin subsequently released from the core can enhance bone formation.

15. SUBJECT TERMS
Infected bone defect, bone filler, moldable, controlled release, antibiotic delivery, osteogenic

16. SECURITY CLASSIFICATION OF:			17. LIMITATION OF ABSTRACT	18. NUMBER OF PAGES	19a. NAME OF RESPONSIBLE PERSON
a. REPORT	b. ABSTRACT	c. THIS PAGE			USAMRMC
U	U	U	UU	40	19b. TELEPHONE NUMBER *(include area code)*

Table of Contents

Page

Introduction

The majority of explosion-induced trauma sustained by armed service members results in loss of tissue and contamination with a variety of materials, biological and nonbiological. Repair of large defects can be challenging under aseptic conditions, but even low levels of microbial contamination initiate a chronic inflammatory response that further undermines surrounding tissues. This project is developing materials to treat infected osseous injuries, such as those that occur in the long bones, head, and face. More specifically, a moldable bone graft substitute providing localized, controlled, sequential release of antimicrobial and osteogenic agents will enable timely and complete healing of large, infected bone defects. The hypothesis being tested is that the proposed multifunctional material will provide superior healing compared to simply grafting with bone substitute, even in the presence of systemically administered antibiotics. The first phase of experiments systematically examined parameters contributing to a bone filler material that is moldable, biodegradable, and provides controlled release of antimicrobial and osteogenic molecules. The second, ongoing, proof-of-principle phase will determine biological performance of materials meeting specific criteria in an animal model of infected bone defects.

Body

Summary of tasks and their status

Task	Proposed Timeline	Status
Task 1: **Develop and characterize a bone filler material**		
Subtask 1a: Formulate moldable bone filler	[Y1, Q1]	Complete
Subtask 1b: Formulate antimicrobial drug delivery component	[Y1, Q1-3]	Complete
Subtask 1b1: Traditional antibiotic therapy	[Y1, Q1-2]	Complete
Subtask 1b2: Enhanced antibiotic therapy	[Yr 1, Q1-4]	Complete
Subtask 1c: Formulate osteotropic drug delivery component	[Yr 1, Q1-3]	Complete
Subtask 1c1: Soluble osteogenic therapy	[Yr 1, Q1-2]	Complete
Subtask 1c2: Targeted osteogenic therapy	[Yr 1, Q2-3]	Complete
Subtask 1d: Formulate composite filler material	[Yr 1, Q2-4]	Complete
Subtask 1e: Determine the release kinetics for the three drug delivery components	[Yr 1, Q1-4]	Complete
Subtask 1f: Measure bioerosion of the composite bone filler	[Yr 1, Q3-4]	Complete
Subtask 1g: Quantify mechanical properties of the composite bone filler	[Yr 1, Q3 – Yr2, Q1]	Complete
Subtask 1h: Assess biological activities of the composite bone filler *in vitro*	[Yr 1, Q3 – Yr 2, Q1]	Complete
Task 2: **Measure biological activity of the bone filler *in vivo* in an infected segmental defect model**		
Subtask 2a: Formulate composite bone fillers based on results from Task 1	[Yr 2, Q1-2]	Complete
Subtask 2b: Implant bone fillers in animal model of infected segmental bone defects	[Yr 2, Q2 - Yr 4, Q3]	60% Complete
Subtask 2c: Measure mechanical properties of repaired bones	[Yr 2, Q2 - Yr 4, Q4]	5% Complete
Subtask 2d: Assess tissue formation via histology and microCT	[Yr 2, Q2 - Yr 4, Q4]	50% Complete

Task 1: **Develop and characterize a bone filler material that is moldable, biodegradable, and provides controlled release of antimicrobial and osteogenic molecules**

- Subtask 1a: Formulate moldable bone filler [Yr 1, Q1]

  Status: Complete (reported in Year 1 Annual Report)

- Subtask 1b: Formulate antimicrobial drug delivery component [Yr 1, Q1-4]
  - Subtask 1b1: Traditional antibiotic therapy [Yr 1, Q1-2]

    Status: Complete (reported in Year 1 Annual Report)
  - Subtask 1b2: Enhanced antibiotic therapy [Yr 1, Q1-4]

    Status: Complete (reported in Year 1 Annual Report)
- Subtask 1c: Formulate osteotropic drug delivery component [Yr 1, Q1-3]
  - Subtask 1c1: Soluble osteogenic therapy [Yr 1, Q1-2]

    Status: Complete (reported in Year 1 Annual Report)
  - Subtask 1c2: Targeted osteogenic therapy [Yr 1, Q2-3]

    Status: Complete (reported in Year 1 Annual Report)

    Publications reporting results are shown in Appendices 1 and 2.
- Subtask 1d: Formulate composite filler material [Yr 1, Q2-4]

  Status: Complete (reported in Year 1 Annual Report)

  Publication reporting results is shown in Appendix 3.
- Subtask 1e: Determine the release kinetics for the three drug delivery components [Yr 1, Q1-4]

  Status: Complete (reported in Year 1 Annual Report)
- Subtask 1f: Measure bioerosion of the composite bone filler [Yr 1, Q3-4]

  Status: Complete (reported in Year 1 Annual Report)

  Publication reporting results is shown in Appendix 3.
- Subtask 1g: Quantify mechanical properties of the composite bone filler [Yr 1, Q3 – Yr2, Q1]

  Status: Completed (reported in Year 2 Annual Report)

  Publication reporting results is shown in Appendix 3.
- Subtask 2a: Formulate composite bone fillers based on results from Task 1 [Yr 2, Q1-2]

  Status: Complete (reported in Year 2 Annual Report)
- Subtask 2b: Implant bone fillers in animal model of infected segmental bone defects [Yr 2, Q2 - Yr 4, Q3]

  Status: On schedule (in relation to revised timeline)

  The goal of this subtask is to test the bone filler in a rat model of an infected segmental defect in the femur.

  Results

  The goal of this subtask is to test the bone filler in a rat model of a chronically infected segmental defect in the femur. Work continued to focus on the animal experiments, with surgeries conducted

one or two times per week. While the initial emphasis was on the shorter follow-up time, procedures allocated to the longer time, i.e., 12 wk, have been initiated. Table 1 shows the full experimental design.

We have been progressing through the large number of procedures. The groups initiated are highlighted in the table. Additional experimental groups are being started in succession. As stated in previous reports, the primary limitation to increasing throughput is availability of our orthopedic and oral surgeon colleagues to perform the procedures. Although the trained surgeons will be necessary for the first procedure in which the defects are created, lab personnel have been trained to perform the second procedure (debridement and implantation).

Table 1. Experimental design with number of animals for testing filler in infected segmental bone defects. Yellow highlighting indicates groups initiated.

Treatment	Time after debridement (wks) 4	12
Control (no filler)		
No infection	6	12
Infection	6	12
No Systemic Antibiotics		
Drug-free	6	12
Antimicrobial	6	12
Osteogenic	6	12
Antimicrobial & Osteogenic	6	12
Antimicrobial (enhanced)	6	12
Osteogenic (enhanced)	6	12
Antimicrobial (enhanced) & Osteogenic (enhanced)	6	12
Systemic Antibiotics		
Drug-free	6	12
Osteogenic	6	12
Osteogenic (enhanced)	6	12

- Subtask 2c: Measure mechanical properties of repaired bones [Yr 2, Q4 - Yr 4, Q4]

  Status: On schedule (in relation to revised timeline)

  Bones have been harvested for preliminary mechanical testing. After potting the epiphyses, specimens will be loaded to failure in torsion.

- Subtask 2d: Assess tissue formation via histology and microCT [Yr 2, Q4 - Yr 4, Q4]

  Status: On schedule (in relation to revised timeline)

  Highlighted observations and representative microCT images from the animal study follow. Specimens that have already been scanned are being processed for calcified tissue histology.

  - As expected, when no implant was placed in the defect, minimal new mineralized material was observed, regardless of infection (Figure 1).

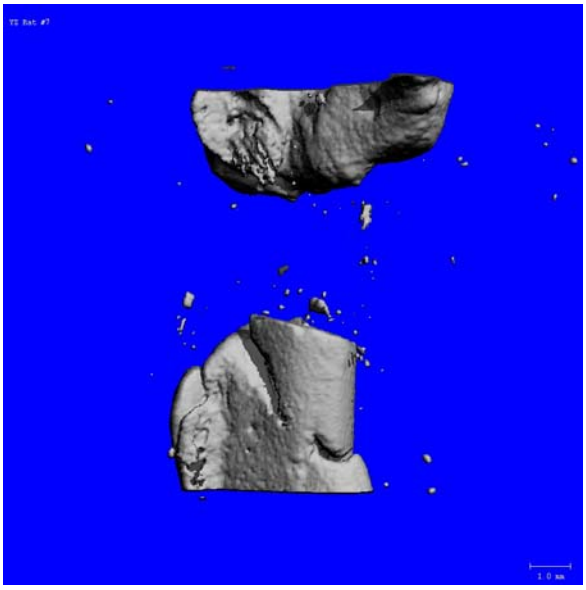

Figure 1. MicroCT image of a non-infected defect four weeks after it was left empty following the sham debridement procedure.

- Blank (drug-free) implants did not enhance repair, and the defects remained devoid of mineralized material. Figure 2(left) shows an infected defect four weeks after placement of a blank implant. Interestingly, although the defect remained radiolucent, calcium sulfate eroded from the implant appears to stimulate some osteoconduction around the fixation plate (Figure 2(right)).

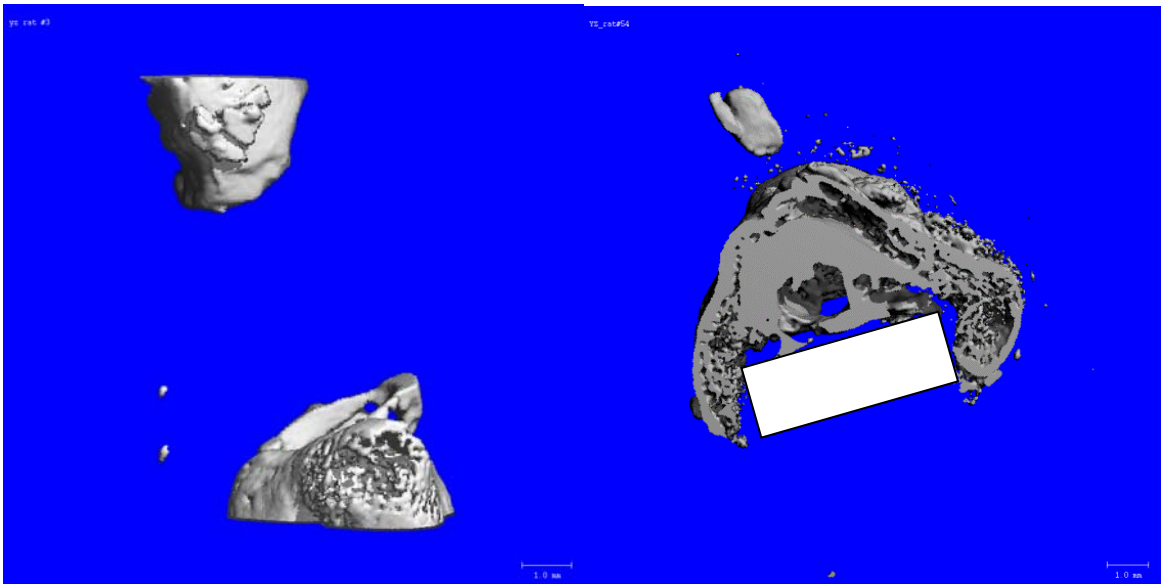

Figure 2. Left: MicroCT image of an infected defect four weeks following implantation of a blank filler. Right: In defects containing some formulation of calcium sulfate-based impalnt, mineralized material was normally deposited around the fixation plate. White rectangle shows approximate location of radiolucent polymeric plate.

- As shown last quarter, simvastatin-loaded implants in non-infected defects stimulated formation of mineralized material within the site (Figure 3).

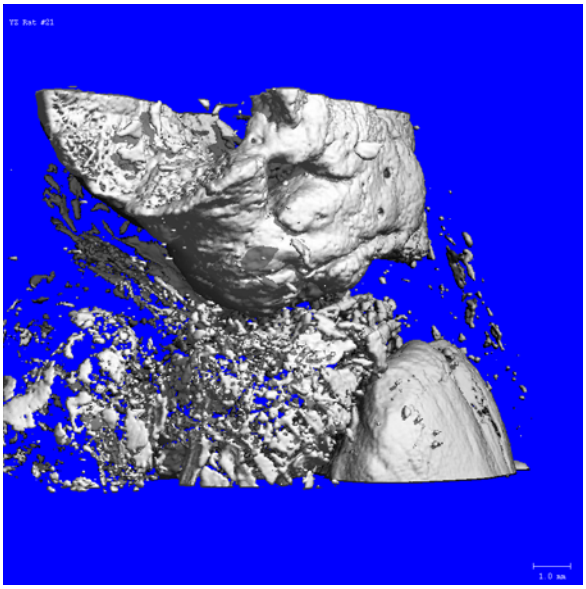

Figure 3. MicroCT image of a non-infected defect four weeks following implantation of a simvastatin-loaded filler.

- Infection reduced the effect of simvastatin-loaded implants. Figure 4 shows side (left) and cut-plane (right) views of an infected defect four weeks following placement of a simvastatin-releasing implant. Furthermore, the mineralized material that formed in the defect had a cystic appearance.

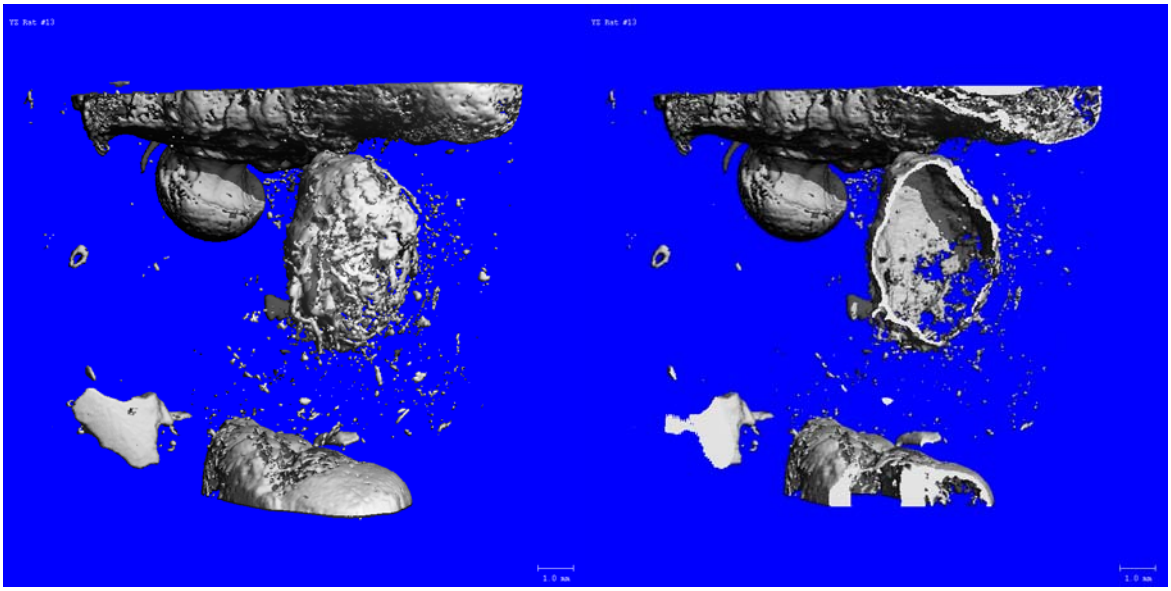

Figure 4. MicroCT images of an infected defect four weeks following implantation of a simvastatin-loaded filler. Left: side view; right: cut-plane view.

- Systemic injections of ceftriaxone marginally enhanced formation of mineralized tissue with simvastatin-treated defects. Figure 5 shows an infected defect four weeks after placement of a simvastatin-loaded implant; the animal received daily injections of antibiotic during this period.

Figure 5. MicroCT image of an infected defect four weeks following implantation of a simvastatin-loaded filler. The animal received daily injections of ceftriaxone.

- Localized release of vancomycin followed by release of simvastatin enhanced formation of mineralized materials within infected defects. Figure 6 shows side (left) and cut-plane (right) views of an infected defect four weeks following placement of a filler loaded with vancomycin-containing microspheres in the moldable shell and simvastatin in its core. Mineralized material was observed both within and around the bony defect.

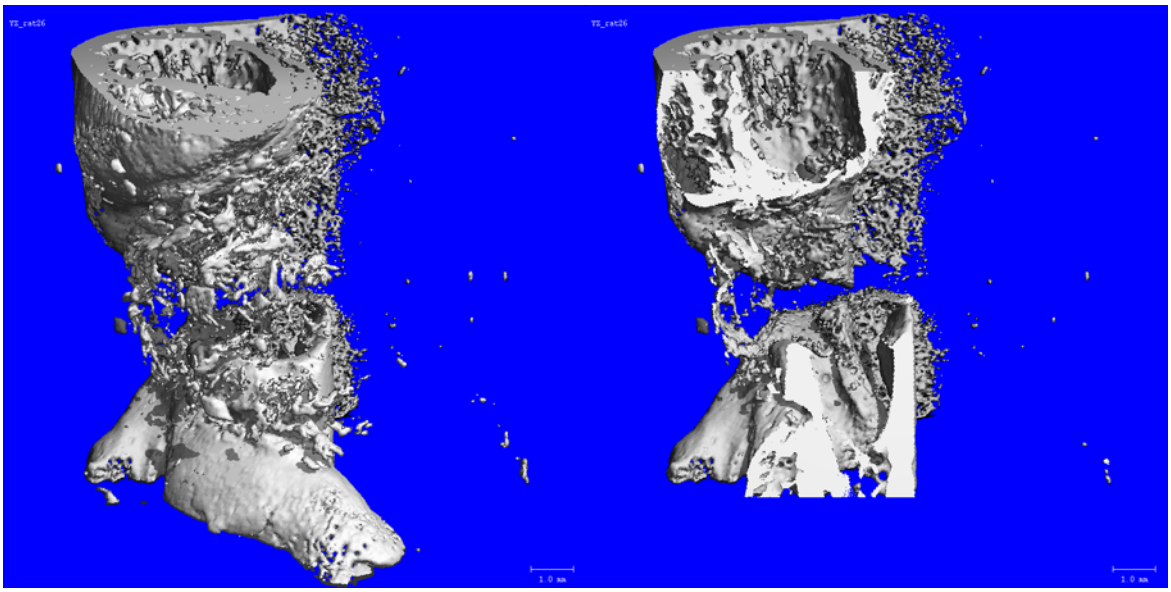

Figure 6. MicroCT images of aninfected defect four weeks following implantation of a filler loaded with vancomycin in the shell and simvastatin in the core. Left: side view; right: cut-plane view.

- The effect of simvastatin-loaded fillers placed in infected defects of animals receiving daily injections of antibiotics was confirmed. At four weeks, mineralized material was observed in and around the defect (Figure 7).

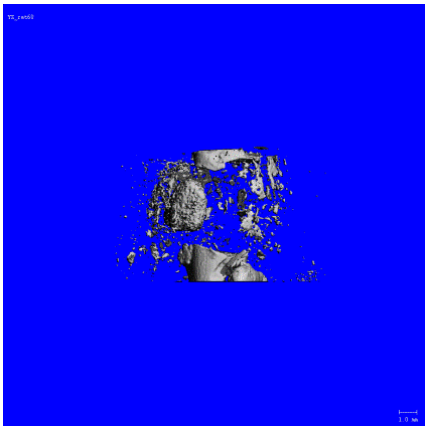

Figure 7. MicroCT image of an infected defect four weeks following implantation of a simvastatin-loaded filler. The animal received daily injections of ceftriaxone.

- Higher dose (6%) simvastatin-loaded samples were tested in the absence of antibiotic. In non-infected defects, the filler stimulated bone formation, but the effect was reduced in the presence of infection (Figure 8).

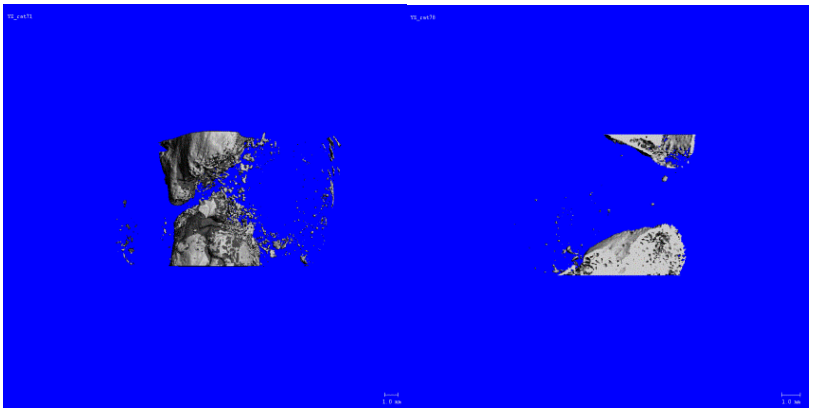

Figure 8. MicroCT images of a non-infected (left) and infected (right) defects four weeks after implantation of bone filler containing 6 wt% simvastatin.

- Filler cores loaded with different doses of simvastatin were compared in conjunction with vancomycin-loaded shell. Both treatments resulted in mineralized material in the defect, with an initial observation that the higher dose (6 wt%) leading to a greater amount (Figure 9).

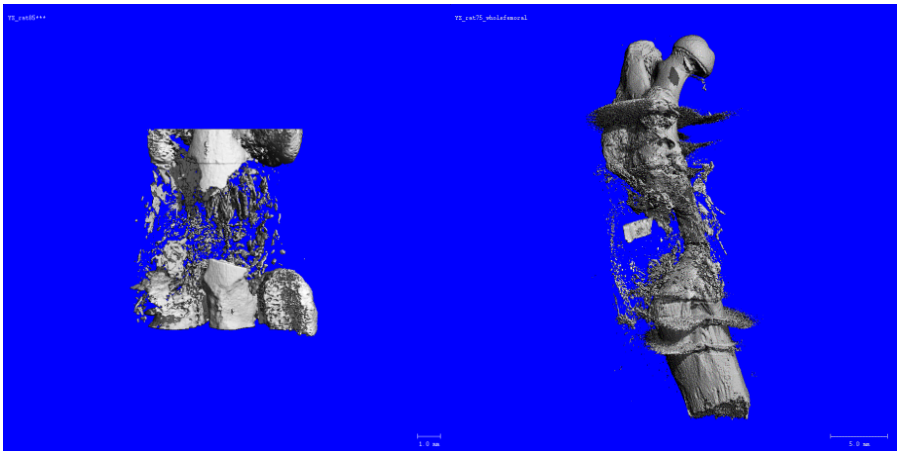

Figure 9. MicroCT images of infected defects four weeks following implantation of low (3 wt%) and high (6 wt%) simvastatin-loaded fillers surrounded by a vancomycin-loaded shell.

- Figure 10 shows initial results for implantation of the "enhanced" antibiotic treatment. This approach involves application of an *in situ* polymerizing biodegradable hydrogel that delivers vancomycin over the core (simvastatin)-shell (blank) filler. Although some mineralized debris was observed in the defect, little narrow of the gap occurred.

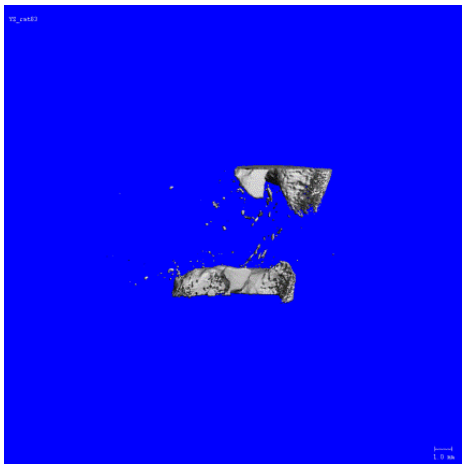

Figure 10. MicroCT image of an infected defect four weeks following implantation of a simvastatin-loaded filler with blank shell that had a vancomycin-releasing biodegradable hydrogel polymerized over it.

- As a positive control to better understand the effect of simvastatin, BMP-2-containing fillers were also placed in non-infected defects. As expected, significant bone formation was observed (Figure 11).

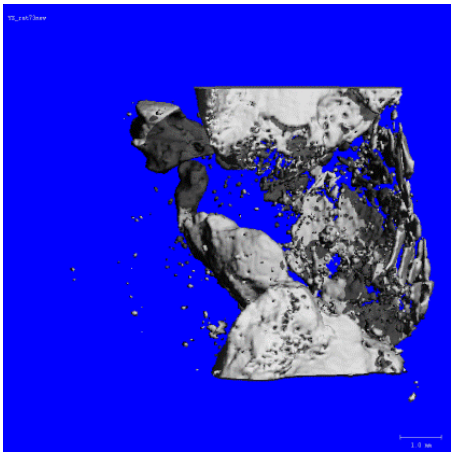

Figure 11. MicroCT image of a non-infected defect four weeks following implantation of a BMP-2-loaded filler (10 µg).

- Longer-term follow-up is needed to assess efficacy of the core-shell filler treatments. Initially, low dose (3 wt%) simvastatin-loaded samples were place in non-infected defects. Figure 12 shows a substantial amount of mineralized material entering the defect from the pre-existing bone ends. The defect was nearly bridged.

Figure 12. MicroCT image of a non-infected defect 12 weeks following implantation of a filler loaded with simvastatin (3 wt%) in the core.

Key Research Accomplishments

- A dose-dependent enhancement of bone formation was observed for loading of simvastatin in the core of the bone filler system.
- As expected, a greater amount of mineralized tissue was observed at a longer follow-up time.
- The effect of localized delivery of antibiotic in enhancing the effect of simvastatin-loaded cores was confirmed.
- Localized delivery of antibiotic seemed to outperform systemic administration through the first month of observation. With the infection at least partially inhibited by sustained release of antibiotics from the implant, simvastatin subsequently released from the core can enhance tissue formation.
- Ongoing animal cohorts being carried out to 12 weeks will provide additional insight into the effectiveness of the bone filler system.

Reportable Outcomes

Publications

McClanahan, J.R., Peyyala, R., Novak, K.F., and Puleo, D.A. (2011). Antibacterial effects of a complexation polymer system for delivering an antimicrobial peptide, *Int. J. Antimicrob. Agents* **38**:530-533. [PMID: 21920706]

Yewle, J.N., Puleo, D.A., and Bachas, L.G. (2011). Enhanced affinity bifunctional bisphosphonates for targeted delivery of therapeutic agents to bone, *Bioconj. Chem.* **22**:2496-2506. [PMID: 22073906]

Yewle, J.N., Wei, Y., Puleo, D.A., Daunert, S., Bachas, L.G. (2012). Oriented immobilization of proteins on hydroxyapatite surface using bifunctional bisphosphonates as linkers, *Biomacromolecules* **13**:1742-1749. [PMID: 22559170]

Brown, M.E., Zou, Y., Dziubla, T.D., and Puleo, D.A. (2012). Effects of composition and setting environment on mechanical properties of a composite bone filler, *J. Biomed. Mater. Res. Part A* (in press).

Orellana, B.R., Thomas, M.V., Hilt, J.Z., and Puleo, D.A. (2012). Bioerodible calcium sulfate hemihydrate/poly(β-amino ester) hydrogel space-making composites (in review).

Abstracts/Presentations

Puleo, D.A. (2011). Using controlled release strategies to modulate tissue regeneration. Presented at the 242nd Annual Meeting of the American Chemical Society, Denver, CO, August 28 - September 2.

Vasilakes, A., Biswal, D., Peyyala, R., Puleo, D.A., Hilt, J.Z., and Dziubla, T.D. (2011). Development of biodegradable hydrogels for the controlled release of antimicrobial and antioxidant agents. Presented at the 2011 AIChE Annual Meeting, October 16-21, Minneapolis, MN.

Orellana, B.R., Thomas, M.V., Hilt, J.Z., and Puleo, D.A. (2012). Drug delivery from space-Making calcium sulfate/poly(β-amino ester) hydrogel composites. Presented at the AADR Annual Meeting, March 21-24, Tampa, FL.

Conclusion

The majority of explosion-induced trauma sustained by armed service members results in loss of tissue and contamination with a variety of materials, biological and nonbiological. This project is developing materials to treat bacterially infected osseous injuries, such as those that occur in long bones, head, and face. More specifically, a moldable bone graft substitute providing localized, controlled, sequential release of antimicrobial and osteogenic agents is being formulated to enable timely and complete healing of large, infected bone defects. Thus far, a moldable, osteoconductive filler, whose mechanical, degradation, and drug release properties can be tailored to different design criteria, has been formulated. Current efforts are directed at systematically examining the potential for these proactive biomaterials to enhance tissue repair in a rodent model of an infected segmental long bone defect. Results thus far have shown that localized delivery of antibiotic outperformed systemic administration through the first month of observation. With the infection at least partially inhibited by sustained release of antibiotics from the implant, simvastatin subsequently released from the core can enhance bone formation.

Bioconjugate Chemistry

Article

pubs.acs.org/bc

Enhanced Affinity Bifunctional Bisphosphonates for Targeted Delivery of Therapeutic Agents to Bone

Jivan N. Yewle,[†] David A. Puleo,[‡] and Leonidas G. Bachas*[,§]

[†]Department of Chemistry, University of Kentucky, Lexington, Kentucky 40506-0055, United States

[‡]Center for Biomedical Engineering, University of Kentucky, Lexington, Kentucky 40506-0070, United States

[§]Department of Chemistry, University of Miami, 1301 Memorial Drive, Coral Gables, Florida 33146-0431, United States

ABSTRACT: Skeletal diseases have a major impact on the worldwide population and economy. Although several therapeutic agents and treatments are available for addressing bone diseases, they are not being fully utilized because of their uptake in nontargeted sites and related side effects. Active targeting with controlled delivery is an ideal approach for treatment of such diseases. Because bisphosphonates are known to have high affinity to bone and are being widely used in treatment of osteoporosis, they are well-suited for drug targeting to bone. In this study, a targeted delivery of therapeutic agent to resorption sites and wound healing sites of bone was explored. Toward this goal, bifunctional hydrazine-bisphosphonates (HBPs), with spacers of various lengths, were synthesized and studied for their enhanced affinity to bone. Crystal growth inhibition studies showed that these HBPs have high affinity to hydroxyapatite, and HBPs with shorter spacers bind more strongly than alendronate to hydroxyapatite. The HBPs did not affect proliferation of MC3T3-E1 preosteoblasts, did not induce apoptosis, and were not cytotoxic at the concentration range tested (10^{-6}–10^{-4} M). Furthermore, drugs can be linked to the HBPs through a hydrazone linkage that is cleavable at the low pH of bone resorption and wound healing sites, leading to release of the drug. This was demonstrated using hydroxyapatite as a model material of bone and 4-nitrobenzaldehyde as a model drug. This study suggests that these HBPs could be used for targeted delivery of therapeutic agents to bone.

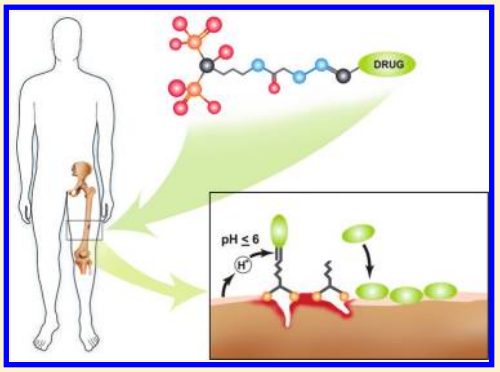

INTRODUCTION

Active targeting of therapeutic agents to bone reduces drug toxicity and improves drug bioavailability at the desired site.[1] Bone tissue is characterized by constant remodeling, whereby it continuously undergoes formation and resorption; perturbations in bone remodeling are associated with several metabolic bone diseases, such as osteoporosis.[2−4] Therefore, molecules that inhibit bone resorption or stimulate bone formation show drug activity against various skeletal disorders.[5] Although a range of therapeutic agents is available to treat skeletal disorders,[6] their clinical application is hampered by their uptake in nontargeted sites and the consequent undesired side effects.[7]

Several bisphosphonates (BPs) show antiresorptive properties and are being prescribed in the treatment of skeletal diseases.[6,8,9] BPs are stable analogues of naturally occurring pyrophosphate and have high affinity to bone and hydroxyapatite (HA).[10] Besides the two phosphonate groups, BPs have two other substituents (R^1 and R^2) on their geminal carbon. BPs with a hydroxyl or an amine group at R^1 facilitate tridentate binding to bone and HA, and show an increased affinity to these materials.[11,12] The overall nature of the R^2 substituent also contributes toward enhancing the bone-seeking ability and pharmacological properties of BPs.[10,13]

Recently, a number of drug targeting and drug delivery strategies have been reported using a range of delivery vehicles,

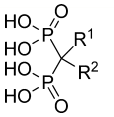

such as polymer scaffolds, liposomes, dendrimers, micelles, hydrogels, peptides, and antibodies.[14−21] However, drug targeting to bone sites requires molecules that have high affinity to bone. Besides BPs, other molecules, such as D-aspartic acid octapeptide,[20,21] polymalonic acid,[22] and tetracycline,[23,24] show affinity to bone. BPs have advantage over other molecules because their affinity can be tuned by changing their R^1 and R^2 substituents. Moreover, in addition to being prescribed as drugs, BPs are also being studied for drug targeting and drug delivery to bone,[25−30] including the administration of radiopharmaceuticals and imaging agents to bone for diagnostic applications.[31−35] For the purpose of drug targeting to bone, various strategies of BP-drug conjugation have been investigated by us and others.[29,35−38] Ideally, for targeted drug delivery to bone, BP-drug conjugates should have a stable linkage between the BP and drug molecule that can survive during systemic circulation of the conjugate following parenteral administration, and at the same time be labile at the

Received: June 15, 2011
Revised: November 10, 2011
Published: November 10, 2011

bone surface to release the drug locally. Most of the strategies mentioned above employ agents that are conjugated to BPs through stable, noncleavable linkages resulting in the administration of the complete conjugate to the treatment site.[25,29,31−33,35] Current approaches that employ cleavable linkages either are too labile to ensure delivery of the drug to the desired site[26,27] or show limited release providing inadequate availability of drug for action.[26] A strategy that involves labile conjugation to one of the phosphonate groups of BP could compromise the affinity of the corresponding BP-drug conjugate toward bone, because it is through the phosphonate groups that BPs bind to the mineral matrix.[27]

Herein, we report a novel strategy for targeted delivery of therapeutic agents to sites of low pH, such as bone resorption lacunae and areas of wound healing, through their conjugation to enhanced affinity bifunctional BPs with a pH-triggered cleavable linkage. In particular, we have synthesized seven novel hydrazine-bisphosphonates (HBPs) (**2**−**8**), which have a hydroxyl group as R^1, while R^2 contains a hydrazine functionality attached through spacers of various length and hydrophobicity (Table 1). Furthermore, experiments were performed to explore the binding affinity, cytotoxicity, drug conjugation, and pH triggered drug release of HBPs.

Table 1. Structure of Alendronate (1) and Hydrazine-Bisphosphonates (HBPs) (2−8)

Cpd	R^1	R^2
1	OH	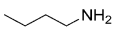
2	OH	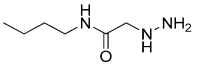
3	OH	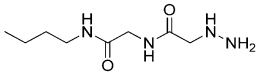
4	OH	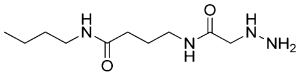
5	OH	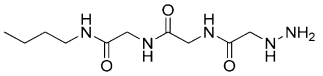
6	OH	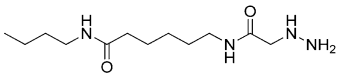
7	OH	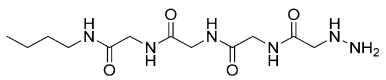
8	OH	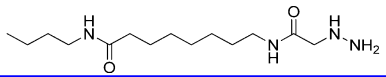

EXPERIMENTAL PROCEDURES

Materials. The osteoblastic cell line MC3T3-E1 was obtained from American Type Culture Collection (CRL-2593; ATCC, Rockville, MD). Alpha minimum essential medium (αMEM) and fetal bovine serum (FBS) were purchased from GIBCO-Invitrogen (Carlsbad, CA). The BCA protein assay kit was obtained from ThermoFisher Scientific (Rockford, IL). The cell proliferation reagent WST-1 was purchased from Roche (Mannheim, Germany). Ac-DEVD-AFC was obtained from Enzo Life Sciences (Plymouth Meeting, PA). 4-Aminobutanoic acid, 6-aminohexanoic acid, 8-aminooctanoic acid, glycine, glycylglycine, glycylglycylglycine, methanesulfonic acid, phosphorous acid, phosphorus trichloride, and 2,3,5,6-tetrafluorophenol (TFP) were purchased from Alfa Aesar (Ward Hill, MA). *N,N′*-Dicyclohexylcarbodiimide (DCC), triethylamine (TEA), tri-BOC-hydrazinoacetic acid (TBHA), reagent grade hydroxyapatite powder, potassium hydroxide, sodium acetate, sodium chloride, sodium hydroxide, etoposide, tris(hydroxymethyl)aminomethane hydrochloride (Tris-HCl), 4-(2-hydroxyethyl)piperazine-1-ethanesulfonic acid (HEPES), 3-[(3-cholamidopropyl)dimethylamino]-1-propanesulfonate (CHAPS), ethylenediaminetetraacetic acid disodium salt dihydrate (EDTA), sodium fluoride (NaF), sodium orthovanadate, leupeptin hemisulfate salt, aprotinin bovine, phenylmethylsulfonylfluoride, DL-dithiothreitol (DTT), glycerol, and Triton X-100 were purchased from Sigma-Aldrich (St. Louis, MO). Calcium chloride, hydrochloric acid, and potassium dihydrogen phosphate were obtained from EMD Chemicals (Gibbstown, NJ). Acetonitrile, chloroform, dichloromethane, diethyl ether, dimethyl sulfoxide (DMSO), hexane, and phosphoric acid were purchased from Mallinckrodt (Hazelwood, MO). The NMR solvents deuterium oxide and deuterated chloroform were purchased from Cambridge Isotope Laboratories (Andover, MA).

Apparatus. ^{1}H NMR, ^{31}P NMR, and ^{13}C NMR spectra were obtained on a Varian INOVA 400 MHz spectrometer (Palo Alto, CA). Electrospray ionization mass spectrometry was performed on a ThermoFinnigan LCQ mass spectrometer (Waltham, MA). HA crystal growth experiments were performed using an Isotemp Refrigerated Circulator and pH meter (Fisher Scientific, Pittsburgh, PA). UV−vis spectra were obtained with an Agilent 8453 UV−visible spectrophotometer (Agilent Technologies, Santa Clara, CA). Deionized water was produced using a Milli-Q water purification system (Millipore, Bedford, MA).

Scheme 1. Synthesis of Alendronate 1 and HBP 2

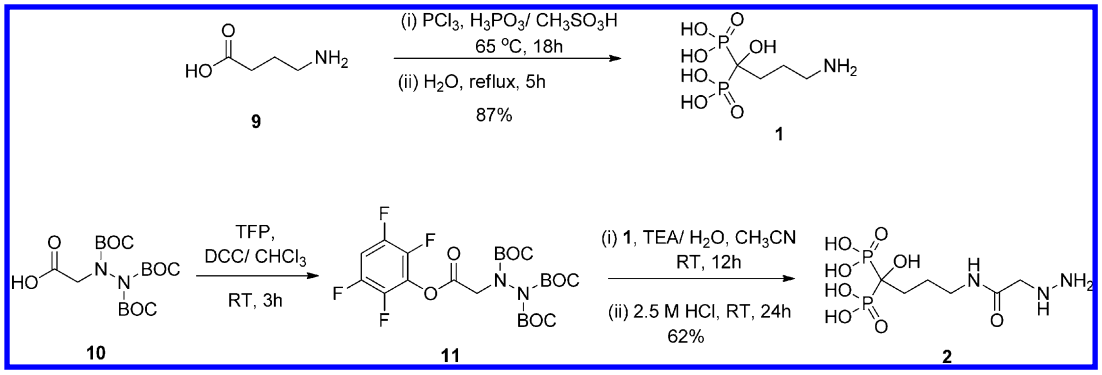

dx.doi.org/10.1021/bc2003132 | Bioconjugate Chem. 2011, 22, 2496−2506

Synthesis of (4-Amino-1-hydroxybutylidene)-bisphosphonic Acid Monosodium Salt (1). (4-Amino-1-hydroxybutylidene)bisphosphonic acid monosodium salt or monosodium alendronate (**1**) was synthesized in an inert atmosphere according to a previously reported procedure from 4-aminobutanoic acid (**9**)[39,40] as outlined in Scheme 1. A 25 mL flask was fitted with an addition funnel and a reflux condenser. Ice-cold water was circulated through the condenser. The system was flushed with nitrogen; and 4-aminobutyric acid (**9**) (4.0 g, 38.7 mmol), phosphorous acid (3.18 g, 38.7 mmol), and methanesulfonic acid (16 mL) were added to the flask. The mixture was heated for 5 min at 65 °C. PCl_3 (9.0 mL, 85.3 mmol) was added over 20 min, and the mixture was stirred for 18 h at 65 °C. The solution was cooled to 25 °C and quenched into 0−5 °C water (40 mL) with vigorous stirring. The reaction flask was rinsed with an additional 16 mL of water, and the combined solution was refluxed for 5 h at 110 °C. The solution was cooled to 23 °C, and the pH was adjusted to 4−4.5 with 50% (v/v) NaOH. The resulting mixture was allowed to react for 10−12 h at 0−5 °C. The white solid obtained was filtered and washed with cold water (20 mL) and 95% ethanol (20 mL). The solid was dried under vacuum at room temperature (RT) to obtain compound **1** as a white solid in 87.1% (9.22 g) yield. ^{1}H NMR (D_2O): δ 3.02 (t, 2H), δ 2.00 (m, 4H). ^{13}C NMR (MeCN/D_2O): δ 72.9 (t), δ 39.33 (s), δ 29.94 (s), δ 21.48 (t). ^{31}P NMR (H_3PO_4/D_2O): δ 18.53. MS (MALDI-TOFMS): 272 $[M+H+Na]^+$.

Synthesis of Tri-*tert*-butyl 2-(2-oxo-2-(2,3,5,6-tetrafluorophenoxy)ethyl)hydrazine-1,1,2-tricarboxylate (11). Tri-BOC-hydrazinoacetate (**10**) (90.0 mg, 0.231 mmol) and TFP (42.1 mg, 0.254 mmol) were dissolved in 5 mL chloroform. DCC (52.3 mg, 0.254 mmol) in 5 mL chloroform was added dropwise to the reaction mixture and stirred at RT. The progress of the reaction was followed by thin layer chromatography (TLC). After complete consumption of **10** (3 h), the 1,3-dicyclohexyl urea formed in the reaction mixture was removed by filtration, and the filtrate was evaporated *in vacuo*. The residue was then suspended in an adequate amount of hexane, the remaining 1,3-dicyclohexyl urea was removed by filtration, and the filtrate was evaporated *in vacuo* to obtain crude compound **11**. The crude material was purified by column chromatography (hexane/acetone 85/15 v/v) to obtain pure compound **11** as a pale yellow liquid in 97% (120.5 mg) yield. ^{1}H NMR (CD_3CN): δ 7.25 (m, 1H), δ 3.20 (s, 2H) δ 1.45 (m, 27H). ^{13}C NMR ($CDCl_3$): δ 168.01 (s), δ 154.35 (s), δ 153.75 (s), δ 150.54 (s), δ 148.70 (s), δ 147.10 (s), δ 146.40 (s), δ 102.10 (s), δ 84.22 (s), δ 83.27 (s), δ 82.21 (s), δ 54.33 (m), δ 28.20 (s).

Synthesis of (4-(2-Hydrazinylacetamido)-1-hydroxybutane-1,1-diyl)bisphosphonic Acid (2). Compound **1** (50.0 mg, 0.154 mmol) was suspended in 1 mL of deionized water, and TEA (93.2 mg, 0.923 mmol) was added to the suspension. After a few seconds of stirring at RT, the suspension became clear. The reaction was stirred at RT for 5 min. Compound **11** (124 mg, 0.231 mmol) was dissolved in 1.5 mL of acetonitrile and added to the reaction mixture. TEA (15.5 mg, 0.154 mmol) was added, and the reaction mixture was stirred at RT for 12 h. The reaction mixture was washed with diethyl ether (10 mL) and evaporated *in vacuo*. The obtained solid was treated with 2 mL of 2.5 M HCl, and the solution was stirred at RT for 24 h. The solvent was removed *in vacuo*, and the crude product was sonicated twice in ethanol at RT for 2 h and filtered to obtain a white solid of pure compound **2** in 62% (31 mg) yield. ^{1}H NMR (D_2O): δ 3.78 (s, 2H), δ 3.28 (t, 2H), δ 1.99 (m, 2H), δ 1.84 (m, 2H). ^{13}C NMR (MeCN/D_2O): δ 170.41 (s), δ 74.17 (t), δ 51.58 (s), δ 40.50 (s), δ 31.75 (s), δ 24.17 (s). ^{31}P NMR (H_3PO_4/D_2O): δ 19.08. MS (+ ESI): 322 $[M+H]^+$.

General Procedure for Synthesis of Compounds 13a−13f. Compound **12a−12f** (0.401 mmol, 1.2 equiv) was suspended in 1 mL of deionized water, and TEA (0.668 mmol, 2.0 equiv) was added to the suspension. After a few seconds of stirring at RT, the suspension became clear. The reaction was stirred at RT for 5 min. Compound **11** (0.334 mmol, 1.0 equiv) was dissolved in 1.5 mL of acetonitrile, and the solution was added to the reaction mixture. TEA (0.167 mmol, 0.5 equiv) was added, and the reaction mixture was stirred at RT for 12 h. The reaction mixture was washed with diethyl ether, and the solvent was evaporated *in vacuo* to obtain crude compound **13a−13f**. The crude product **13a−13f** was used in the next reaction without further purification.

*Compound **13a**.* Following the procedure shown for **13a−13f**, compound **13a** was obtained by amide coupling of compound **11** and glycine (**12a**) as a paste in 95% yield. ^{1}H NMR ($CDCl_3$): δ 4.10 (s, 2H), δ 3.98 (s, 2H), δ 1.45 (m, 27H). ^{13}C NMR ($CDCl_3$): δ 174.56 (s), δ 168.46 (s), δ 154.46 (s), δ 153.86 (s), δ 150.65 (s) δ 84.52 (s), δ 83.16 (s), δ 82.45 (s), δ 54.93 (m), δ 45.91 (m), δ 28.22 (s).

*Compound **13b**.* Following the procedure shown for **13a−13f**, compound **13b** was obtained by amide coupling of compound **11** and 4-aminobutenoic acid (**12b**) as a paste in 97% yield. ^{1}H NMR ($CDCl_3$): δ 4.10 (s, 2H), δ 3.60 (d, 2H), δ 2.35 (m, 2H), δ 1.30 (m, 2H), δ 1.45 (m, 27H). ^{13}C NMR ($CDCl_3$): δ 182.70 (s), δ 170.70 (s), δ 154.30 (s), δ 153.40 (s), δ 150.56 (s) δ 84.24 (s), δ 83.56 (s), δ 82.10 (s), δ 54.30 (m), δ 39.41 (m), δ 35.60 (m), δ 28.41 (s), δ 23.42 (m).

*Compound **13c**.* Following the procedure shown for **13a−13f**, compound **13c** was obtained by amide coupling of compound **11** and glycylglycine (**12c**) as a paste in 94% yield. ^{1}H NMR ($CDCl_3$): δ 4.02 (s, 2H), δ 3.99 (s, 2H), δ 3.80 (s, 2H), δ 1.45 (m, 27H). ^{13}C NMR ($CDCl_3$): δ 174.44 (s), δ 169.24 (s), δ 168.43 (s), δ 154.34 (s), δ 153.55 (s), δ 151.20 (s), δ 85.12 (s), δ 83.66 (s), δ 83.05 (s), δ 55.15 (m), δ 45.24 (m), δ 43.31 (m), δ 28.15 (s).

*Compound **13d**.* Following the procedure shown for **13a−13f**, compound **13d** was obtained by amide coupling of compound **11** and 6-aminohexanoic acid (**12d**) as a paste in 96% yield. ^{1}H NMR ($CDCl_3$): δ 4.03 (s, 2H), δ 3.33 (d, 2H), δ 2.21 (t, 2H), δ 1.61 (m, 2H), δ 1.45 (m, 27H), δ 1.28 (m, 2H). ^{13}C NMR ($CDCl_3$): δ 178.04 (s), δ 170.20 (s), δ 154.44 (s), δ 153.34 (s), δ 151.84 (s), δ 85.11 (s), δ 83.24 (s), δ 83.48 (s), δ 54.35 (m), δ 38.92 (m), δ 34.32 (m), δ 29.15 (s), δ 28.40 (s), δ 26.37 (s), δ 24.75 (s).

*Compound **13e**.* Following the procedure shown for **13a−13f**, compound **13e** was obtained by amide coupling of compound **11** and glycylglycylglycine (**12e**) as a paste in 93% yield. ^{1}H NMR ($CDCl_3$): δ 4.01 (s, 2H), δ 3.98 (d, 2H), δ 3.91 (d, 2H), δ 3.80 (d, 2H), δ 1.42 (m, 27H). ^{13}C NMR ($CDCl_3$): δ 174.45 (s), δ 169.75 (s), δ 169.51 (s), δ 168.01 (s), δ 154.55 (s), 151.40 (s), 151.14 (s), δ 85.40 (s), δ 85.29 (s), δ 83.51 (s), δ 55.49 (m), δ 45.30 (m), δ 43.77 (m), δ 43.34 (s), δ 28.19 (s).

*Compound **13f**.* Following the procedure shown for **13a−13f**, compound **13f** was obtained by amide coupling of compound **11** and 8-aminooctanoic acid (**12f**) as a paste in 95% yield. ^{1}H NMR ($CDCl_3$): δ 4.02 (s, 2H), δ 3.23 (m, 2H), δ 2.22 (t, 2H), δ 1.59 (m, 4H), δ 1.45 (m, 27H), δ 1.25 (m,

6H). ^{13}C NMR ($CDCl_3$): δ 178.40 (s), δ 170.05 (s), δ 154.14 (s), 151.25 (s), 151.19 (s), δ 85.17 (s), δ 85.39 (s), δ 83.89 (s), δ 38.90 (m), δ 34.00 (t), δ 30.10 (m), δ 29.12 (s), δ 29.65 (s), δ 26.58 (s), δ 24.54 (s).

General Procedure for Synthesis of Compounds 14a−14f. Compound **13a−13f** (0.386 mmol, 1.0 equiv) and TFP (0.425 mmol, 1.1 equiv) were dissolved in 15 mL chloroform. DCC (0.425 mmol, 1.1 equiv) in 10 mL chloroform was added dropwise to the reaction mixture and stirred at RT. The progress of the reaction was followed by TLC. After complete consumption of **13a−13f** (3 h), the 1,3-dicyclohexyl urea formed in the reaction mixture was removed by filtration, and the filtrate was evaporated *in vacuo*. The residue was then suspended in an adequate amount of hexane, the remaining 1,3-dicyclohexyl urea was removed by filtration, and the filtrate was evaporated *in vacuo* to obtain crude compound **14a−14f**. The crude product was purified by column chromatography (CH_2Cl_2/MeOH 90/10 v/v) to obtain the pure compound as a pale yellow liquid.

*Compound **14a***. Following the procedure shown for **14a−14f**, compound **14a** was obtained from **13a** by treatment of TFP and DCC as a sticky liquid. ^{1}H NMR ($CDCl_3$): δ 6.60 (s, 1H), δ 4.25 (s, 2H), δ 4.10 (s, 2H), δ 1.42 (m, 27H). ^{13}C NMR ($CDCl_3$): δ 174.02 (s), δ 168.32 (s), δ 154.21 (s), δ 153.14 (s), δ 150.78 (s), δ 148.72 (d), δ 146.89 (d), δ 146.10 (s), δ 101.80 (s), δ 84.12 (s), δ 83.85 (s), δ 82.64 (s), δ 54.41 (m), δ 45.00 (m), δ 28.44 (s).

*Compound **14b***. Following the procedure shown for **14a−14f**, compound **14b** was obtained from **13b** by treatment of TFP and DCC as a sticky liquid. ^{1}H NMR ($CDCl_3$): δ 6.60 (s, 1H), δ 4.05 (s, 2H), δ 3.20 (d, 2H), δ 2.67 (m, 2H), δ 1.97 (m, 2H), δ 1.42 (m, 27H). ^{13}C NMR ($CDCl_3$): δ 182.47 (s), δ 170.12 (s), δ 154.10 (s), δ 153.45 (s), δ 151.10 (s), δ 148.69 (d), δ 147.23 (d), δ 146.80 (s), δ 102.10 (s), δ 84.58 (s), δ 83.74 (s), δ 82.36 (s), δ 54.33 (m), δ 39.45 (m), δ 33.56 (m), δ 23.47 (s), δ 28.56 (s).

*Compound **14c***. Following the procedure shown for **14a−14f**, compound **14c** was obtained from **13c** by treatment of TFP and DCC as a sticky liquid. ^{1}H NMR ($CDCl_3$): δ 6.98 (s, 1H), δ 4.38 (s, 2H), δ 4.11 (s, 2H), δ 3.41 (s, 2H), δ 1.45 (m, 27H). ^{13}C NMR ($CDCl_3$): δ 170.28 (s), δ 169.52 (s), δ 167.00 (s), δ 156.00 (s), δ 151.12 (s), δ 150.02 (s), 148.23 (d), δ 147.45 (d), δ 146.69 (s), δ 102.47 (s), δ 85.67 (s), δ 85.00 (s), δ 83.90 (s), δ 55.87 (s), δ 45.65 (s), δ 43.06 (m), δ 28.14 (s).

*Compound **14d***. Following the procedure shown for **14a−14f**, compound **14d** was obtained from **13d** by treatment of TFP and DCC as a sticky liquid. ^{1}H NMR ($CDCl_3$): δ 6.97 (s, 1H), δ 4.05 (s, 2H), δ 3.95 (s, 2H), δ 2.31 (m, 2H), δ 2.62 (m, 4H), δ 1.80 (m, 2H), δ 1.45 (m, 27H). ^{13}C NMR ($CDCl_3$): δ 177.12 (s), δ 170.89 (s), δ 154.69 (s), δ 153.78 (s), δ 151.11 (s), 148.60 (d), δ 147.05 (d), δ 146.44 (s), δ 102.10 (s), δ 85.25 (s), δ 83.73 (s), δ 83.92 (s), δ 54.33 (m), δ 38.96 (m), δ 33.56 (m), δ 29.78 (s), δ 28.40 (s), δ 26.58 (s), δ 24.45 (s).

*Compound **14e***. Following the procedure shown for **14a−14f**, compound **14e** was obtained from **13e** by treatment of TFP and DCC as a sticky liquid. ^{1}H NMR ($CDCl_3$): δ 6.75 (s, 1H), δ 4.42 (d, 2H), δ 4.10 (m, 4H), δ 3.85 (d, 2H), δ 1.50 (m, 27H). ^{13}C NMR ($CDCl_3$): δ 170.81 (s), δ 170.10 (s), δ 170.05 (s), δ 165.87 (s), δ 156.00 (s), 154.80 (s), 151.20 (s), 148.48 (d), δ 147.23 (d), δ 146.10 (s), δ 103.76 (s), δ 85.79 (s), δ 85.51 (s), δ 84.07 (s), δ 55.96 (m), δ 49.46 (s), δ 43.61 (s), δ 40.82 (s), δ 28.11 (s).

*Compound **14f***. Following the procedure shown for **14a−14f**, compound **14f** was obtained from **13f** by treatment of TFP and DCC as a sticky liquid. ^{1}H NMR ($CDCl_3$): δ 6.98 (s, 1H), δ 4.05 (s, 2H), δ 3.95 (s, 2H), δ 2.40 (s, 2H), δ 1.65 (m, 4H), δ 1.38 (m, 6H), δ 1.45 (m, 27H). ^{13}C NMR ($CDCl_3$): δ 178.58 (s), δ 170.89 (s), δ 154.45 (s), 151.69 (s), 151.51 (s), 148.72 (d), δ 147.20 (d), δ 146.40 (s), δ 102.10 (s), δ 85.93 (s), δ 85.54 (s), δ 83.12 (s), δ 38.95 (m), δ 33.50 (t), δ 30.32 (m), δ 29.45 (s), δ 29.10 (s), δ 26.70 (s), δ 25.73 (s).

General Procedure for Synthesis of Compounds 3−8. Compound **1** (0.154 mmol, 1.0 equiv) was suspended in 1 mL of deionized water, and TEA (1.077 mmol, 7.0 equiv) was added to the suspension. After a few seconds of stirring at RT, the suspension became clear. The reaction was stirred at RT for 5 min. Crude compound **14a−14f** (0.231 mmol, 1.5 equiv) was dissolved in 1.5 mL of acetonitrile and added to the reaction mixture. TEA (0.154 mmol, 1.0 equiv) was added, and the reaction mixture was stirred at RT for 12 h. The reaction mixture was washed with diethyl ether (10 mL) and evaporated *in vacuo*. The obtained solid was treated with 2 mL of 2.5 M HCl, and the solution was stirred at RT for 24 h. The solvent was removed *in vacuo*; the crude product was sonicated twice in ethanol at RT for 2 h, and filtered to obtain pure compounds **3−8**.

*Compound **3***. Following the procedure shown for **3−8**, compound **1** was coupled to compound **14a** by amide linkage, followed by an acid treatment to obtain pure compound **3** as a white solid in 55% yield. ^{1}H NMR (D_2O): δ 3.95 (s, 2H), δ 3.84 (s, 2H), δ 3.26 (t, 2H), δ 1.98 (m, 2H), δ 1.84 (m, 2H). ^{13}C NMR (MeCN/D_2O): δ 172.10 (s), δ 171.74 (s), δ 74.15 (t), δ 51.40 (s), δ 47.62 (s) δ 40.60 (s), δ 31.70 (s), δ 24.09 (s). ^{31}P NMR (H_3PO_4/D_2O): δ 19.16. MS (+ ESI): 379 $[M+H]^+$.

*Compound **4***. Following the procedure shown for **3−8**, compound **1** was coupled to compound **14b** by amide linkage, followed by an acid treatment to obtain pure compound **4** as a white solid in 63% yield. ^{1}H NMR (D_2O): δ 3.73 (s, 2H), δ 3.22 (t, 4H), δ 2.25 (t, 2H), δ 1.95 (m, 2H), δ 1.80 (m, 4H). ^{13}C NMR (MeCN/D_2O): δ 176.87 (s), δ 170.46 (s), δ 74.16 (t), δ 51.54 (s), δ 40.66 (s), δ 39.52 (s), δ 34.04 (s), δ 31.84 (s), δ 25.66 (t), δ 24.16 (s). ^{31}P NMR (H_3PO_4/D_2O): δ 19.32. MS (+ ESI): 407 $[M+H]^+$.

*Compound **5***. Following the procedure shown for **3−8**, compound **1** was coupled to compound **14c** by amide linkage, followed by an acid treatment to obtain pure compound **5** as a white solid in 56% yield. ^{1}H NMR (D_2O): δ 4.04 (s, 2H), δ 3.92 (s, 2H), δ 3.86 (s, 2H), δ 3.25 (t, 2H), δ 1.96 (m, 2H), δ 1.84 (m, 2H). ^{13}C NMR (MeCN/D_2O): δ 171.55 (s), δ 170.79 (s), δ 170.62 (s), δ 72.82 (t), δ 50.04 (s), δ 42.15 (s) δ 41.88 (s), δ 39.26 (s), δ 30.06 (s), δ 22.71 (s). ^{31}P NMR (H_3PO_4/D_2O): δ 19.08. MS (+ ESI): 436 $[M+H]^+$.

*Compound **6***. Following the procedure shown for **3−8**, compound **1** was coupled to compound **14d** by amide linkage, followed by an acid treatment to obtain pure compound **6** as a white solid in 59% yield. ^{1}H NMR (D_2O): δ 3.73 (s, 2H), δ 3.22 (q, 4H), δ 2.25 (t, 2H), δ 1.98 (m, 2H), δ 1.82 (m, 2H), δ 1.59 (t, 2H), δ 1.52 (t, 2H), δ 1.30 (m, 2H). ^{13}C NMR (MeCN/D_2O): δ 177.70 (s), δ 169.94 (s), δ 73.95 (t), δ 51.36 (s), δ 40.43 (s) δ 39.86 (s), δ 36.37 (s), δ 31.64 (s), δ 28.62 (s), δ 26.15 (s), δ 25.68 (s), δ 23.99 (s). ^{31}P NMR (H_3PO_4/D_2O): δ 19.14. MS (+ ESI): 435 $[M+H]^+$.

*Compound **7***. Following the procedure shown for **3−8**, compound **1** was coupled to compound **14e** by amide linkage,

dx.doi.org/10.1021/bc2003132 | *Bioconjugate Chem.* 2011, 22, 2496−2506

followed by an acid treatment to obtain pure compound **7** as a white solid in 54% yield. ^{1}H NMR (D_2O): δ 3.73 (s, 2H), δ 3.22 (q, 4H), δ 2.25 (t, 2H), δ 2.00 (m, 2H), δ 1.82 (m, 2H), δ 1.55 (t, 2H), δ 1.45 (t, 2H), δ 1.30 (s, 6H). ^{13}C NMR (MeCN/D_2O): δ 178.82 (s), δ 170.70 (s), δ 74.58 (t), δ 52.25 (s), δ 49.01 (s), δ 41.25 (s), δ 40.95 (s), δ 37.36 (s), δ 32.54 (s), δ 29.73 (s), δ 29.57 (s), δ 27.41 (s), δ 26.88 (s), δ 24.81 (s). ^{31}P NMR (H_3PO_4/D_2O): δ 19.38. MS (+ ESI): 493 $[M+H]^+$.

Compound ***8***. Following the procedure shown for **3**−**8**, compound **1** was coupled to compound **14f** by amide linkage, followed by an acid treatment to obtain pure compound **8** as a white solid in 57% yield. ^{1}H NMR (D_2O): δ 4.06 (s, 2H), δ 4.0 (s, 2H), δ 3.92 (s, 2H), δ 3.86 (s, 2H), δ 3.25 (t, 2H), δ 1.98 (m, 2H), δ 1.84 (m, 2H). ^{13}C NMR (MeCN/D_2O): δ 173.19 (s), δ 172.01 (s), δ 172.17 (s), δ 171.92 (s), δ 74.15 (t), δ 51.45 (s) δ 43.73 (s), δ 43.49 (s), δ 43.15 (s), δ 40.60 (s), δ 31.67 (s), δ 24.15 (s). ^{31}P NMR (H_3PO_4/D_2O): δ 19.15. MS (+ ESI): 463 $[M+H]^+$.

Crystal Growth Inhibition Assay for Binding Affinity Study. As BPs target bone surfaces under active formation and resorption of HA,[41] a crystal growth inhibition assay was performed to measure the affinities of HBPs to HA. This method has commonly been used to examine BP binding affinity.[42,43] Kinetic experiments of HA crystal growth were performed in a nitrogen atmosphere in magnetically stirred (400 rpm) double-jacketed vessels at pH 7.4 and 37.0 ± 0.1 °C, as described in a previously reported procedure.[42,43] In brief, the reaction solution with final ionic strength of 0.15 M was prepared by mixing calcium chloride (2.0 mmol), potassium dihydrogen phosphate (2.0 mmol), and sodium chloride (132.0 mmol) followed by degassing and filtration. The titrant with final ionic strength of 0.15 M was prepared by mixing calcium chloride (2.0 mmol), potassium hydroxide (10.0 mmol), and sodium chloride (134.0 mmol) followed by degassing and filtration. The reaction was initiated by adding 5 mg seed mass of HA crystallites into 100 mL of reaction solution. The constant thermodynamic driving force for growth of HA crystals was maintained by keeping the pH constant at 7.4 with addition of titrant. The volume of titrant added was recorded as a measure of HA crystal growth. Crystal growth inhibition experiments were performed in presence of at least six different concentration of each of HBPs (**2**−**8**). For positive control, experiments were performed in presence of six different concentrations of alendronate (**1**), whereas for negative control, experiments were performed in the absence of any BP.

Cell Culture. The MC3T3-E1 cells were cultured in prewarmed αMEM medium that was supplemented with 10% FBS at 37 °C in a humidified atmosphere composed of 5% CO_2. The cells were seeded into 96-well plates at a density of 1×10^4 cells/well for *in vitro* quantification of intracellular protein and caspase activity. One day after seeding, the cultures were treated with various concentrations (1×10^{-6}, 1×10^{-5}, and 1×10^{-4} M) of HBPs. Cells without HBPs were used as a negative control, while cells treated with 10^{-6}, 10^{-5}, or 10^{-4} M of etoposide were used as positive controls. The plates were incubated again for 24, 48, and 72 h before use for further analysis. The experiments were conducted in triplicate and repeated at least three times to ascertain the reproducibility of the results.

Intracellular Protein Quantification. Intracellular protein was measured using a commercially available BCA assay kit. Briefly, the medium was removed, and the adherent cells were washed with PBS. The cultures were lysed by 10 min incubation in 50 μL of lysate buffer (20 mM Tris-HCl, pH 7.4, 150 mM NaCl, 1 mM EDTA, 10 mM NaF, 1 mM sodium orthovanadate, 5 μg/mL leupeptin, 0.14 U/mL aprotinin, 1 mM phenylmethylsulfonylfluoride, and 1% (v/v) Triton X-100), followed by 2 s of sonication. Volumes of 10 μL of the cell lysate samples and standards (solutions of known concentrations of bovine serum albumin) were added to the wells of a 96-well microtiter plate followed by addition of 200 μL of the working reagent; the well contents were mixed thoroughly by shaking the plate for 2 min. The plate was incubated at 37 °C for 30 min and then cooled to RT. The absorbance of the samples was measured at 562 nm on a plate reader. The amount of protein in the sample was calculated using a standard plot.

Cell Cytotoxicity Assay. The cytotoxicity of the HBPs was determined using a colorimetric WST-1 assay. The assay was conducted after 72 h of HBP treatment in accordance with the manufacturer's instructions. In brief, cultures in 96-well plates were incubated with 10 μL/well of cell proliferation reagent WST-1 at 37 °C for 60 min in a humidified atmosphere composed of 5% CO_2. The plate was cooled to RT, and the absorbance of the samples was measured at 450 nm on a plate reader.

Apoptosis Assay. Apoptosis was determined by measuring the intracellular caspase-3 activity. The cultures were lysed by 10 min of incubation in 50 μL of lysate buffer (20 mM Tris-HCl, pH 7.4, 150 mM NaCl, 1 mM EDTA, 10 mM NaF, 1 mM sodium orthovanadate, 5 μg/mL leupeptin, 0.14 U/mL aprotinin, 1 mM phenylmethylsulfonylfluoride, and 1% (v/v) Triton X-100), followed by 2 s of sonication. The cell lysate was treated with 50 μM Ac-DEVD-AFC in 50 mM HEPES buffer (pH 7.4, 100 mM NaCl, 0.1% CHAPS, 10 mM DTT, 1 mM EDTA, and 10% (v/v) glycerol) at RT for 60 min in the dark. The caspase-3 activity was determined by measuring the fluorescence at λ_{em} = 510 nm (λ_{ex} = 485).

Synthesis of Compound 16. Compound **2** (10.0 mg, 0.028 mmol) was suspended in 10 mL of deionized water. The reaction mixture was acidified with 10 μL of acetic acid. 4-Nitrobenzaldehyde (**15**) (8.4 mg, 0.056 mmol) was dissolved in DMSO and added to the above suspension. The reaction was stirred at RT for 48 h. The solvent was evaporated *in vacuo* to obtain crude product **16**. Compound **16** was dissolved in water and washed with ethyl acetate to remove excess reactant **15**. The water layer containing **16** was used in the next reaction without further purification.

Synthesis of Compound 19. 4-Nitrobenzoic acid (**18**) (100.0 mg, 0.598 mmol) and TFP (109.3 mg, 0.658 mmol) were dissolved in 5 mL acetone. DCC (135.8 mg, 0.658 mmol) in 5 mL acetone was added dropwise to the reaction mixture and stirred at RT. The progress of the reaction was followed by TLC. After complete consumption of **18** (3 h), the 1,3-dicyclohexyl urea formed in the reaction mixture was removed by filtration, and the filtrate was evaporated *in vacuo*. The residue was then suspended in an adequate amount of acetonitrile, the remaining 1,3-dicyclohexyl urea was removed by filtration, and the filtrate was evaporated *in vacuo* to obtain crude compound **19**. Compound **19** was used in the next reaction without further purification.

Synthesis of Compound 20. Compound **1** (60.0 mg, 0.185 mmol) was suspended in 1 mL of deionized water and TEA (111.9 mg, 1.108 mmol) was added to the suspension. After a few seconds of stirring at RT, the suspension became clear. The reaction was stirred at RT for 5 min. Crude

dx.doi.org/10.1021/bc2003132 | *Bioconjugate Chem.* 2011, 22, 2496−2506

compound **19** (92.2 mg, 0.277 mmol) was dissolved in 1.5 mL of acetonitrile and added to the reaction mixture. TEA (18.7 mg, 0.185 mmol) was added, and the reaction mixture was stirred at RT for 12 h. The reaction mixture was washed with 10 mL diethyl ether several times, and the water layer was lyophilized to obtain a sticky solid. The reaction product was then sonicated twice in ethanol for 2 h at RT and filtered to obtain pure compound **20**. ^{1}H NMR (D_2O): δ 8.33 (d, 2H), δ 7.95 (d, 2H), δ 3.45 (t, 2H), δ 1.98 (m, 4H). ^{31}P NMR (H_3PO_4/D_2O): δ 18.23. MS (- ESI): 397 $[M-H]^-$.

***In Vitro* Studies of Drug Targeting and Drug Release.** Compound **16** is a HBP-drug conjugate, where a model drug (4-NBA) is conjugated to HBP **2** via hydrazone linkage. The conjugate was immobilized on HA surface and studied for its release at various pH solutions. In brief, compound **16** (1 mg) in water was equally distributed into three Eppendorf tubes and diluted to get 1.0 mL of total volume each. Excess of HA (50.0 mg) was added to each Eppendorf tube, and the tubes were stirred at RT for 0.5 h. After centrifugation at 1000 rpm for 5 min, the supernatant was discarded. The HA was washed twice with 1.0 mL water, followed by centrifugation, and the supernatant was discarded. A volume of 1.0 mL acetate solution (0.1 M sodium acetate, 0.05 M sodium chloride) of pH 5.0, 6.0, and 7.4 was added in three Eppendorf tubes, respectively. The Eppendorf tubes were incubated at 37 °C with continuous shaking. The suspensions were centrifuged at particular time points, and the absorbance of the supernatants was measured (λ = 265 nm, 1 cm cuvette) to calculate the amount of 4-NBA released from the immobilized conjugate.

For the control studies, the above experiment was repeated with compound **20**. Compound **20** is a BP-drug conjugate, where the model drug (4-NBA) is conjugated to alendronate via amide linkage. The conjugate was immobilized on the HA surface and studied for its release at various pH solutions. In brief, compound **20** (1 mg) in water was equally distributed into three Eppendorf tubes and diluted to get 1.0 mL of total volume each. Excess of HA (50.0 mg) was added to each Eppendorf tube, and the tubes were stirred at RT for 0.5 h. After centrifugation at 1000 rpm for 5 min, the supernatant was discarded. The HA was washed twice with 1 mL water, followed by centrifugation, and the supernatant was discarded. A volume of 1.0 mL acetate solution (0.1 M sodium acetate, 0.05 M sodium chloride) of pH 5.0, 6.0, and 7.4 was added in three Eppendorf tubes, respectively. The Eppendorf tubes were incubated at 37 °C with continuous shaking. The suspensions were centrifuged at particular time points, and the absorbance of the supernatants was measured (λ = 265 nm, 1 cm cuvette) to calculate the amount of 4-NBA released from the immobilized conjugate.

RESULTS AND DISCUSSION

BPs have high affinity toward bone and HA. After administration, BPs bind to bone surfaces where they can be internalized into osteoclasts and cause their apoptosis.[44−46] In other words, BPs control bone resorption through apoptosis of osteoclasts. However, this could be a drawback of the BP treatment because it disturbs the bone remodeling cycle. In general, bone remodeling is a lifelong process, whereby osteoblasts and osteoclasts work simultaneously for bone formation and bone resorption, respectively. Bone formation and bone resorption are interdependent processes, and therefore, osteoblastic function of bone formation also gets affected by controlling osteoclastic bone resorption. Along with controlling bone resorption, subsequent bone formation at resorption sites is crucial; this can be achieved by delivering therapeutic agents to bone resorption sites using bisphosphonates. Active drug targeting at sites of bone metastases and calcified neoplasms using polymeric carrier was reported previously. Alendronate and an antiangiogenic agent, TNP-470, were conjugated to *N*-(2-hydroxypropyl)methacrylamide (HPMA) through a cathepsin K sensitive tetrapeptide (Gly-Gly-Pro-Nle).[47,48] Because of alendronate conjugation, HPMA was found to be distributed to bone tumors and the endothelial compartments of bone metastases with a good antitumor efficacy. However, one could eliminate the polymeric carrier and make a simpler and smaller conjugate by coupling drugs directly to high affinity BPs via hydrolyzable bonds. Therefore, our overall goal is to make BPs capable of delivering drug molecules, including bone growth factors, at bone resorption sites. The first goal was to design novel BPs that demonstrate high binding affinity to HA and contain a functional group that could be used to conjugate therapeutic agents to BPs through an acid-labile linkage. Substituents (R^1 and R^2) at the germinal carbon of the BP contribute toward bone affinity; in particular, the presence of a hydroxyl at R^1 enhances bone affinity by enabling tridentate binding to HA.[10−12] In that regard, we chose 1-hydroxy-1,1-bisphosphonic acid as the basic backbone of bifunctional BPs.

The designed 1-hydroxy-1,1-bisphosphonic acid backbone has a hydroxyl at R^1, while the R^2 substituent was used to introduce a different functional group that could be subsequently used for attachment of therapeutic agents. The attachment of a therapeutic agent to BP is possible through several reversible and irreversible linkages such as amide, ester, imine, hydrazone, ether, and thioether coupling. However for drug delivery at wound healing sites and resorption sites, where the pH is acidic,[49,50] acid-labile linkages such as those provided by hydrazones and imines are more appropriate. Imine hydrolyses rapidly at pH $\leq$ 7.0,[51] while hydrazone is stable at physiological pH. Further, the rate of hydrolysis of the hydrazone linkage increases gradually with decrease in pH from 7.4.[52,53] Therefore, the hydrazone linkage presents advantages over the imine linkage when sustained drug release is desired at the bone surface. Hence, the hydrazine functionality was introduced in 1-hydroxy-1,1-bisphosphonic acid at R^2 to obtain bifunctional HBPs.

It is important that the HBP-drug conjugate should not only be stable during systemic circulation, but should also bind to the bone surface before releasing the drug at the desired site. The attached drug may sterically affect this interaction between the BP and the bone surface. Consequently, a spacer was introduced in the synthesized HBPs between the BPs and the terminal hydrazine. HBPs with several spacers of varying length and hydrophobicity were synthesized.

A straightforward synthesis was used to create the desired HBPs (**2**−**8**). Compound **2** has the shortest spacer attaching hydrazine to 1-hydroxy-1,1-bisphosphonic acid. To synthesize HBP **2**, monosodium alendronate was prepared first in an inert atmosphere according to a previously reported procedure from 4-aminobutanoic acid by reaction with phosphorous acid and phosphorus trichloride in methanesulfonic acid and subsequent hydrolysis.[39,40] The reactive ester of TBHA (**10**) was prepared by dropwise addition of DCC in chloroform to a mixture of TBHA and TFP in chloroform at RT. This reactive ester was then coupled with monosodium alendronate in basic condition at RT to obtain BOC-protected HBP **2**. The BOC-protection

dx.doi.org/10.1021/bc2003132 | *Bioconjugate Chem.* 2011, 22, 2496−2506

Scheme 2. Synthesis of HBPs 3−8

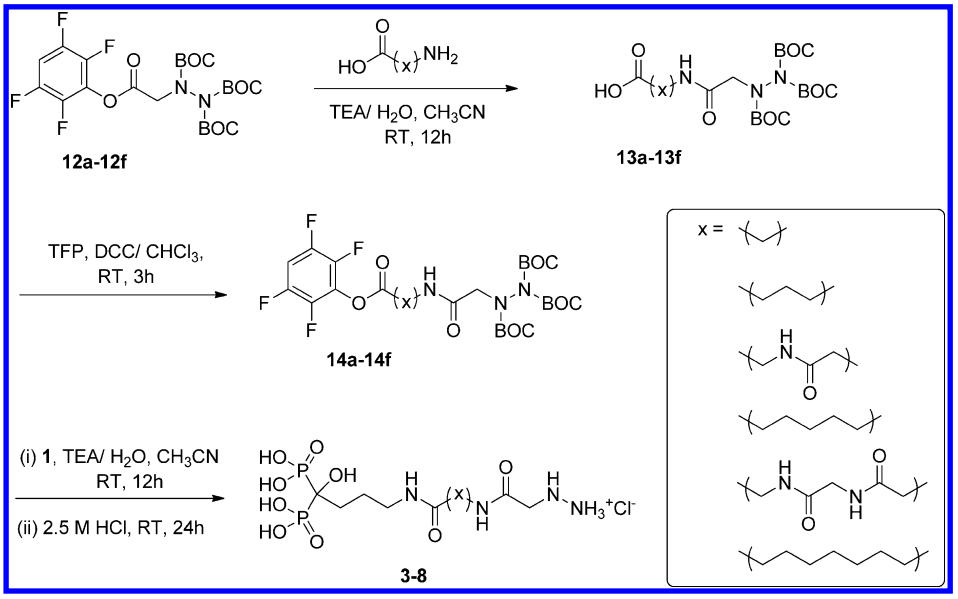

of the hydrazine group was removed with treatment of 2.5 M HCl to obtain HBP **2**. The crude product was sonicated twice in ethanol at RT for 2 h and filtered to obtain pure HBP **2** (Scheme 1).

Using a similar strategy, six other analogues of HBP **2** (**3**−**8**) with spacers of different length and hydrophobicity were synthesized by introducing various amino acids, such as glycine (**12a**), 4-aminobutanoic acid (**9**), glycylglycine (**12c**), 6-aminohexanoic acid (**12d**), glycylglycylglycine (**12e**), and 8-aminooctanoic acid (**12f**), respectively (Scheme 2). All seven HBPs were obtained and were characterized with ^{1}H NMR, ^{31}P NMR, ^{13}C NMR, and electrospray ionization mass spectrometry.

The binding affinities of the HBPs were measured and compared with alendronate, which is a commercially available BP having high affinity to HA. BPs are known to inhibit the crystal growth of HA and target bone surfaces under active formation and resorption of HA.[41] Therefore, a crystal growth inhibition assay, which is a widely used method for determination of binding affinity of BP,[42,43] was performed to measure the affinities of HBPs to HA. During the experiments, a favorable environment for crystal growth of HA was maintained. The crystal growth of HA was measured in the presence of various concentration HBPs. The pH was maintained at 7.4 by addition of titrant, and the volume of titrant added was recorded as a measure of HA crystal growth. A range of experiments were performed in presence of various concentrations (0, 1.0×10^{-7}, 2.5×10^{-7}, 5.0×10^{-7}, 7.5×10^{-7}, and 1.0×10^{-6} M) of HBPs and alendronate. For every experiment of HA crystal growth, a plot of the volume of titrant added vs time was generated. A typical set of plots is depicted in Figure 1. The growth rate (R) at any instant can be described by

$$R = \beta \frac{dV}{dt} \quad (1)$$

where dV/dt is the rate of titrant addition, and β is a constant whose value reflects the titrant concentration with respect to the surface area of HA during crystal formation; β was considered as constant for all experiments.

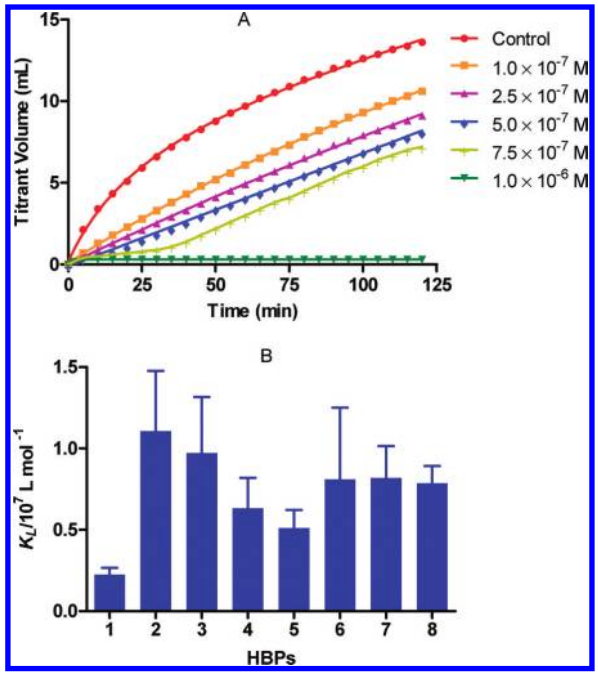

Figure 1. (A) Plot of HA crystal growth in the presence of varying concentrations of HBP **2** at pH 7.4 and 37 °C (seed mass = 5 mg). (B) Relative adsorption affinity constants (K_L) of alendronate (**1**) and HBPs **2**−**8** measured at varying concentrations of BPs ($C = 1.0 \times 10^{-7}$, 2.5×10^{-7}, 5.0×10^{-7}, and 7.5×10^{-7} M) at pH 7.4 and 37 °C. Data are the average ± one standard deviation ($n = 4$).

It can be noted from Figure 1 that the HA crystals appear to grow nonlinearly during the early stage of the experiment due to initial seeding of the HA crystals. The flat line parallel to the X-axis indicates the complete prevention of crystal growth. A pseudo-Langmuir adsorption isotherm can be used to describe the rates of HA crystal growth and can be expressed by

$$\frac{R_0}{R_0 - R_i} = 1 + \frac{1}{K_L C} \quad (2)$$

dx.doi.org/10.1021/bc2003132 | Bioconjugate Chem. 2011, 22, 2496−2506

where C is the concentration of BP added, and R_0 and R_i are the rates of HA crystal growth in the absence and presence of BP, respectively.

By rearranging eqs 1 and 2, the relative adsorption affinity constants (K_L) can be described by

$$K_L = \frac{\frac{dV_0}{dt} - \frac{dV_i}{dt}}{C\frac{dV_i}{dt}} \quad (3)$$

where dV_0/dt and dV_i/dt are the rates of titrant addition at early stage of the experiment in the absence and presence of BP, respectively.

The relative trend of binding affinities of alendronate (**1**) and HBPs (**2**–**8**) at various concentrations of BPs is shown in Figure 1. The shorter length HBPs (**2** and **3**) showed significantly higher binding affinities than alendronate ($p < 0.05$). Overall, all seven HBPs showed high binding affinities to HA, which makes them suitable for drug targeting.

Apart from its targeting ability, the ideal drug-carrier should not induce unnecessary toxic effects, especially against bone-forming cells (osteoblasts). HBPs could also have toxic affects toward other cells and tissues or affect cell differentiation, which could cause substantial morbidity.[54] The primary purpose of this study was to demonstrate the potential of HBPs for targeted delivery of the attached drugs at bone-resorption sites through *in vitro* experiments. Therefore, HBPs at various concentrations (10^{-6}–10^{-4} M) were evaluated for their possible cytotoxicity and apoptotic effect against preosteoblasts. The intracellular protein measured after 24, 48, and 72 h treatment of HBPs showed no abnormal changes in cell proliferation (Figure 2). The amount of protein in the HBP-treated cells was similar to the control over a period of 72 h. Cell viability studies were performed and metabolic activity was quantified using the commercially available WST-1 kit. MC3T3-E1 cells exposed to HBPs for 72 h showed activity similar to that of control (Figure 3). Although the metabolic activity of cells exposed to 10^{-4} M HBPs for 72 h showed 10% decrease in cell viability, the difference was not statistically significant.

Because caspases are required for cell apoptosis, the possibility of HBP-induced cell apoptosis was evaluated by measuring caspase-3 activity. Caspase-3 is a cysteine-aspartic acid protease and cleaves Ac-DEVD-AFC releasing the fluorogenic AFC, which can be quantified by fluorescence spectroscopy.[55] Apoptosis of MC3T3-E1 preosteoblasts was confirmed by treatment with 10^{-6}, 10^{-5}, or 10^{-4} M etoposide for 72 h, which resulted in 2–3-fold increase in caspase-3 activity (results not shown). As shown in Figure 4, however, HBPs did not induce apoptosis in MC3T3-E1 preosteoblasts after 72 h of exposure; all treatments resulted in statistically similar levels of caspase activity. Because HBPs showed no apoptotic and cytotoxic effects on preosteoblasts, HBPs could be utilized as a vehicle for drug delivery applications.

HBP **2** was used to demonstrate the targeted delivery of therapeutic agents to bone. In particular, in vitro drug targeting to HA and drug release from the HA surface was demonstrated using 4-NBA as a model drug. 4-NBA was conjugated with HBP **2** in DMSO/water, and then the conjugate was immobilized on HA by adding excess of HA particles to the reaction mixture at RT. HA with the attached conjugate was separated by centrifugation and washed thoroughly with water to remove unconjugated 4-NBA (Scheme 3). The triggered

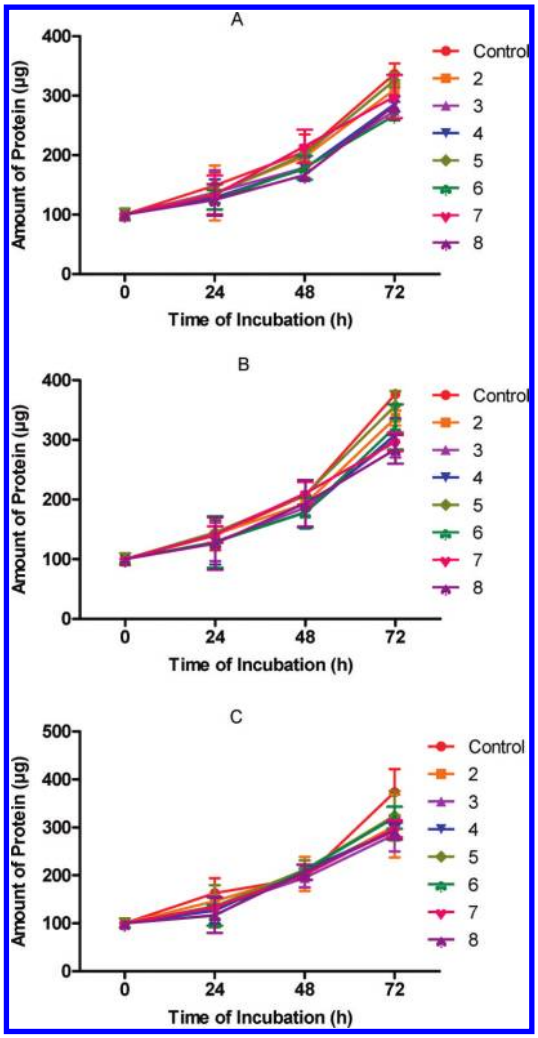

Figure 2. Intracellular protein contents showing MC3T3-E1 cell growth for 72 h after HBP treatment. Plots A, B, and C show results for exposure to HBPs at 1×10^{-6}, 1×10^{-5}, and 1×10^{-4} M, respectively. Error bars denote standard deviation.

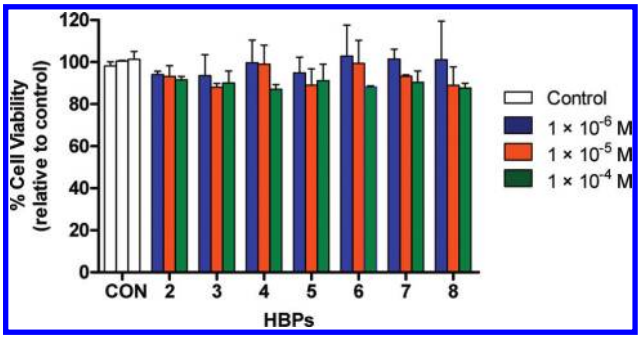

Figure 3. MC3T3-E1 cell viability measured after 72 h of incubation with no HBP (CON) and HBPs **2**–**8** at different concentrations (1×10^{-6}, 1×10^{-5}, and 1×10^{-4} M). The data are expressed as percentage of the control. The white, blue, orange, and green bars represent treatment of no HBP (control), 1×10^{-6}, 1×10^{-5}, and 1×10^{-4} M HBPs, respectively. Error bars denote standard deviations.

release of 4-NBA from the immobilized 4-NBA-HBP conjugate on HA was demonstrated at various pH as shown in Figure 5. HA with the attached conjugate was resuspended in 0.1 M sodium acetate (pH 5.0, 6.0, or 7.4) and incubated at 37 °C. The suspensions were centrifuged at particular time points, and

dx.doi.org/10.1021/bc2003132 | *Bioconjugate Chem.* 2011, 22, 2496–2506

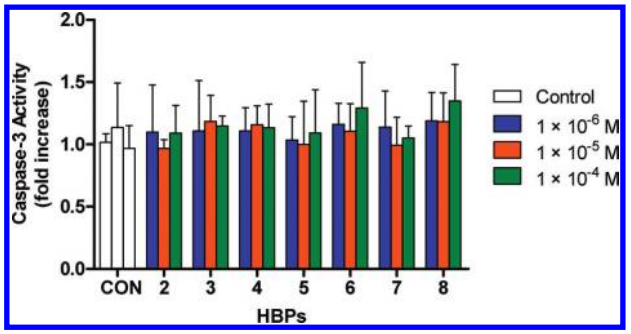

Figure 4. Apoptosis of MC3T3-E1 cells measured 72 h following addition of no HBP (CON) and HBPs **2**–**8** at three different concentrations (1×10^{-6}, 1×10^{-5}, and 1×10^{-4} M). The data are expressed as percentage of the control. The white, blue, orange, and green bars represent treatment of no HBP (control), 1×10^{-6}, 1×10^{-5}, and 1×10^{-4} M HBPs, respectively. Error bars denote standard deviations.

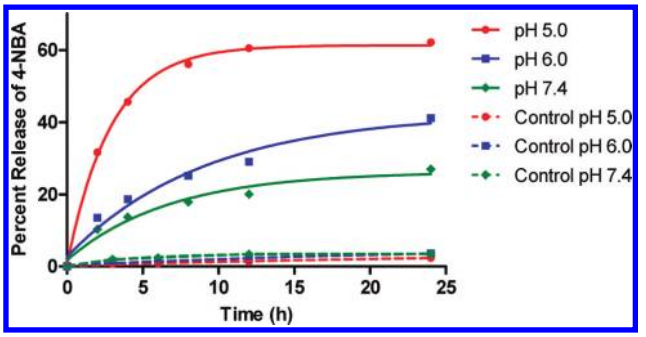

Figure 5. Percent release of 4-NBA (percentage of cleaved hydrazone bonds) from the immobilized conjugate on HA surface at 37 °C. Solid line and dotted line represent 4-NBA release from **17** and **21**, respectively.

the absorbance of the supernatants was measured at 265 nm using a UV–vis spectrophotometer to calculate the amount of released 4-NBA. It was observed that, in the first 12 h of incubation, there was approximately 60%, 30%, and 20% of 4-NBA released from the immobilized conjugate at pH 5.0, 6.0, and 7.4, respectively. Since HBPs have higher affinity for bone than does alendronate, they are expected to carry and deliver the attached drug at bone resorption sites as well as calcified bone tumors. Similar to this study, drug release at resorption sites was previously reported using a polymeric system with a spacer composed of a cathepsin K sensitive tetrapeptide (Gly-Gly-Pro-Nle).[56] Cathepsin K, which is expressed at higher level in osteoclasts, could cleave the polymer at the cathepsin K sensitive tetrapeptide and initiate drug release. However, cleavage of the polypeptide by cathepsin K could be affected by steric hindrance, which could change the rate of drug release. On the other hand, HBPs are not crowded molecules, and therefore, the rate of hydrolysis of the hydrazone and consequent drug release is expected to be affected less by steric effects.

To confirm that release of 4-NBA occurs via hydrazone cleavage rather than through desorption of the conjugate from the HA surface, 4-NBA was conjugated to alendronate (**1**) through formation of an amide bond. The conjugate was immobilized on HA surface by adding excess of HA particles, and then the particles were washed thoroughly with water to

Scheme 3. Synthesis, Immobilization of Model Drug–BP Conjugate, and Incubation at 37 °C in Acetate Solutions of Various pH[a]

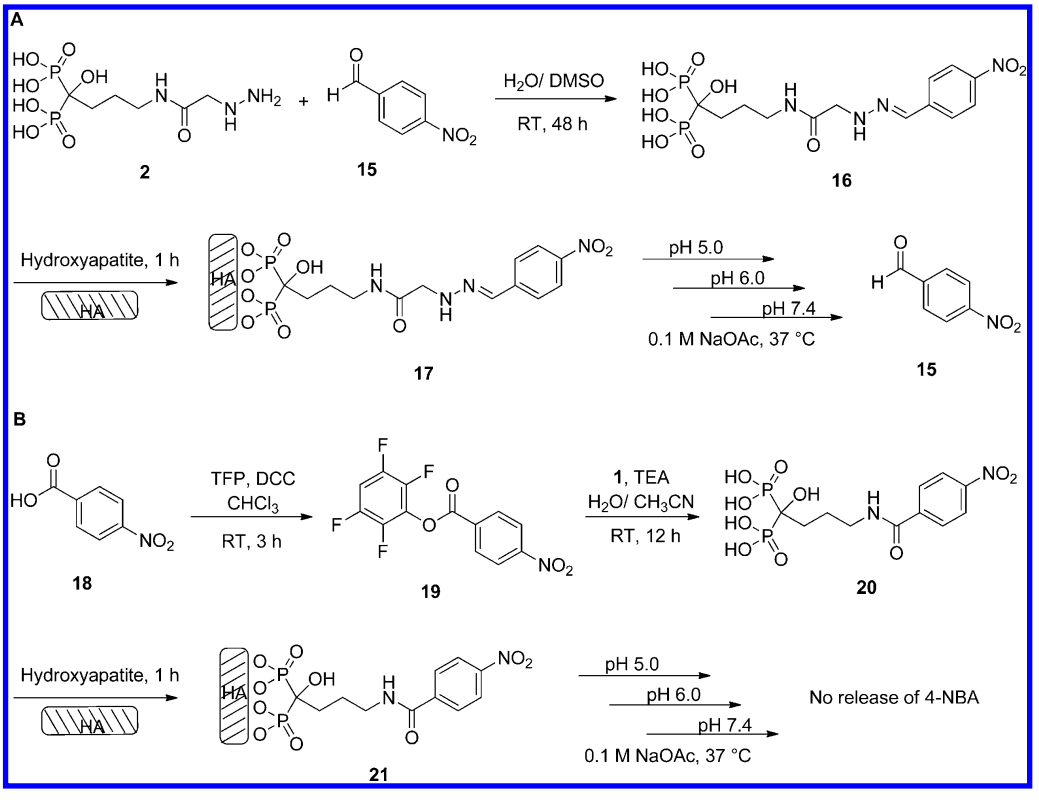

[a]Hatched area represents HA particles.

dx.doi.org/10.1021/bc2003132 | Bioconjugate Chem. 2011, 22, 2496–2506

remove unconjugated 4-NBA and nonspecifically adsorbed conjugate molecules. HA with the attached conjugate was treated similarly as described above, and the amount of released 4-NBA was measured by UV−vis spectroscopy (Scheme 3). From the control experiments, it was observed that there was no significant release of 4-NBA through desorption from the immobilized conjugate **21** (Figure 5).

CONCLUSION

In conclusion, we have reported the synthesis of novel, bifunctional HBPs (**2**−**8**), which show high binding affinities to HA. Through *in vitro* experiments, HBPs demonstrated no apoptotic and cytotoxic effects on MC3T3-E1, a preosteoblast cell. 4-NBA, a model drug, was bound to HA through a HBP, and its *in vitro* release at various pH was recorded. It was observed that hydrolysis of hydrazone bonds in the conjugate and subsequent release of 4-NBA was slow at physiological pH but much faster at pH lower than physiological, such as the pH in bone resorption sites and sites of wound healing.[49,50] Consequently, HBP−drug conjugates could be useful in local delivery of attached drugs to the resorptive microenvironment of bone tissue. Overall, this approach should improve the therapeutic index by boosting pharmacological efficacy and diminishing undesirable side effects.

AUTHOR INFORMATION

Corresponding Author

*Tel: 305-284-4021. Fax: 305-284-5637. E-mail: bachas@miami.edu.

ACKNOWLEDGMENTS

This research was supported by the US Army Medical Research and Materiel Command (W81XWH-09-1-0461) and the National Institutes of Health (AR048700). J.Y. thanks the University of Kentucky for a Research Challenge Trust Fund fellowship supporting this research. We thank Drs. M. Watson, A. Cammers, Y. Wei, E. Dikici, and E. Zahran for useful discussions.

REFERENCES

(1) Langer, R. (2001) Drug delivery: Drugs on target. *Science 293*, 58−59.
(2) Harada, S., and Rodan, G. A. (2003) Control of osteoblast function and regulation of bone mass. *Nature 423*, 349−355.
(3) Goltzman, D. (2002) Discoveries, drugs and skeletal disorders. *Nat. Rev. Drug Discovery 1*, 784−796.
(4) Salo, J., Lehenkari, P., Mulari, M., Metsikkö, K., and Väänänen, H. K. (1997) Removal of osteoclast bone resorption products by transcytosis. *Science 276*, 270−273.
(5) Deal, C. (2009) Future therapeutic targets in osteoporosis. *Curr. Opin. Rheumatol. 21*, 380−385.
(6) Vondracek, S. F., and Linnebur, S. A. (2009) Diagnosis and management of osteoporosis in the older senior. *Clin. Interventions Aging 4*, 121−136.
(7) Rodan, G. A., and Martin, T. J. (2000) Therapeutic approaches to bone diseases. *Science 289*, 1508−1514.
(8) Polascik, T. J. (2009) Bisphosphonates in oncology: Evidence for the prevention of skeletal events in patients with bone metastases. *Drug Des., Dev. Ther. 3*, 27−40.
(9) Lumachi, F., Brunello, A., Roma, A., and Basso, U. (2008) Medical treatment of malignancy-associated hypercalcemia. *Curr. Med. Chem. 15*, 415−421.
(10) Zhang, S., Gangal, G., and Uludağ, H. (2007) 'Magic bullets' for bone diseases: Progress in rational design of bone-seeking medicinal agents. *Chem. Soc. Rev. 36*, 507−531.
(11) van Beek, E. R., Lowik, C., Que, I., and Papapoulos, S. (1996) Dissociation of binding and antiresorptive properties of hydroxy bisphosphonates by substitition of the hydroxyl with an amino group. *J. Bone Miner. Res. 11*, 1492−1497.
(12) Sunberg, R. J., Ebetino, F. H., Mosher, C. T., and Roof, C. F. (1991) Designing drugs for stronger bones. *CHEMTECH 21*, 305−309.
(13) Chapurlat, R. D., and Delmas, P. D. (2006) Drug insight: Bisphosphonates for postmenopausal osteoporosis. *Nat. Clin. Pract. Endocrinol. Metab. 2*, 211−219.
(14) Peppas, N. A. (2004) Intelligent therapeutics: Biomimetic systems and nanotechnology in drug delivery. *Adv. Drug Delivery Rev. 56*, 1529−1531.
(15) Peppas, N. A. (2006) Vecteurs de médicaments innovants et ≪ intelligents ≫: leurs applications pharmaceutiques. *Ann. Pharm. Fr. 64*, 260−275.
(16) Langer, R., and Peppas, N. A. (2003) Advances in biomaterials, drug delivery, and bionanotechnology. *AIChE J. 49*, 2990−3006.
(17) Oh, Y.-K., Senter, P. D., and Song, S.-C. (2009) Intelligent drug delivery systems. *Bioconjugate Chem. 20*, 1813−1815.
(18) MacEwan, S. R., and Chilkoti, A. (2010) Elastin-like polypeptides: Biomedical applications of tunable biopolymers. *Pept. Sci. 94*, 60−77.
(19) Betre, H., Liu, W., Zalutsky, M. R., Chilkoti, A., Kraus, V. B., and Setton, L. A. (2006) A thermally responsive biopolymer for intra-articular drug delivery. *J. Controlled Release 115*, 175−182.
(20) Wang, D., Miller, S. C., Shlyakhtenko, L. S., Portillo, A. M., Liu, X.-M., Papangkorn, K., Kopečková, P., Lyubchenko, Y., Higuchi, W. I., and Kopeček, J. (2007) Osteotropic peptide that differentiates functional domains of the skeleton. *Bioconjugate Chem. 18*, 1375−1378.
(21) Wang, D., Sima, M., Mosley, R. L., Davda, J. P., Tietze, N., Miller, S. C., Gwilt, P. R., Kopečková, P., and Kopeček, J. (2006) Pharmacokinetic and biodistribution studies of a bone-targeting drug delivery system based on N-(2-Hydroxypropyl)methacrylamide copolymers. *Mol. Pharmaceutics 3*, 717−725.
(22) Thompson, W. J., Thompson, D. D., Anderson, P. S., Rodan, G. A. (1989) Polymalonic acids as boneaffinity agents, EP 0341961.
(23) Orme, M. W., and Labroo, V. M. (1994) Synthesis of [beta]-estradiol-3-benzoate-17-(succinyl-12A-tetracycline): A potential bone-seeking estrogen. *Bioorg. Med. Chem. Lett. 4*, 1375−1380.
(24) Zheng, H., Weng, L. (1997) Bone resorption inhibition/osteogenesis promotion pharmaceutical composition, U.S. Patent 5,698,542.
(25) Hirabayashi, H., Takahashi, T., Fujisaki, J., Masunaga, T., Sato, S., Hiroi, J., Tokunaga, Y., Kimura, S., and Hata, T. (2001) Bone-specific delivery and sustained release of diclofenac, a non-steroidal anti-inflammatory drug, via bisphosphonic prodrug based on the osteotropic drug delivery system (ODDS). *J. Controlled Release 70*, 183−191.
(26) Gil, L., Han, Y., Opas, E. E., Rodan, G. A., Ruel, R., Seedor, J. G., Tyler, P. C., and Young, R. N. (1999) Prostaglandin E2-bisphosphonate conjugates: Potential agents for treatment of osteoporosis. *Bioorg. Med. Chem. 7*, 901−919.
(27) Ora, M., Lönnberg, T., Florea-Wang, D., Zinnen, S., Karpeisky, A., and Lönnberg, H. (2008) Bisphosphonate derivatives of nucleoside antimetabolites: Hydrolytic stability and hydroxyapatite adsorption of 5′-β,γ-methylene and 5′-β,γ-(1-hydroxyethylidene) triphosphates of 5-fluorouridine and ara-cytidine. *J. Org. Chem. 73*, 4123−4130.
(28) El-Mabhouh, A., Angelov, C., McEwan, A., Jia, G., and Mercer, J. (2004) Preclinical investigations of drug and radionuclide conjugates of bisphosphonates for the treatment of metastatic bone cancer. *Cancer Biother. Radiopharm. 19*, 627−640.
(29) Herczegh, P., Buxton, T. B., McPherson, J. C. I., Kovács-Kulyassa, Á., Brewer, P. D., Sztaricskai, F., Stroebel, G. G., Plowman, K. M., Farcasiu, D., and Hartmann, J. F. (2002) Osteoadsorptive bisphosphonate derivatives of fluoroquinolone antibacterials. *J. Med. Chem. 45*, 2338−2341.

(30) Wang, J. B., Yang, C. H., Yan, X. M., Wu, X. H., and Xie, Y. Y. (2005) Novel bone-targeted agents for treatment of osteoporosis. *Chin. Chem. Lett. 16*, 859−862.
(31) Blower, P. (2006) Towards molecular imaging and treatment of disease with radionuclides: The role of inorganic chemistry. *Dalton Trans.*, 1705−1711.
(32) Ogawa, K., Mukai, T., Inoue, Y., Ono, M., and Saji, H. (2006) Development of a novel ^{99m}Tc-chelate-conjugated bisphosphonate with high affinity for bone as a bone scintigraphic agent. *J. Nucl. Med. 47*, 2042−2047.
(33) Martin, Torres, de Rosales, R., Finucane, C., Foster, J., Mather, S. J., and Blower, P. J. (2010) ^{188}Re(CO)$_3$-dipicolylamine-alendronate: A new bisphosphonate conjugate for the radiotherapy of bone metastases. *Bioconjugate Chem. 21*, 811−815.
(34) Zaheer, A., Lenkinski, R. E., Mahmood, A., Jones, A. G., Cantley, L. C., and Frangioni, J. V. (2001) In vivo near-infrared fluorescence imaging of osteoblastic activity. *Nat. Biotechnol. 19*, 1148−1154.
(35) Årstad, E., Hoff, P., Skattebøl, L., Skretting, A., and Breistøl, K. (2003) Studies on the synthesis and biological properties of non-carrier-added [^{125}I and ^{131}I]-labeled arylalkylidenebisphosphonates: Potent bone-seekers for diagnosis and therapy of malignant osseous lesions. *J. Med. Chem. 46*, 3021−3032.
(36) Ehrick, R. S., Capaccio, M., Puleo, D. A., and Bachas, L. G. (2007) Ligand-modified aminobisphosphonate for linking proteins to hydroxyapatite and bone surface. *Bioconjugate Chem. 19*, 315−321.
(37) Uludağ, H. (2002) Bisphosphonates as a foundation of drug delivery to bone. *Curr. Pharm. Des. 8*, 1929−1944.
(38) Doschak, M. R., Kucharski, C. M., Wright, J. E. I., Zernicke, R. F., and Uludağ, H. (2009) Improved bone delivery of osteoprotegerin by bisphosphonate conjugation in a rat model of osteoarthritis. *Mol. Pharmaceutics 6*, 634−640.
(39) Kieczykowski, G. R., Jobson, R. B., Melillo, D. G., Reinhold, D. F., Grenda, V. J., and Shinkai, I. (1995) Preparation of (4-amino-1-hydroxybutylidene)bisphosphonic acid sodium salt, MK-217 (alendronate sodium). An improved procedure for the preparation of 1-hydroxy-1,1-bisphosphonic acids. *J. Org. Chem. 60*, 8310−8312.
(40) Chebbi, I., Migianu-Griffoni, E., Sainte-Catherine, O., Lecouvey, M., and Seksek, O. (2010) In vitro assessment of liposomal neridronate on MDA-MB-231 human breast cancer cells. *Int. J. Pharm. 383*, 116−122.
(41) Rodan, G. A., and Fleisch, H. A. (1996) Bisphosphonates: Mechanisms of action. *J. Clin. Invest. 97*, 2692−2696.
(42) Koutsoukos, P., Amjad, Z., Tomson, M. B., and Nancollas, G. H. (1980) Crystallization of calcium phosphates. A constant composition study. *J. Am. Chem. Soc. 102*, 1553−1557.
(43) Nancollas, G. H., Tang, R., Phipps, R. J., Henneman, Z., Gulde, S., Wu, W., Mangood, A., Russell, R. G. G., and Ebetino, F. H. (2006) Novel insights into actions of bisphosphonates on bone: Differences in interactions with hydroxyapatite. *Bone 38*, 617−627.
(44) Fleisch, H. (1998) Bisphosphonates: mechanisms of action. *Endocr. Rev. 19*, 80−100.
(45) Rodan, G. A. (1998) Mechanisms of action of bisphosphonates. *Annu. Rev. Pharmacol. Toxicol. 38*, 375−388.
(46) Roelofs, A. J., Thompson, K., Gordon, S., and Rogers, M. J. (2006) Molecular mechanisms of action of bisphosphonates: Current status. *Clin. Cancer Res. 12*, 6222s−6230s.
(47) Segal, E., Pan, H., Ofek, P., Udagawa, T., Kopečková, P., Kopeček, J., and Satchi-Fainaro, R. (2009) Targeting angiogenesis-dependent calcified neoplasms using combined polymer therapeutics. *PloS ONE 4*, e5233.
(48) Segal, E., Pan, H., Benayoun, L., Kopečková, P., Shaked, Y., Kopeček, J., and Satchi-Fainaro, R. (2011) Enhanced anti-tumor activity and safety profile of targeted nano-scaled HPMA copolymer-alendronate-TNP-470 conjugate in the treatment of bone malignances. *Biomaterials 32*, 4450−4463.
(49) Schneider, L., Korber, A., Grabbe, S., and Dissemond, J. (2007) Influence of pH on wound-healing: A new perspective for wound-therapy? *Arch. Dermatol. Res. 298*, 413−420.
(50) Teitelbaum, S. L. (2000) Bone resorption by osteoclasts. *Science 289*, 1504−1508.
(51) Xu, S., Krämer, M., and Haag, R. (2006) pH-Responsive dendritic core-shell architectures as amphiphilic nanocarriers for polar drugs. *J. Drug Targeting 14*, 367−374.
(52) Kale, A. A., and Torchilin, V. P. (2007) Design, synthesis, and characterization of pH-sensitive PEG−PE conjugates for stimuli-sensitive pharmaceutical nanocarriers: The effect of substitutes at the hydrazone linkage on the pH stability of PEG−PE conjugates. *Bioconjugate Chem. 18*, 363−370.
(53) Sawant, R. M., Hurley, J. P., Salmaso, S., Kale, A., Tolcheva, E., Levchenko, T. S., and Torchilin, V. P. (2006) SMART" drug delivery systems: Double-targeted pH-responsive pharmaceutical nanocarriers. *Bioconjugate Chem. 17*, 943−949.
(54) Prommer, E. E. (2009) Toxicity of bisphosphonates. *J. Palliat. Med. 12*, 1661−1665.
(55) Lazebnik, Y. A., Kaufmann, S. H., Desnoyers, S., Poirier, G. G., and Earnshaw, W. C. (1994) Cleavage of poly(ADP-ribose) polymerase by a proteinase with properties like ICE. *Nature 371*, 346−347.
(56) Pan, H., Kopečková, P., Wang, D., Yang, J., Miller, S., and Kopeček, J. (2006) Water-soluble HPMA copolymer—prostaglandin E1 conjugates containing a cathepsin K sensitive spacer. *J. Drug Targeting 14*, 425−435.

Article

pubs.acs.org/Biomac

Oriented Immobilization of Proteins on Hydroxyapatite Surface Using Bifunctional Bisphosphonates as Linkers

Jivan N. Yewle,[†] Yinan Wei,[†] David A. Puleo,[‡] Sylvia Daunert,[‡] and Leonidas G. Bachas*[,§]

[†]Department of Chemistry and [‡]Center for Biomedical Engineering, University of Kentucky, Lexington, Kentucky 40506-0055, United States

[‡]Department of Biochemistry and Molecular Biology, Miller School of Medicine, University of Miami, Florida 33146-0431, United States

[§]Department of Chemistry, University of Miami, 1301 Memorial Drive, Coral Gables, Florida 33146-0431, United States

ABSTRACT: Oriented immobilization of proteins is an important step in creating protein-based functional materials. In this study, a method was developed to orient proteins on hydroxyapatite (HA) surfaces, a widely used bone implant material, to improve protein bioactivity by employing enhanced green fluorescent protein (EGFP) and β-lactamase as model proteins. These proteins have a serine or threonine at their N-terminus that was oxidized with periodate to obtain a single aldehyde group at the same location, which can be used for the site-specific immobilization of the protein. The HA surface was modified with bifunctional hydrazine bisphosphonates (HBPs) of various length and lipophilicity. The number of functional groups on the HBP-modified HA surface, determined by a 2,4,6-trinitrobenzenesulfonic acid (TNBS) assay, was found to be 2.8×10^{-5} mol/mg of HA and unaffected by the length of HBPs. The oxidized proteins were immobilized on the HBP-modified HA surface in an oriented manner through formation of a hydrazone bond. The relative protein immobilization amounts through various HBPs were determined by fluorescence and bicinchoninic acid (BCA) assay and showed no significant effect by length and lipophilicity of HBPs. The relative amount of HBP-immobilized EGFP was found to be 10−15 fold that of adsorbed EGFP, whereas the relative amount of β-lactamase immobilized through HBPs (**2**, **3**, **4**, **6**, and **7**) was not significantly different than adsorbed β-lactamase. The enzymatic activity of HBP-immobilized β-lactamase was measured with cefazolin as substrate, and it was found that the catalytic efficiency of HBP-immobilized β-lactamase improved 2−5 fold over adsorbed β-lactamase. The results obtained demonstrate the feasibility of our oriented immobilization approach and showed an increased activity of the oriented proteins in comparison with adsorbed proteins on the same hydroxyapatite surface matrix.

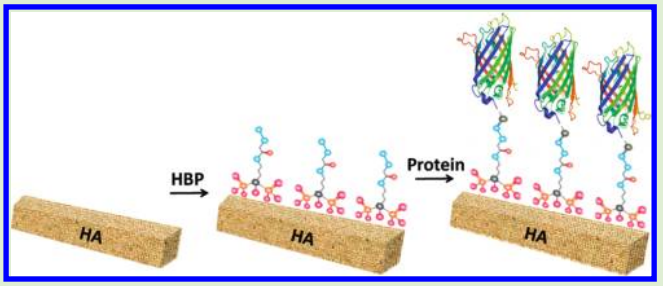

INTRODUCTION

Approaches to immobilize proteins are widely investigated because of their diverse applications in various fields such as protein microarrays, biosensors, biotechnology, chemical manufacturing, nanotechnology, single-molecule enzymology, and drug discovery.[1] Oriented immobilization methods that maintain the native structure and proper orientation of the target protein are desirable because through oriented immobilization the proteins can be predisposed in a manner that is optimal for binding to their respective ligands. Proteins have been immobilized on surfaces via three different approaches: physical adsorption, bioaffinity binding, and covalent bonding. Physical adsorption is the most straightforward type of immobilization in which proteins are adsorbed on the surface with weak noncovalent interactions. Conversely, because of the random and weak nature of the attachment, proteins may lose their activity as a result of blocking of the active site or leaching from the surface after immobilization.[2] Bioaffinity immobilization of proteins is mainly based on the specific interaction between two biomolecules, such as enzymes binding to surfaces modified with their corresponding substrates, cofactors, or inhibitors. The use of bioaffinity for immobilization may result in blockage of the active site of the protein and reduction of its activity. In addition, bioaffinity is usually a reversible interaction under specific conditions; therefore, it may lead to reversible immobilization.[3,4] Covalent immobilization yields proteins bound to a solid surface through a strong covalent linkage. Functional groups, such as amines, carboxylates, thiols, or hydroxyls, in the side chain of exposed amino acids in the protein have been used in the formation of irreversible linkages with surfaces.[2] Because multiple copies of the same functional group usually exist on the protein's surface, covalent immobilization is usually not selective. Oriented immobilization is achieved only when the protein contains just one copy of the reactive functional group, which is usually realized through selective chemical reactions or by protein engineering.[5] Several methods, such as Staudinger ligation, thiol−ene reaction, thiazolidine ring formation, cycloaddition,

Received: December 29, 2011
Revised: April 26, 2012
Published: May 4, 2012

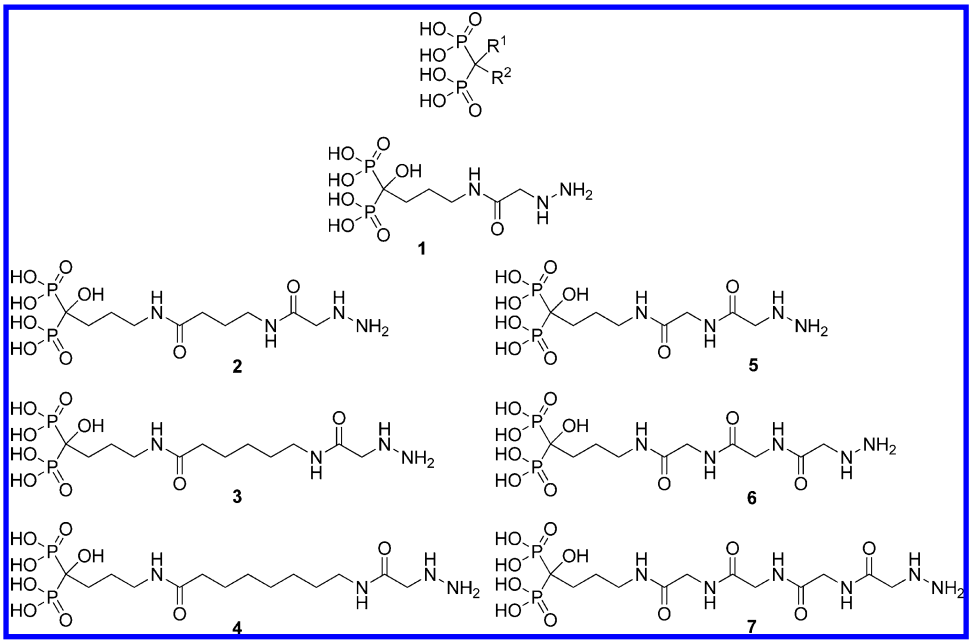

Figure 1. General structure of BP and structures of previously synthesized HBPs, which were used as bifunctional linkers for coupling EGFP and β-lactamase to HA. The HBPs shown are bifunctional molecules having phosphonates and hydrazine as terminal functionalities connected with spacers of various length and lipophilicity. HBPs-**2**, -**3**, and -**4** are relatively more lipophilic than HBP-**5**, -**6**, and -**7**, respectively.

and Diels–Alder product formation, have been explored for oriented immobilization of proteins and small molecules for various applications.[5−7] However, they have not been adequately explored for bone implant applications.

A host of materials, such as titanium, stainless steel, cobalt-based alloys, and HA, have been explored as bone implant materials.[8] Naturally occurring HA has similar composition to bone mineral; therefore, it has been widely used for orthopedic implants as well as an implant coating material. The interface between implants and the body plays a crucial role in determining success or failure of the prosthesis. Stability of the bone-to-implant interface can be improved chemically by incorporating organic material and physically by optimizing the surface topography of implants.[9−11] Covering the implant surface with biomolecule is one of the most effective ways of stimulating specific cell and tissue response at the bone–implant interface.[12−14] Moreover, oriented immobilization of therapeutic biomolecules on HA could provide additional benefits to implants, such as faster osseointegration, prevention of infection, and so on. Herein, a novel, versatile approach of oriented immobilization of proteins is described by employing rationally designed bifunctional bisphosphonates (BPs).

BPs are chemical analogues of endogenous pyrophosphate and have been investigated for protein immobilization applications on natural and artificial biomaterials, such as bone and HA.[15−18] BPs are bone-seeking molecules, having high affinity to bone and HA. They are organic molecules with, typically, two substituents (R^1 and R^2) in their structure, along with two phosphonate groups attached to their geminal carbon. Various BPs analogues and their conjugates have been utilized in treatment of skeletal diseases, such as osteoporosis, bone metastasis, and hypercalcemia.[19,20] Furthermore, BPs have been used to administer radiopharmaceuticals and imaging agents for diagnostic purposes.[21] Studies have also focused on determining the affinity to bone and HA of BPs conjugated with protein.[16−18] However, to date, BPs have not been conjugated site-selectively to proteins. In the aforementioned studies, BPs were attached nonspecifically to multiple sites of proteins, which led to random orientation of proteins on the surface.[15] In this study, our objective was to demonstrate that bifunctional BPs could facilitate the oriented immobilization of proteins on HA. Toward this goal, we used seven bifunctional HBPs, with various length and lipophilicity, as linkers between the protein and the HA surface. All seven HBPs were previously synthesized in our laboratory, and their high affinity toward HA surface was established.[22] EGFP with an N-terminal serine and β-lactamase with an N-terminal threonine were used as model proteins to demonstrate their site-specific immobilization on the HA surface. Specifically, both proteins were oxidized selectively to obtain an N-terminal aldehyde and immobilized on the HA surface through HBPs. The overall purpose of the present studies was to investigate the feasibility of oriented immobilization of protein on HA through HBPs and to evaluate the bioactivity of HBP-immobilized protein. Such biomaterial should find application in bone regeneration and targeted protein delivery therapies.

EXPERIMENTAL SECTION

Materials. Reagent grade HA powder, 4-(2-hydroxyethyl)-piperazine-1-ethanesulfonic acid sodium salt (HEPES), tris-(hydroxymethyl)aminoethane hydrochloride (Tris-HCl), ampicillin, isopropyl-1-β-D-thiol-1-galactopyranoside (IPTG), ethylenediaminetetraacetic acid (EDTA), 2,4,6-trinitrobenzenesulfonic acid (TNBS), sodium borate decahydrate, potassium hydroxide, sodium acetate, sodium chloride, sodium hydroxide, sodium periodate, ethylene glycol, agarose, β-lactamase from *Enterobacter cloacae*, and Luria–Bertani (LB) broth were purchased from Sigma-Aldrich (St. Louis, MO). Calcium chloride, hydrochloric acid, potassium dihydrogen phosphate, and sodium phosphate were obtained from EMD Chemicals (Gibbstown, NJ). The pEGFP vector was obtained from Clontech Laboratories (Mountain View, CA). The pTWIN1 vector and all restriction endonucleases were obtained from New England BioLabs (Ipswich, MA). Oligonucleotide primers used in PCR were custom-synthesized by Integrated DNA Technologies (Coralville, IA). The BCA assay kit was purchased from Pierce Chemical (Rockford, IL). All solutions and buffers were prepared using deionized water, which was

dx.doi.org/10.1021/bm201865r | *Biomacromolecules* 2012, 13, 1742–1749

produced using a Milli-Q water purification system (Millipore, Bedford, MA). All chemicals were reagent grade or better.

Apparatus. All UV−vis spectroscopy experiments were performed with an Agilent 8453 UV−visible spectrophotometer (Agilent Technologies, Santa Clara, CA). All UV−vis spectroscopy readings are background-subtracted. Fluorescence measurements were performed on a Cary Eclipse fluorescence spectrophotometer (Varian, Walnut Creek, CA). Polymerase chain reactions (PCRs) were performed in a Perkin-Elmer GeneAmp PCR system 2400 (Norwalk, CT). Cell lysates were centrifuged using an Avanti J-25I centrifuge (Beckman Coulter, Brea, CA). HA samples were centrifuged using centrifuge-5417R (Eppendorf, Wesseling-Berzdorf, Germany).

Substrate and Linkers Used for Protein Immobilization. Reagent-grade HA powder was used as solid support for immobilization experiments. Slurries of HA in various buffers were used without any pretreatment for protein immobilization. Seven HBPs (**1**−**7**) of various length and lipophilicity, which were previously synthesized in our laboratory,[22] were used as linkers between the HA and the protein for immobilization of proteins (Figure 1).

Modification of Proteins. Two different proteins were used as model proteins, EGFP and β-lactamase. EGFP and β-lactamase were oxidized at their N-terminus, which was a serine and threonine, respectively.

The gene encoding EGFP was cloned by PCR using plasmid pEGFP as the template and the primers, GGT GGT TGC TCT TCC AAC TCG ACT CTA GAG GAT CCC CGG GTA CCG (forward) and GGT CTG CAG TTA CTT GTA CAG CTC GTC CAT GCC GAG (reverse). The restriction enzymes *Sap*I (forward primer) and *Pst*I (reverse primer) digestion sites are underlined. The PCR product was purified with agarose gel electrophoresis and then doubly digested with *Sap*I and *Pst*I. The pTWIN1 vector was similarly digested with the same pair of enzymes. After digestion, the PCR product and the vector were gel-purified and ligated to yield plasmid pTWIN1-EGFP. In this construct, a stretch of 12 residues "STLEDPRVPVAT" was added to the N-terminus of EGFP. This sequence serves two purposes. First, it introduced a serine at the N-terminus of the protein after internal self-splicing, which can be used after oxidation (vide infra) for immobilization. Second, it worked as a spacer between the surface and EGFP to reduce the risk of compromising fluorescence emission. The DNA sequence of the pTWIN1-EGFP was confirmed by DNA sequencing (Davis Sequencing, Davis, CA). Plasmid pTWIN1-EGFP was then transformed into *E. coli* cells for protein expression. Cells were grown in cultures of LB broth containing 100 μg/mL of ampicillin at 37 °C with shaking at 250 rpm. When the OD600 of the culture reached 0.6 to 0.7, expression was induced with the addition of 100 μg/mL of IPTG. Cultures were incubated for an additional 4 h under the same conditions. The cells were harvested by centrifugation at 6000 rpm for 20 min at 20 °C. The supernatant was discarded, and the pellet was resuspended in 5 mL of Tris-HCl buffer (20 mM Tris-HCl, 500 mM NaCl, 1 mM EDTA, pH 8.5). Resuspended bacteria were sonicated on ice for 5 min with 10 s on/off pulses to lyse the cells. The cellular debris was removed by centrifugation for 25 min at 10 000 rpm and 20 °C. The protein in the supernatant was purified using affinity chromatography according to the manufacturer's recommendations (Green Fluorescent Protein Purification Kit, BIO-RAD Laboratories, Hercules, CA). In brief, the supernatant containing the protein was added to the binding buffer (4 M $(NH_4)_2SO_4$, pH 7.0) to obtain a protein-buffer solution (2 M $(NH_4)_2SO_4$, pH 7.0). The disposable column was equilibrated with 2 M $(NH_4)_2SO_4$, pH 7.0, and then loaded with the protein-buffer solution. The column was washed for a total of three times with a wash buffer (1.3 M $(NH_4)_2SO_4$, pH 7.0). The bound EGFP protein was eluted with a low salt elution buffer (10 mM Tris-HCl, 1 mM EDTA, pH 7.0). The purity of the eluting fractions was evaluated by SDS-PAGE using 12.5% polyacrylamide PhastGels (GE Healthcare, Piscataway, NJ), followed by gel development using silver staining. The protein concentration was measured using the BCA protein assay with bovine serum albumin (BSA) as the standard.

EGFP was oxidized using a sodium periodate treatment, which converts the N-terminal serine to an N-terminal aldehyde moiety.[23] Purified EGFP at a concentration of 1.0 mg/mL in phosphate buffer (10 mM sodium phosphate, 200 mM NaCl, pH 7.0) was used for the reaction. Sodium periodate was prepared freshly in water and added to the EGFP solution at five-fold molar excess. The mixture was incubated for 20 min at room temperature (RT). The reaction was quenched by the addition of seven-fold molar excess of ethylene glycol over sodium periodate (Scheme 1). The reaction mixture was then dialyzed against the same buffer (10 mM sodium phosphate, 200 mM NaCl, pH 7.0) overnight at 4 °C.

Scheme 1. Oriented Immobilization of β-Lactamase and EGFP on HA through HBPs

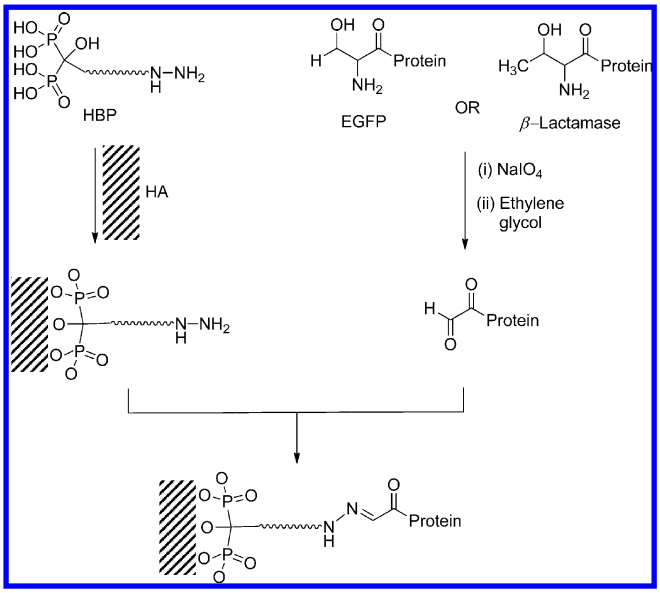

β-Lactamase was treated with sodium periodate to convert the N-terminal threonine to a N-terminal aldehyde (Scheme 1). The reaction mixture was dialyzed against HEPES buffer (50 mM HEPES, pH 7.4) overnight at 4 °C. The concentration of the proteins was determined using the BCA protein assay with BSA as the standard.

Measurement of Fluorescence and Enzyme Activity of Modified Proteins. Equal amounts of EGFP and oxidized EGFP in phosphate buffer (10 mM sodium phosphate, 200 mM NaCl, pH 7.0) were used for fluorescence measurement to determine the change in fluorescence after oxidation. The fluorescence of EGFP and oxidized EGFP were measured at excitation and emission wavelengths of 485 and 520 nm, respectively, under the same conditions.

Enzymatic activities of β-lactamase and oxidized β-lactamase were measured to determine the effect of oxidation on protein activity. Equal amount of β-lactamase and oxidized β-lactamase were used for kinetic experiments. The enzymatic activity of β-lactamase and oxidized β-lactamase was measured using the substrate cefazolin. β-Lactamase catalyzes the hydrolysis of the β-lactam ring of cefazolin, leading to a decrease in absorbance at 263 nm. In particular, β-lactamase and oxidized β-lactamase in HEPES buffer (50 mM HEPES, pH 7.4) were incubated with a 100 μM cefazolin solution freshly prepared in the same buffer for 20, 40, 60, 80, and 100 s at RT. The absorbance at 263 nm was measured for each sample, and the absorbance versus time was plotted.

Surface Modification with HBPs. HBPs were immobilized on HA particles and quantified by reaction with TNBS, which reacts with hydrazine groups to form trinitrophenyl derivatives.[24−26] HA particles (1.0 mg) were treated with 1×10^{-4} M HBPs in HEPES buffer (50 mM HEPES, pH 7.4) for 1 h at RT. The samples were washed thoroughly with the same buffer, followed by deionized water (Scheme 1). HA particles without treatment with HBP were used as control. HBP-treated samples along with the control were incubated with 0.1% (w/v) TNBS in 3% (w/v) sodium borate at 70 °C for 5 min. The samples were washed with deionized water and then hydrolyzed with 1

dx.doi.org/10.1021/bm201865r | *Biomacromolecules* 2012, 13, 1742−1749

M NaOH at 70 °C for 10 min. The released yellow product was proportional to the number of hydrazine groups. The amount of immobilized HBPs was measured indirectly by measuring the absorbance of the hydrolyzed reaction products at 410 nm. Standard curves were prepared by direct hydrolysis of TNBS in 1 M NaOH.

Immobilization and Quantification of Protein. EGFP was immobilized on HA particles using seven HBPs (**1**−**7**). HBP-modified HA particles (1.0 mg) were treated with 0.1 mg of oxidized EGFP in phosphate buffer (10 mM sodium phosphate, 200 mM NaCl, pH 7.0) for 1 h at 4 °C (Scheme 1). For the control studies, oxidized EGFP was simply adsorbed on HA particles under the same conditions. The samples were centrifuged for 5 min at 3000 rpm, and the amount of immobilized EGFP was determined by measuring the fluorescence of the supernatant at excitation and emission wavelengths of 485 and 520 nm, respectively.

β-Lactamase was immobilized on HA particles using seven HBPs (**1**−**7**). For immobilization on the HA particles, 1.0 mg of HBP-modified HA particles was treated with 0.3 mg of oxidized β-lactamase in HEPES buffer (50 mM HEPES, pH 6.5) for 1 h at RT (Scheme 1). For the control studies, β-lactamase was simply adsorbed on HA particles under the same conditions. The samples were thoroughly washed with HEPES buffer (50 mM HEPES, pH 7.0) and deionized water. The amount of β-lactamase immobilized on HA was measured using the BCA protein assay with BSA as the standard by a slight modification in the manufacturer's protocol. β-Lactamase-immobilized HA samples were incubated directly in the working reagent of BCA assay for 1 h at 37 °C. The samples were centrifuged for 5 min at 3000 rpm, and the absorbance of the supernatants was measured at 570 nm.

To determine the extent of washing necessary for removal of physically adsorbed β-lactamase from the HBP-modified surface, we have optimized the number of washes to remove the physically adsorbed β-lactamase. The enzymatic activity of β-lactamase was measured after each wash, and it was observed that after the second wash the amount of the enzyme on the HBP-modified HA surface remains same. Therefore, to ensure the complete removal of physically adsorbed β-lactamase, we thoroughly washed the HA particles (after β-lactamase treatment) at least three times.

Enzymatic Activity of β-Lactamase and Determination of Kinetic Constants. The enzymatic activity of β-lactamase immobilized on HA particles, adsorbed β-lactamase, and free β-lactamase in solution was measured using the substrate cefazolin and monitoring the hydrolysis reaction at 263 nm. In brief, cefazolin solutions were prepared at different concentrations (0, 20, 40, 60, 80, 100, 120, 140, 160, 180, 200 μM) in HEPES buffer (50 mM HEPES, pH 7.4). A fixed volume of β-lactamase-immobilized HA particles was added to each cefazolin solution and treated for 15 s at RT. Similarly, HA particles with adsorbed β-lactamase and free β-lactamase in solution were exposed to various concentrations of cefazolin for 15 s at RT. Each reaction mixture was centrifuged immediately, and the absorbance of the supernatant was measured at 263 nm. The reaction rates were calculated from the change in absorbance. The substrate saturation curves of various β-lactamase samples with cefazolin were fitted into Michaelis−Menten kinetics using GraphPad, and the corresponding K_M, k_{cat}, and k_{cat}/K_M values were calculated.

Statistical Analysis. Data presented are mean ± standard deviation. A minimum of three replicates were used for each experiment. One-way analysis of variance (ANOVA) was conducted using GraphPad software (San Diego, CA). The results were considered significantly different when $p < 0.05$.

RESULTS AND DISCUSSION

Immobilization of biomolecules has been the subject of active investigation. To ensure activity, factors such as the interaction between the biomolecule and the immobilization surface and the orientation of the biomolecule on the surface need to be considered.[27] Various methods have been explored for immobilization of proteins on solid surfaces, including several bone implant interfaces.[28−31] However, the majority of the methods employed are based on linking the protein covalently to the implant surface via surface-exposed functional groups on the protein, including amino, carboxylate, and thiol groups. Such methods result in linkages that are mostly random, and multiple bonds may form between each protein molecule and the surface. Therefore, such immobilization approaches may compromise the activity of the protein. In addition, the active site of the immobilized protein may be blocked during random immobilization, which may lead to drastically decreased bioactivity. In addition, the structure of the protein may also be affected by protein−surface interactions, steric hindrance, or both. Oriented immobilization may minimize or overcome the drawbacks of random orientation. Successful oriented immobilization requires selective functionalization of biomolecules, tailoring of the surface, or both.[24] Various approaches have been explored for oriented immobilization of biomolecules. Most of these approaches rely on the formation of a specific covalent linkage between the protein and the target surface or a specific interaction between two biomolecules.[6] However, oriented immobilization has been rarely reported for immobilization of biomolecules on biomaterials.

In this study, EGFP and β-lactamase were used as model proteins to develop an oriented immobilization method of proteins on mineralized biomaterials, such as HA. EGFP is a green fluorescent protein, which was modified genetically to contain an N-terminal serine. β-lactamase is an enzyme produced by a broad spectrum of bacteria that hydrolyzes β-lactam antibiotics to produce a change in the absorption spectrum, which can be used to monitor enzymatic activity. It is a very efficient catalyst and instills resistance to β-lactam antimicrobial agents, such as penicillins, cephalosporins, and cefamycins by breaking their four-member ring structure. β-Lactamase from *Enterobacter cloacae* has a threonine at its N-terminus. Serine and threonine are the only amino acids that have a vicinal amino alcohol. Vicinal diols and amino alcohols can be oxidized with periodate to obtain an aldehyde functional group that can be used for attachment. In our work, the N-terminal serine and threonine in EGFP and β-lactamase, respectively, were oxidized with periodate to obtain a single aldehyde, which was used to attach the proteins to the HA surface. The rate of oxidation of vicinal diol is 100−1000 fold slower than vicinal amino alcohol.[32] Therefore, this method of generating N-terminal aldehydes could also be applied to glycoproteins without degrading the carbohydrate region.

The fluorescence emission at 520 nm of EGFP and oxidized EGFP were measured and compared (data not shown). No significant change in fluorescence was observed after oxidation of EGFP. To evaluate the effect of oxidation of β-lactamase, we determined the enzymatic activities of the same amount of β-lactamase and oxidized β-lactamase using 100 μM cefazolin as the substrate. The enzymatic activity of β-lactamase was reduced by ∼30% upon periodate treatment, indicating that oxidation has some effect on the protein. Therefore, it can be stated that sodium periodate oxidation of the N-terminus serine or threonine of a protein might affect the activity of the protein, and this could vary from protein to protein. Other than vicinal amino alcohols and diols, amino acids that can be oxidized by periodate treatment are methionine, cysteine, tyrosine, tryptophan, and histidine. However, these amino acids are much less reactive toward periodate. Under the mild experimental conditions used for the oxidation of the N-terminal serine and threonine of EGFP and β-lactamase, respectively, damage to other periodate-reactive groups of the proteins is limited, which is manifested by no change in the

dx.doi.org/10.1021/bm201865r | *Biomacromolecules* 2012, 13, 1742−1749

fluorescence of EGFP and limited change in the activity of β-lactamase.

In this study, HA was used as a solid surface for protein immobilization. The unit cell of HA has a chemical formula of $Ca_{10}(PO_4)_6(OH)_2$, with two primary sites capable of binding, namely, Ca^{2+} for anions and PO_4^{3-} for cations.[33] HA has a similar composition as that of the mineral component of bone and is a bioactive prosthetic material, which can undergo in vivo bone bonding.[34,35] Because of these properties, HA has been widely used in bone implant applications. Moreover, as a result of the development of several effective coating techniques, such as direct current plasma spraying, radio-frequency plasma spraying, and suspension plasma spraying, HA has been broadly used as a coating material for various metal implants.[35,36] Given the extensive use of HA in bone implant applications, the focus in this study was the site-specific immobilization of proteins on the HA surface. Because BPs have a high affinity toward HA, bifunctional BPs were used as linkers between proteins and the HA surface.

BPs have been approved for the treatment of various skeletal diseases and therefore are biocompatible and could be used for implant modification. BPs have excellent antiresorptive properties and affinity to bone. The two phosphonates of BPs account for their bone-seeking ability via Ca^{2+} chelation. However, the R^1 and R^2 groups of BPs also contribute to their bone affinity. Because BPs with hydroxyl or amine at R^1 demonstrate tridentate binding and thus higher affinity to bone or HA,[33] for this study, we chose a series of hydrazine-BP (HBP) derivatives previously reported by our laboratory. The enhanced affinity of HBPs was measured using a crystal growth inhibition study.[22,37] HBPs have a hydrazine on their R^2 substituent that is linked with various length and lipophilicity spacer arms to the BP group. Hydrazine reacts with aldehyde at low pH (4.5 to 7.4),[38−41] where the lysine amine groups of the protein are protonated, rendering them unreactive. Moreover, hydrazines react faster than amines to aldehydes and ketones, and reaction of hydrazines with aldehydes results in the formation of a stable hydrazone bond. In that regard, HBPs are well-suited bifunctional linkers for the oriented immobilization of proteins containing an aldehyde and were used to target and immobilize proteins on the surface of HA particles.

It has been observed that several factors affect the bioactivity of immobilized proteins, including the surface density of functional groups as well as the length and lipophilicity of the spacer between the surface and the protein.[42−44] Higher density of functional groups on the surface could cause a higher number of immobilized biomolecules, which may result in steric hindrance as a result of crowding, thus blocking the active site of biomolecules. A lower density of functional groups should result in a lower number of the immobilized biomolecules, but this does not necessarily cause improvement in the accessibility and activity of the biomolecule;[45] the latter could occur if the site from which the biomolecule is immobilized misorients the protein in a way that its binding/active site is blocked by the immobilization surface. In other words, the activity of the biomolecule does not solely depend on the density of the functional groups on the surface or the number of biomolecules immobilized on the surface. The objective was to investigate the effect of the above-mentioned factors on the accessibility and activity of the immobilized protein. Therefore, HBPs of various length and lipophilicity were used for immobilization of proteins. The surface density of hydrazines on the HA surface following treatment with various HBPs was determined with a TNBS assay, as shown in Figure 2. The TNBS assay is generally used for the detection of

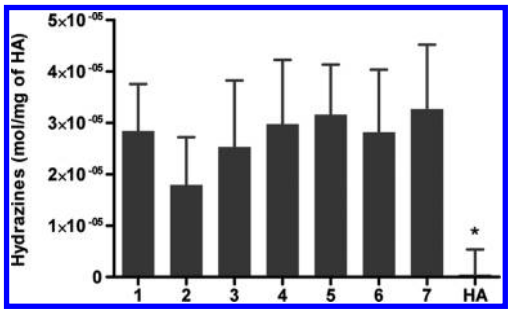

Figure 2. Surface density of hydrazine groups on HA surfaces modified with seven different HBPs (**1**−**7**) by TNBS assay. An amount of 1 mg HA particles was treated with 1×10^{-4} M of the corresponding HBP (**1**−**7**). HA refers to unmodified HA. Data are the average ± one standard deviation (n = 9). (* indicates the values are significantly different from others $p < 0.05$.)

amine groups; however, it has also been used for quantification of hydrazines.[25,26] The results of the TNBS assay show that neither the length nor the lipophilicity of the spacer affects significantly the surface density of the hydrazine on the surface of HA.

Oxidized EGFP was immobilized on the HBP-modified HA particles, and the amount of immobilized EGFP was measured using fluorescence. The extent of binding was determined by measuring the difference between the fluorescence of the supernatant before and after the immobilization of oxidized EGFP on HA (Figure 3). The change in length and lipophilicity

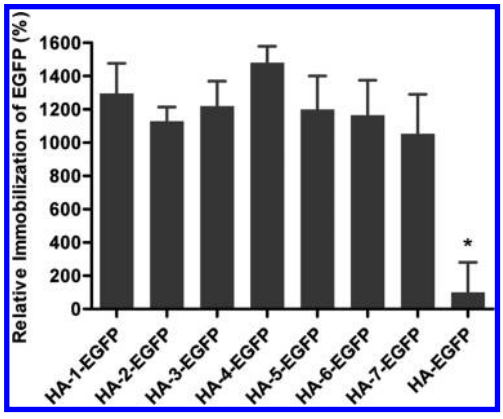

Figure 3. Immobilization of EGFP on HA surfaces determined by fluorescence. EGFP was immobilized on HA surfaces via seven different HBPs (**1**−**7**) and by simple adsorption. The corresponding EGFP is denoted as HA-1-EGFP through HA-7-EGFP. HA-EGFP refers to EGFP physically adsorbed on HA in the absence of HBP. The Y axis is normalized relative to the amount of EGFP immobilized by adsorption (HA-EGFP). Data are the average ± one standard deviation (n = 3). (* indicates the values are significantly different from others $p < 0.05$.)

of HBPs had no statistically significant effect on the amount of EGFP immobilized. However, it was observed that the use of HBPs as linkers for the immobilization of EGFP increased significantly the amount of EGFP immobilized over EGFP that was simply adsorbed on HA ($p < 0.05$). The lower amount of adsorbed EGFP can be explained by the tendency of HA to adsorb proteins with an overall positive charge while repelling

proteins that are overall negatively charged.[46,47] EGFP has a pI of 5.7 and possesses an overall negative charge at pH of 7.0, which is the pH at which the experiments were conducted. On the contrary, BPs have high affinity for HA. Consequently, modification with HBP results in higher amounts of immobilized EGFP.

Oxidized β-lactamase was also immobilized on the HBP-modified HA particles through a stable hydrazone linkage between the aldehyde at the N-terminus of oxidized β-lactamase and surface hydrazines. The amount of immobilized β-lactamase was measured using the BCA assay (Figure 4). The

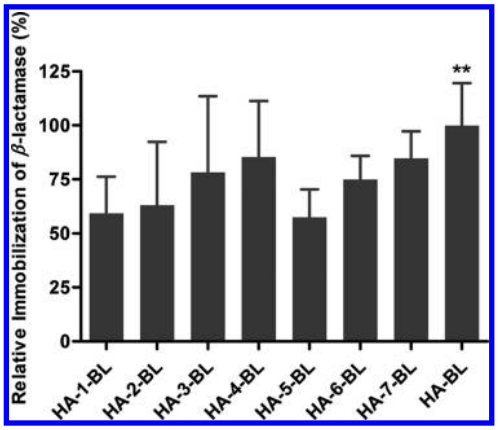

Figure 4. Immobilization of β-lactamase on HA surfaces determined by the BCA protein assay. β-Lactamase was immobilized on HA surfaces via seven different HBPs (**1**−**7**) (HA-1-BL through HA-7-BL) and by simple adsorption (HA-BL). The *Y* axis is normalized relative to the amount of β-lactamase immobilized by adsorption (HA-BL). Data are the average ± one standard deviation (n = 6). (** indicates the values are significantly different from HA-1-BL and HA-5-BL p < 0.05.)

lowest binding was observed when β-lactamase was attached to HA through the shorter chain HBP **1** and **5** (p < 0.05). β-Lactamase that was simply adsorbed on HA and immobilized through HBP **2**, **3**, **4**, **6**, and **7** gave statistically indistinguishable results in terms of the amount of immobilized enzyme (p < 0.05). In general, HA has an elevated affinity to proteins that possess a positive charge.[46,47] β-Lactamase from *Enterobacter cloacae* has a pI of 7.8;[48] therefore, the protein has an overall positive charge at pH 6.5, which is the pH at which the experiments were conducted. This explains why β-lactamase adsorbs readily on HA. From Figure 4, it can also be stated that the lipophilicity of the HBPs does not show any significant effect on the amount of immobilized β-lactamase.

The enzymatic activities of HBP-immobilized β-lactamase and adsorbed β-lactamase were determined through the hydrolysis of the substrate cefazolin. For comparison purposes, the activity of free β-lactamase in solution was also measured using the same substrate under similar reaction conditions. The hydrolysis of cefazolin was also determined in the presence of "bare" HA and HBP-modified HA as negative controls. The reaction data were fitted to a Michaelis−Menten kinetic model. The Michaelis constant (K_M) and the maximum velocity (V_{max}) were calculated using GraphPad. The turnover number of β-lactamase (k_{cat}), which represents the maximum number of the substrate molecules that undergoes hydrolysis per catalytic site of the active enzyme per unit time, was also calculated using the following equation.

$$k_{cat} = \frac{V_{max}}{[E]} \tag{S1}$$

where $[E]$ is the enzyme concentration. The catalytic efficiency, k_{cat}/K_M, of immobilized β-lactamase, adsorbed β-lactamase, and free β-lactamase in solution was calculated. In general, the catalytic efficiency of the enzyme indicates how fast the chemical reaction proceeds in the forward direction.

The kinetic parameters obtained with cefazolin and surface-immobilized β-lactamase, adsorbed β-lactamase, and free β-lactamase in solution are shown in Table 1. The K_M values of

Table 1. Kinetic Parameters Describing the Enzymatic Activity of Free β-Lactamase in Solution, Adsorbed β-Lactamase, and Immobilized β-Lactamase through HBPs[a]

β-Lactamase in various form	K_M (10^{-6} M)	k_{cat} (10^{-3} s^{-1})	k_{cat}/K_M (s^{-1} M^{-1})
free β-lactamase in solution	24.2 ± 3.8	7.43 ± 0.47	310 ± 34
adsorbed β-lactamase	124 ± 25	1.36 ± 0.26	11.1 ± 1.2
β-lactamase immobilized through HBP 1	70.7 ± 5.0	3.73 ± 0.03	52.9 ± 3.2
β-lactamase immobilized through HBP 2	81.2 ± 8.9	2.88 ± 0.10	35.6 ± 2.6
β-Lactamase immobilized through HBP 3	85.0 ± 5.0	1.90 ± 0.07	22.3 ± 0.7
β-Lactamase immobilized through HBP 4	82.3 ± 8.3	1.82 ± 0.07	22.3 ± 1.5
β-lactamase immobilized through HBP 5	77.3 ± 4.1	3.84 ± 0.14	49.8 ± 4.2
β-lactamase immobilized through HBP 6	80.9 ± 5.2	2.64 ± 0.04	32.7 ± 2.4
β-lactamase immobilized through HBP 7	89.7 ± 6.4	2.02 ± 0.00	22.8 ± 1.6

[a]Data are represented by mean values (n = 3) ± standard deviation.

the immobilized β-lactamase were all higher than free β-lactamase in solution. The k_{cat} and k_{cat}/K_M values of immobilized β-lactamase were all lower than free β-lactamase in solution. From these findings, it can be concluded that the enzymatic activity of immobilized β-lactamase is reduced compared with free β-lactamase in solution. This is consistent with prior literature that indicates higher K_M and lower k_{cat} values when enzymes are immobilized.[49,50] However, the K_M values for immobilized β-lactamase are significantly lower than that of adsorbed β-lactamase (p < 0.05). The k_{cat} values of immobilized β-lactamase, which indicate the number of cefazolin molecule hydrolyzed per β-lactamase molecule per second, were also significantly higher than that of adsorbed β-lactamase (p < 0.05). Therefore, β-lactamase immobilized through HBPs hydrolyzed the substrate more effectively than adsorbed β-lactamase. Specifically, the catalytic efficiencies of β-lactamase immobilized through HBP **1**, **2**, **5**, and **6** were significantly higher than those of adsorbed β-lactamase (p < 0.05). As stated above, statistically equivalent amounts of the enzyme were attached on HA when β-lactamase was simply adsorbed or immobilized through HBP **2**, **3**, **4**, **6**, and **7**. Despite having the same amount of immobilized enzyme, the lowest turnover number was observed with adsorbed β-lactamase. This is because direct adsorption of the protein leads to random orientation on the surface, which may result in loss of structural integrity and activity because of steric hindrance and interactions with the HA surface.[51,52] Overall, HBP-immobilized β-lactamase showed higher k_{cat} than adsorbed β-lactamase.

dx.doi.org/10.1021/bm201865r | *Biomacromolecules* 2012, 13, 1742−1749

Further work will be necessary to determine the actual orientation of the immobilized protein on the HA surface. Because this strategy of oriented immobilization of proteins was developed using HA, which is widely used as a bone implant material, the next logical step would be to orient bone-related proteins on the HA implant surface to improve cell/tissue interactions with the implant surface.

CONCLUSIONS

Oriented immobilization of proteins on solid surfaces anchors them at preferred locations, enhancing their usefulness for a target desired application. Immobilization of proteins in their bioactive as well as accessible state is critical for inducing their specific biological actions. The objective of the present work was to demonstrate the ability of bifunctional HBPs to immobilize a target protein in an oriented manner on HA surfaces, a type of biomaterial widely used in orthopedic implants. It was expected that such functionalization of the HA surface with a protein would result in improved bioactivity compared with simply adsorption. Our data demonstrate that the length or lipophilicity of HBPs has no significant effect on the amount of protein (EGFP and β-lactamase) immobilized on HA surface. Regarding the study of β-lactamase immobilized through various HBPs, we demonstrated that the immobilized enzyme had enhanced bioactivity compared with adsorbed β-lactamase. In summary, we showed that HBPs could be used for effective and bioactive immobilization on HA of any protein that has an intrinsic N-terminal serine or threonine or onto which either of these amino acids can be introduced at the N-terminus. It is envisioned that the proposed approach of oriented immobilization of bioactive proteins will broaden the possibility of immobilizing a wide variety of therapeutic proteins and peptide agents onto biomaterial surfaces, thus potentially improving the biocompatibility of orthopedic implants.

AUTHOR INFORMATION

Corresponding Author

*Address: Department of Chemistry, University of Miami, 1301 Memorial Drive, Coral Gables, Florida 33146-0431, United States. Tel: 305-284-4021. Fax: 305-284-5637. E-mail: bachas@miami.edu.

Notes

The authors declare no competing financial interest.

ACKNOWLEDGMENTS

This work was funded by the U.S. Army Medical Research and Materiel Command (W81XWH-09-1-0461). J.Y. acknowledges support from the University of Kentucky in the form of an RCTF fellowship. We thank Dr. Emre Dikici and Dr. Xin Liu (University of Kentucky, Lexington, KY) for useful discussions. S.D. is grateful for support from the Gill Eminent Professorship of the University of Kentucky and the Lucille P. Markey Chair in Biochemistry and Molecular Biology of the Miller School of Medicine of the University of Miami.

REFERENCES

(1) Wong, L. S.; Khan, F.; Micklefield, J. Selective covalent protein immobilization: strategies and applications. *Chem. Rev.* **2009**, *109*, 4025−4053.

(2) Rusmini, F.; Zhong, Z.; Feijen, J. Protein immobilization strategies for protein biochips. *Biomacromolecules* **2007**, *8*, 1775−1789.

(3) Tetala, K. K. R.; Beek, T. A. V. Bioaffinity chromatography on monolithic supports. *J. Sep. Sci.* **2010**, *33*, 422−438.

(4) Saleemuddin, M.: Bioaffinity based immobilization of enzymes. In *Thermal Biosensors, Bioactivity, Bioaffinitty*; Bhatia, P., Danielsson, B., Gemeiner, P., Grabley, S., Lammers, F., Mukhopadhyay, A., Ramanathan, K., Saleemuddin, M., Scheper, T., Stefuca, V., Thiericke, R., Xie, B., Eds.; Springer: Berlin/Heidelberg, 1999; Vol. *64*, pp 203−226.

(5) Lin, P.-C.; Weinrich, D.; Waldmann, H. Protein biochips: oriented surface immobilization of proteins. *Macromol. Chem. Phys.* **2010**, *211*, 136−144.

(6) Rao, S. V.; Anderson, K. W.; Bachas, L. G. Oriented immobilization of proteins. *Microchim. Acta* **1998**, *128*, 127−143.

(7) Köhn, M. Immobilization strategies for small molecule, peptide and protein microarrays. *J. Pept. Sci.* **2009**, *15*, 393−397.

(8) Hench, L. L. Prosthetic implant materials. *Annu. Rev. Mater. Sci.* **1975**, *5*, 279−300.

(9) Yuan, Y.; Chesnutt, B. M.; Wright, L.; Haggard, W. O.; Bumgardner, J. D. Mechanical property, degradation rate, and bone cell growth of chitosan coated titanium influenced by degree of deacetylation of chitosan. *J. Biomed. Mater. Res., Part B* **2008**, *86B*, 245−252.

(10) Dohan Ehrenfest, D. M.; Coelho, P. G.; Kang, B.-S.; Sul, Y.-T.; Albrektsson, T. Classification of osseointegrated implant surfaces: materials, chemistry and topography. *Trends Biotechnol.* **2010**, *28*, 198−206.

(11) Wazen, R. M.; Lefebvre, L.-P.; Baril, E.; Nanci, A. Initial evaluation of bone ingrowth into a novel porous titanium coating. *J. Biomed. Mater. Res., Part B* **2010**, *94B*, 64−71.

(12) Richert, L.; Variola, F.; Rosei, F.; Wuest, J. D.; Nanci, A. Adsorption of proteins on nanoporous Ti surfaces. *Surf. Sci.* **2010**, *604*, 1445−1451.

(13) Martin, H. J.; Schulz, K. H.; Bumgardner, J. D.; Walters, K. B. XPS study on the use of 3-aminopropyltriethoxysilane to bond chitosan to a titanium surface. *Langmuir* **2007**, *23*, 6645−6651.

(14) Variola, F.; Brunski, J. B.; Orsini, G.; Tambasco de Oliveira, P.; Wazen, R.; Nanci, A. Nanoscale surface modifications of medically relevant metals: state-of-the art and perspectives. *Nanoscale* **2011**, *3*, 335−353.

(15) Ehrick, R. S.; Capaccio, M.; Puleo, D. A.; Bachas, L. G. Ligand-modified aminobisphosphonate for linking proteins to hydroxyapatite and bone surface. *Bioconjugate Chem.* **2007**, *19*, 315−321.

(16) Uludağ, H.; Kousinioris, N.; Gao, T.; Kantoci, D. Bisphosphonate conjugation to proteins as a means to impart bone affinity. *Biotechnol. Prog.* **2000**, *16*, 258−267.

(17) Uludağ, H.; Yang, J. Targeting systemically administered proteins to bone by bisphosphonate conjugation. *Biotechnol. Prog.* **2002**, *18*, 604−611.

(18) Gittens, S. A.; Matyas, J. R.; Zernicke, R. F.; Uludağ, H. Imparting bone affinity to glycoproteins through the conjugation of bisphosphonates. *Pharm. Res.* **2003**, *20*, 978−987.

(19) Costa, L.; Major, P. P. Effect of bisphosphonates on pain and quality of life in patients with bone metastases. *Nat. Clin. Pract. Oncol.* **2009**, *6*, 163−174.

(20) Lumachi, F.; Brunello, A.; Roma, A.; Basso, U. Medical treatment of malignancy-associated hypercalcemia. *Curr. Med. Chem.* **2008**, *15*, 415−421.

(21) Blower, P. Towards molecular imaging and treatment of disease with radionuclides: the role of inorganic chemistry. *Dalton Trans.* **2006**, 1705−1711.

(22) Yewle, J. N.; Puleo, D. A.; Bachas, L. G. Enhanced affinity bifunctional bisphosphonates for targeted delivery of therapeutic agents to bone. *Bioconjugate Chem.* **2011**, *22*, 2496−2506.

(23) Mikolajczyk, S. D.; Meyer, D. L.; Starling, J. J.; Law, K. L.; Rose, K.; Dufour, B.; Offord, R. E. High yield, site-specific coupling of N-terminally modified β-lactamase to a proteolytically derived single-sulfhydryl murine Fab'. *Bioconjugate Chem.* **1994**, *5*, 636−646.

(24) Sharon, J. L.; Puleo, D. A. The use of N-terminal immobilization of PTH(1−34) on PLGA to enhance bioactivity. *Biomaterials* **2008**, *29*, 3137−3142.
(25) Puleo, D. A.; Kissling, R. A.; Sheu, M. S. A technique to immobilize bioactive proteins, including bone morphogenetic protein-4 (BMP-4), on titanium alloy. *Biomaterials* **2002**, *23*, 2079−2087.
(26) Puleo, D. A. Retention of enzymatic activity immobilized on silanized Co-Cr-Mo and Ti-6Al-4V. *J. Biomed. Mater. Res., Part A* **1997**, *37*, 222−228.
(27) Huang, W.; Wang, J.; Bhattacharyya, D.; Bachas, L. G. Improving the activity of immobilized subtilisin by site-specific attachment to surfaces. *Anal. Chem.* **1997**, *69*, 4601−4607.
(28) Ito, Y. Covalently immobilized biosignal molecule materials for tissue engineering. *Soft Matter* **2008**, *4*, 46−56.
(29) Morra, M. Biochemical modification of titanium surfaces: peptides and ECM proteins. *Eur. Cell. Mater.* **2006**, *12*, 1−15.
(30) Gittens, S. A.; Bansal, G.; Zernicke, R. F.; Uludağ, H. Designing proteins for bone targeting. *Adv. Drug Delivery Rev.* **2005**, *57*, 1011−1036.
(31) Pan, H.; Kopečková, P.; Wang, D.; Yang, J.; Miller, S.; Kopeček, J. Water-soluble HPMA copolymer—prostaglandin E1 conjugates containing a cathepsin K sensitive spacer. *J. Drug Targeting* **2006**, *14*, 425−435.
(32) Fields, R.; Dixon, H. B. F. A spectrophotometric method for the microdetermination of periodate. *Biochem. J.* **1968**, *108*, 883−887.
(33) Zhang, S.; Gangal, G.; Uludağ, H. 'Magic bullets' for bone diseases: progress in rational design of bone-seeking medicinal agents. *Chem. Soc. Rev.* **2007**, *36*, 507−531.
(34) Wolke, J.; de Blieck-Hogervorst, J.; Dhert, W.; Klein, C.; de Groot, K. Studies on the thermal spraying of apatite Bioceramics. *J. Therm. Spray Technol.* **1992**, *1*, 75−82.
(35) Bouyer, E.; Gitzhofer, F.; Boulos, M. The suspension plasma spraying of bioceramics by induction plasma. *JOM* **1997**, *49*, 58−62.
(36) Søballe, K. Hydroxyapatite ceramic coating for bone implant fixation. *Acta Orthop. Scand., Suppl.* **1993**, *255*, 1−58.
(37) Nancollas, G. H.; Tang, R.; Phipps, R. J.; Henneman, Z.; Gulde, S.; Wu, W.; Mangood, A.; Russell, R. G. G.; Ebetino, F. H. Novel insights into actions of bisphosphonates on bone: differences in interactions with hydroxyapatite. *Bone* **2006**, *38*, 617−627.
(38) Greenfield, R. S.; Kaneko, T.; Daues, A.; Edson, M. A.; Fitzgerald, K. A.; Olech, L. J.; Grattan, J. A.; Spitalny, G. L.; Braslawsky, G. R. Evaluation in vitro of adriamycin immunoconjugates synthesized using an acid-sensitive hydrazone linker. *Cancer Res.* **1990**, *50*, 6600−6607.
(39) Raddatz, S.; Mueller-Ibeler, J.; Kluge, J.; Wäß, L.; Burdinski, G.; Havens, J. R.; Onofrey, T. J.; Wang, D.; Schweitzer, M. Hydrazide oligonucleotides: new chemical modification for chip array attachment and conjugation. *Nucleic Acids Res.* **2002**, *30*, 4793−4802.
(40) Antsypovich, S. I.; Von Kiedrowski, G. A novel versatile phosphoramidite building block for the synthesis of 5′- and 3′-hydrazide modified oligonucleotides. *Nucleosides, Nucleotides Nucleic Acids* **2005**, *24*, 211−226.
(41) *Thermo Scientific Pierce Crosslinking Technical Handbook*; Thermo Fisher Scientific: Waltham, MA, 2009.
(42) Watanabe, J.; Ishihara, K. Multiple protein-immobilized phospholipid polymer nanoparticles: effect of spacer length on residual enzymatic activity and molecular diagnosis. *Nanobiotechnology* **2007**, *3*, 76−82.
(43) Cao, T.; Wang, A.; Liang, X.; Tang, H.; Auner, G. W.; Salley, S. O.; Ng, K. Y. S. Investigation of spacer length effect on immobilized *Escherichia coli* pili-antibody molecular recognition by AFM. *Biotechnol. Bioeng.* **2007**, *98*, 1109−1122.
(44) Nouaimi, M.; Möschel, K.; Bisswanger, H. Immobilization of trypsin on polyester fleece via different spacers. *Enzyme Microb. Technol.* **2001**, *29*, 567−574.
(45) Brogan, K. L.; Schoenfisch, M. H. Influence of antibody immobilization strategy on molecular recognition force microscopy measurements. *Langmuir* **2005**, *21*, 3054−3060.
(46) Lee, W.-H.; Loo, C.-Y.; Van, K. L.; Zavgorodniy, A. V.; Rohanizadeh, R. Modulating protein adsorption onto hydroxyapatite particles using different amino acid treatments. *J. R. Soc. Interface* **2012**, *9*, 918−927.
(47) Marina, J, G. The interaction of proteins with hydroxyapatite: II. Role of acidic and basic groups. *Anal. Biochem.* **1984**, *136*, 433−439.
(48) Seeberg, A. H.; Tolxdorff-Neutzling, R. M.; Wiedemann, B. Chromosomal beta-lactamases of *Enterobacter cloacae* are responsible for resistance to third-generation cephalosporins. *Antimicrob. Agents Chemother.* **1983**, *23*, 918−925.
(49) Cabana, H.; Alexandre, C.; Agathos, S. N.; Jones, J. P. Immobilization of laccase from the white rot fungus *Coriolopsis polyzona* and use of the immobilized biocatalyst for the continuous elimination of endocrine disrupting chemicals. *Bioresour. Technol.* **2009**, *100*, 3447−3458.
(50) Wang, J.; Bhattacharyya, D.; Bachas, L. G. Orientation specific immobilization of organophosphorus hydrolase on magnetic particles through gene fusion. *Biomacromolecules* **2001**, *2*, 700−705.
(51) Cao, L. Covalent Enzyme Immobilization. In *Carrier-Bound Immobilized Enzymes*; Wiley-VCH: Weinheim, Germany, 2006; pp 169−316.
(52) De Maio, A.; El-Masry, M. M.; De Luca, P.; Grano, V.; Rossi, S.; Pagliuca, N.; Gaeta, F. S.; Portaccio, M.; Mita, D. G. Influence of the spacer length on the activity of enzymes immobilised on nylon/polyGMA membranes - Part 2: Non-isothermal conditions. *J. Mol. Catal. B: Enzym.* **2003**, *21*, 253−265.

Society For Biomaterials

Effects of composition and setting environment on mechanical properties of a composite bone filler

Matthew E. Brown,[1] Yuan Zou,[1] Thomas D. Dziubla,[2] David A. Puleo[1]

[1]Center for Biomedical Engineering, University of Kentucky, Lexington, Kentucky 40506
[2]Department of Chemical and Materials Engineering, University of Kentucky, Lexington, Kentucky 40506

Received 23 December 2011; revised 30 July 2012; accepted 31 July 2012
Published online in Wiley Online Library (wileyonlinelibrary.com). DOI: 10.1002/jbm.a.34399

Abstract: Large bone defects can be difficult to treat, even with autografts. Bone graft substitutes, such as calcium sulfate (CS), calcium phosphate cements, and hydroxyapatite, are receiving significant attention because of their biocompatibility and potential for incorporation of therapeutic agents. To create a bone filler capable of treating irregularly shaped, often infected, bony defects, microspheres and a plasticizer were added to CS, resulting in a moldable composite capable of being loaded with biomolecules. Different compositions and setting environments, such as immersion in saline, a humidified incubator, or room temperature air, were investigated to determine their effects on mechanical strength and degradation rate of the composites. Addition of any other components to the CS, such as plasticizers or microspheres composed of biopolymers (gelatin, hyaluronan [HY], cellulose acetate phthalate, and carboxymethylcellulose), increased its functionality but reduced mechanical strength. The compressive modulus and strength of the composite fillers ranged from 10 to 350 MPa and 5 to 20 MPa, respectively, depending on the composition. This moldable bone filler degraded in 18–20 days when placed in solution and was able to set in harsh environments given a composition that did not retain too much water. By combining a plasticizing agent, such as HY with CS, a composite material has been developed that is moldable, sets *in situ*, and maintains its mechanical stability. With these desirable properties for a bone graft substitute and the potential to be loaded with bioactive drugs, this composite material merits further investigation for the future treatment of bony defects. © 2012 Wiley Periodicals, Inc. J Biomed Mater Res Part A: 00A:000–000, 2012.

Key Words: bone filler, bone graft substitute, calcium sulfate, composite, moldable

How to cite this article: Brown ME, Zou Y, Dziubla TD, Puleo DA. 2012. Effects of composition and setting environment on mechanical properties of a composite bone filler. J Biomed Mater Res Part A 2012:00A:000–000.

INTRODUCTION

High energy trauma, resulting from events such as explosions, can cause large bony defects that cannot heal spontaneously.[1,2] Because of the large variability in size and location associated with these wounds, treatment can be complicated and require multiple procedures.[2–5] Approximately 80% of injuries in Operations Enduring Freedom and Iraqi Freedom are the result of explosions.[6–8]

The most common method of treatment begins with debridement to remove necrotic tissue followed by an autogenous bone graft to replace the missing bone.[3,9] Autografts, which involve harvesting the donor bone from the patient, have been the gold standard for bone grafts for more than 100 years.[5,9] Major reasons for their success are the incorporation of osteogenic cells and the use of an osteoconductive matrix in the grafting material.[1] Harvesting donor bone from the patient significantly reduces the risk of rejection when implanted.[1,10] Even with all their success, autografts still have several drawbacks, including the need for a second surgery to obtain the donor bone and donor site morbidity that can cause pain and future complications for the patient.[10] Allografts are an alternative to autografts that removes the need for the patient to donate the bone grafting material and instead obtains it from cadavers.[1] This method does not require a second surgery site, but it increases the risk of disease transmission and infection.[1,10]

Because of the inherent limitations of traditional bone grafts, substitute bone grafting materials have been an area of intense research interest. Many of these materials are designed to be biodegradable, osteoconductive, and provide some mechanical support.[1,9,11] Ceramics, such as calcium sulfate (CS), calcium phosphate cements (CPC), and hydroxyapatite (HA), and various polymers, such as polyurethane and poly(lactic-co-glycolic acid), are being investigated for use as bone graft substitutes.[12–15] CS has a long history of clinical use and is biodegradable, biocompatible, and osteoconductive.[3,16,17] With the incorporation of antibiotics and growth factors, CS can be used to treat infections

Correspondence to: D. A. Puleo; e-mail: puleo@uky.edu
Contract grant sponsor: U.S. Army Medical Research Acquisition Activity; contract grant number: W81XWH-09-1-0461
Contract grant sponsor: Kentucky NASA EPSCoR; contract grant number: NNX08BA13A
Contract grant sponsor: IGERT support from the National Science Foundation; contract grant number: DGE-0653710 (to M.E.B.)

TABLE I. Formulations of Moldable Bone Filler Used in Different Experiments Expressed as Weight Percentages

Sample set	Component (wt %)						
	CS	CMC	HY	CAPP	Gms	Gentamicin	Vancomycin
Setting environment	90	5	0	2.5	2.5	0	0
Composition effects on mechanical strength over time	85	5	0	5	5	0	0
	80	10	0	5	5	0	0
	100	0	0	0	0	0	0
Polymer comparison	95	0	5	0	0	0	0
	95	5	0	0	0	0	0
Mass loss	85	5	0	5	5	0	0
Set time	87	5	0	0	5	1.5	1.5
	87	0	5	0	5	1.5	1.5
	95	0	5	0	0	0	0

CS, calcium sulfate; CMC, carboxymethylcellulose; HY, hyaluronan; CAPP, cellulose acetate phthalate/Pluronic F-127.

and stimulate bone formation, further increasing the material's effectiveness in bone regeneration.[11,18,19] Along with making more bioactive grafting substitutes, there is significant interest in developing moldable or injectable systems with the addition of biopolymers that can be more easily applied to a wound and can fill the void better than preset materials.[13,15,16,20,21]

The current work focused on the development of a composite bone graft substitute, composed of CS, microspheres, and a plasticizer, that can eventually be modified to deliver biomolecules for the treatment of large bony defects, such as may result from explosions. A key factor in the effectiveness of bone graft fillers is the ability to fill the defect completely to prevent soft tissue in-growth; this moldable bone filler will be capable of filling any irregularly shaped defect and setting *in vivo*. The handling properties and moldability of CS were significantly improved by the addition of a plasticizer, such as carboxymethylcellulose (CMC) or hyaluronan (HY), which have already been used in human patients for wound healing applications in products such as OP-1 putty and Orthovisc®. Addition of these biomacromolecules to CS created a material that is easy to work and is still capable of setting *in vivo*. The effects of composition and environment on mechanical properties and degradation time were evaluated to determine a balance between setting time and mechanical strength.

MATERIALS AND METHODS

General sample preparation

CS (hemihydrate 98%; Sigma), CMC (medium viscosity; Sigma), or HY (molecular weight [MW] 7.46×10^3, 1.323×10^5, 3.574×10^5, or 2×10^6 Da; LifeCore Biomedical), gelatin microspheres (Gms), cellulose acetate phthalate/Pluronic F-127 microspheres (CAPPms), gentamicin (Sigma), and vancomycin (Sigma). Sample compositions used in the various studies can be seen in Table I. A series of different compositions were investigated as the composite material was continuing in development, each experiment providing valuable information for the experiments to follow.

Microsphere preparation is detailed in the following section. The relative amounts of each component were varied to determine the effects while maintaining a strong, moldable material. All components were dry mixed by hand before addition of deionized water. The amount of water required varied (usually between 300 and 600 μL/g) depending on the relative amounts of components in the composite, and samples were fabricated such that a nonsticky, moldable material was formed. The moldable filler was then packed into cylindrical Delrin molds (6.5 deep × 3.2 mm diameter), and samples were removed once they could be pushed out without deformation, which took between 10 and 20 min depending on the composition. Pictures demonstrating the moldable nature of the filler can be seen in Figure 1.

Microsphere preparation

Gelatin microspheres were prepared using methods adapted from Zou et al.[22,23] A solution of 10% gelatin in deionized water was added to 200 mL of stirring olive oil (40°C) in a dropwise manner. The mixture was then chilled to 10°C with stirring for 30 min before the addition of 60 mL of chilled (4°C) acetone for an hour with continuous stirring. The solution was centrifuged (123*g* force for 5 min) before microspheres were collected by filtration (11 μm; Whatman). The microspheres were then crosslinked by being placed in stirring 20 m*M* glutaraldehyde for 12 h at 4°C. The crosslinked microspheres were collected and immersed in 50 m*M* glycine solution for 2 h to block residual aldehyde groups.

CAPPms were prepared by first dissolving cellulose acetate phthalate (CAP) and Pluronic in acetone at a weight ratio of a 2.33:1 (CAP:Pluronic) while shaking.[24] This emulsion was added rapidly into four volumes of corn oil and sonicated (25W) for 5 s. The CAP/oil solution was then added to 5.3 volumes of deionized water along with 0.5 volume of Triton X-100 solution; the combined solution was then homogenized at 1509.2*g* force for 5 min. The resulting suspension was centrifuged at 277*g* force for 5 min to separate the CAPPms, and the oil and water phases were removed by aspiration.

Both types of microspheres were lyophilized for 24 h before use. Characterization of microspheres was reported

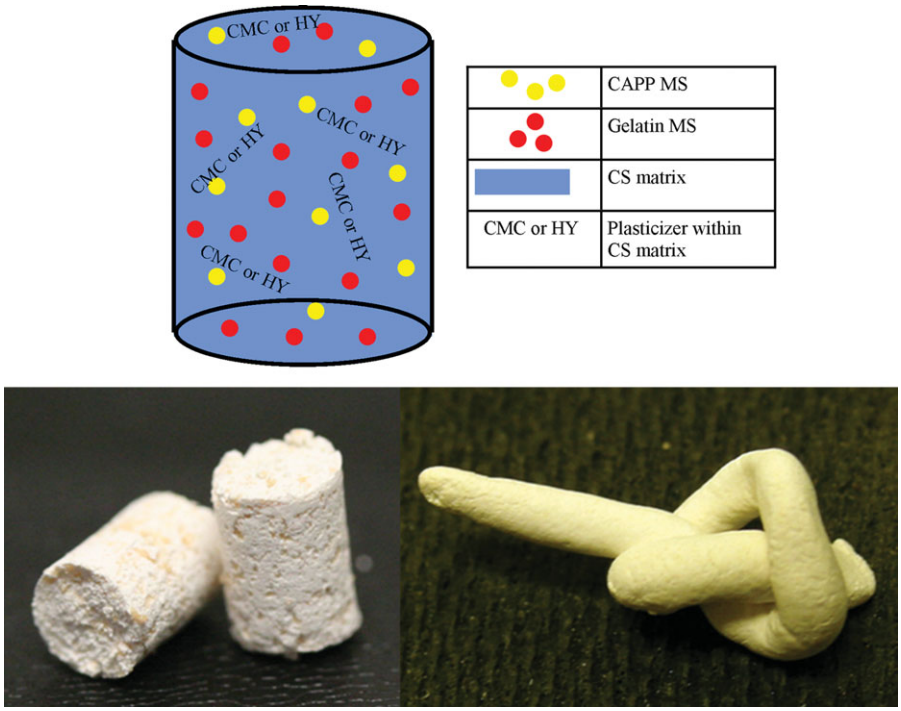

FIGURE 1. Schematic image of the cylindrical bone filler samples used for mechanical testing (top); plasticizers, CMC or HY, were dispersed throughout the CS matrix to improve the handling properties of the CS. A picture of actual bone filler samples (bottom left) and a demonstration of the moldable nature of the CS composite material (bottom right). [Color figure can be viewed in the online issue, which is available at wileyonlinelibrary.com.]

previously,[23,25] and microscopic observations showed their diameter to range from 70 to 150 μm and 70 to 110 μm for gelatin and CAP–Pluronic, respectively. In future work, these microspheres could be loaded with bioactive drugs for the treatment of infected bony defects.

Mechanical properties of composite material

To test the properties of set composites with HY compared with CMC, mechanical testing was performed on samples 10–20 min after fabrication. Samples were removed from the mold as soon as possible and allowed to air dry for 10 min, at which point compression testing was performed. The aim of this part of the study was to determine how quickly the different compositions were able to set.

Setting environment

Once bone filler samples were removed from the mold, they were placed in one of three environments to set: (1) oven at 40°C; (2) a fully humidified cell culture incubator at 37°C; or (3) immersion in 1.5- or 3-mL phosphate-buffered saline (PBS), pH 7.4 at 37°C. Samples were dried in an oven for comparison against other preset calcium phosphate or CS bone grafting materials/cements. The cell culture incubator and immersion in PBS were examined to simulate two extremes of the simulated *in vivo* environment. Different volumes of PBS were used to determine what effect the surface area (sample) to volume (PBS) ratio had on the degradation rate of the bone filler samples.

Mechanical properties and degradation

Compression testing was performed on cylindrical samples using a Bose ELF 3300 mechanical testing system. Samples were removed from their respective setting environment, or the mold in the case of the set time experiments, and tested immediately afterward. Load was applied at 5 N/s until failure, and the compressive modulus (M) and ultimate compressive strength (UCS) were calculated.

Nondestructive degradation studies were performed by placing composite samples directly into either 1.5- or 3-mL static PBS at 37°C. While avoiding any crystalline particulate matter that precipitated, the solution was changed every 3 days, and at each time point, three samples were removed, dried for 24 h at 40°C, and then weighed. Volumes of 1.5 or 3 mL of PBS were used because calculations based on solubility of CS indicated the volumes would maintain sink conditions while being small enough to enable detection of released drugs in future studies. The water solubility of CS is approximately 2.4 mg/mL. In the case of the smaller volume, the samples would have needed to degrade 42% over the 3-day interval between samplings to reach the solubility limit of CS. Pilot study data (not shown) showed that samples reached steady state mass after 4 h when dried at 40°C. The initial and final weights after degradation were then used to determine the percent mass loss for each sample.

Statistical analysis

One-way and two-way analysis of variance (ANOVA) was performed using Prism (GraphPad). Statistical analysis was

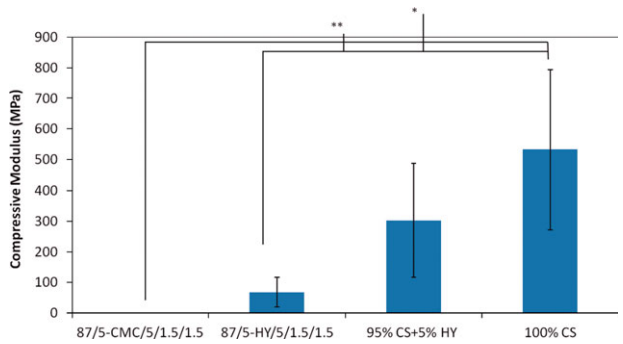

FIGURE 2. Effect of composition on initial mechanical properties of composites. All samples were evaluated within 20 min of fabrication, and 1.323×10^5 Da HY was used in all samples containing HY. (Data are mean ± SD, $n = 6, 6, 5,$ or 5 for the groups evaluated, respectively; $p < 0.001$, $*p < 0.01$, $**p < 0.001$). [Color figure can be viewed in the online issue, which is available at wileyonlinelibrary.com.]

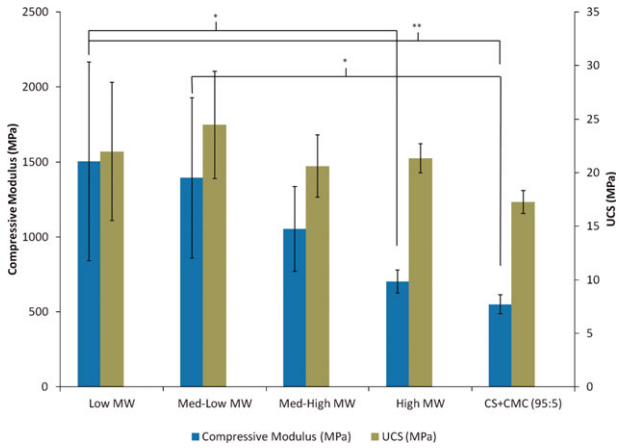

FIGURE 3. Effect of type of biopolymer on mechanical properties of CS with 5 wt % of CMC or varying MW hyaluronan. Low = 7.46×10^3, Med-low = 1.32×10^5, Med-high = 3.57×10^5, High = 2.0×10^6 Da. (Data are mean ± SD, $n = 11, 11, 5, 5,$ and 7 for the groups evaluated, respectively; $*p < 0.05$, $**p < 0.01$). [Color figure can be viewed in the online issue, which is available at wileyonlinelibrary.com.]

determined at p values less than 0.05. Bonferroni's *post hoc* test was performed as needed. Because certain testing groups were small, normality tests and data skew were used to test the validity of using ANOVA statistical methods.

RESULTS

Initial mechanical properties of composite material

Bone filler samples that contained HY instead of CMC had significantly ($p < 0.05$) better mechanical properties when tested shortly after mixing (Fig. 2). The samples containing CMC were still moldable even after testing, which resulted in low mechanical stiffness of the cylinders. Samples that contained microspheres showed inferior mechanical strength to those containing CS and HY alone.

The type of plasticizer used in the composite influenced the mechanical properties, but no significant difference was seen between the different MW HY samples (Fig. 3). Samples containing low and med–low MW HY had compressive moduli ranging from 1400 to 1500 MPa, significantly higher ($p < 0.05$) than samples containing CMC with an average compressive modulus of 550 MPa.

Setting environment

The elastic modulus of the bone filler composites and CS controls under different setting conditions can be seen in Figure 4. Composite samples placed in wet environments, such as a cell culture incubator or submerged in PBS, showed significantly lower ($p < 0.05$) mechanical properties after 24 h compared with those dried in air. A UCS of 0.86 MPa and compressive modulus of 42 MPa was seen in samples placed in an incubator compared with 11 and 453 MPa seen in samples air dried. Samples that were placed directly into PBS retained their cylindrical shape but did not fully set and were unable to be mechanically tested.

Mechanical properties over time and degradation

The relative amounts of the composite material components were shown to have a significant ($p < 0.0001$) effect on the mechanical properties (Fig. 5). Addition of larger amounts of plasticizer or microspheres to the composites resulted in lower mechanical properties over time ($p < 0.0001$). All three compositions became stronger over the first few days as the CS was able to fully set in the humid environment.

The type of plasticizer used, either CMC or HY, did not have any significant effect on the degradation rate of the bone filler composite (Fig. 6). The time until complete degradation was approximately 18 days for both polymers examined. The samples began degrading by erosion, getting smaller throughout the 18 days; however, some samples began to fragment toward the end of the degradation period. The ratio of sample surface area to volume of PBS in which they were incubated (SA/vol.), however, seemed to have a slight effect on the degradation profile by increasing the degradation rate with a higher SA/vol. ratio, but the results were not significant.

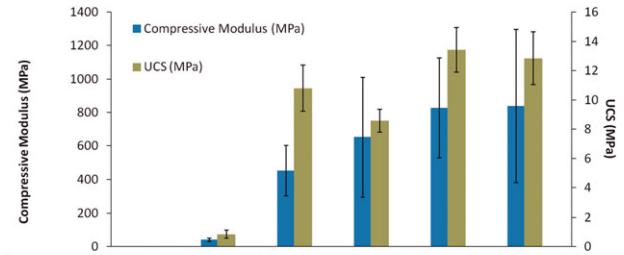

CS	90	90	90	100	100	100
CMC	5	5	5	0	0	0
CAPPms	2.5	2.5	2.5	0	0	0
Gms	2.5	2.5	2.5	0	0	0
Set Condition	PBS	Incubator	Air	PBS	Incubator	Air

FIGURE 4. Effect of setting environment on compressive modulus. 90/5/2.5/2.5 PBS set was not tested because the samples were too fragile to even remove from the PBS without deforming or breaking. (Data are mean ± SD, $n = 4, 4, 11, 8, 6,$ and 4 for the groups evaluated, respectively; One-way ANOVA for compressive modulus and UCS $p < 0.0001$). [Color figure can be viewed in the online issue, which is available at wileyonlinelibrary.com.]

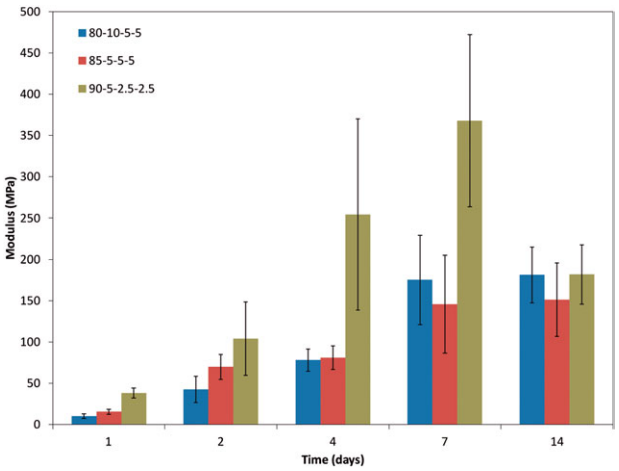

FIGURE 5. Effect of composition on modulus of the moldable bone filler dried in a humidified environment. (Data are mean ± SD, $n = 4$; two-way ANOVA $p < 0.0005$). [Color figure can be viewed in the online issue, which is available at wileyonlinelibrary.com.]

DISCUSSION

CS as a bone filler

CS has been used in many different forms as a bone graft substitute, such as injectable treatments, moldable putties, or as preset pellets.[3,15,26] CS-based materials have many useful properties for bone regeneration, such as being osteoconductive, biodegradable, and biocompatible.[3,16] CS paste alone is sticky and sets quickly, which makes it difficult to work with in a clinical setting; the addition of a plasticizing polymer to the CS matrix makes the material injectable or moldable and generally increases the working time.[15,16,20] Although CS has many useful natural properties, it is not osteoinductive, a key factor in the success of a bone grafting material in large defects.[1] CS-based materials also do not posses any inherent antimicrobial properties and require the same repeated debridement/irrigation procedures as traditional grafts.[3,17] Antibiotics and osteogenic molecules can be added to CS to create a material that is antibacterial, osteoinductive, and osteoconductive.[11,16,27] In the current study, a moldable, biocompatible, and biodegradable bone filler material was created that could be loaded with different bioactive agents. The degradation and mechanical strength were shown to be tailorable depending on the ratio of components within the composite, and the properties also depended considerably on the environmental conditions around the samples as discussed below. Although this composite material is not within the range needed for a fully weight-bearing material (addressed further in the next section), it is strong enough to be used in a similar manner as traditional bone grafts.

Compositional effects on mechanical properties

Much of the recent research into bone filler substitutes has examined composite materials that are easier to handle and apply clinically.[15,16,28] These materials are often created by the addition of a plasticizing agent that can make the composite injectable or moldable.[15,26] Antibiotics or growth factors are often included in these composite bone fillers to increase the therapeutic effects by fighting infections or actively promoting the growth of bone.[27,29–32] The ability to load both antibiotics and osteogenic molecules into the same moldable grafting material is not commonly done and creates a bone grafting substitute that has larger therapeutic applications.

The mechanical properties of bone vary considerably depending on the type of bone, the location of the bone, and the health of the patient.[1] The difference in mechanical properties between cortical and cancellous bone is large, with the compressive modulus of cortical bone ranging from 7 to 25 GPa, whereas that of cancellous bone ranging from 0.1 to 1 GPa.[1,26] The UCS of cortical bone and cancellous bone ranges from 50 to 150 and less than 1 MPa, respectively.[1] Many bone filler materials aim to have similar mechanical properties to the bone they temporarily replace to reduce complications with surrounding bone and make the materials more load bearing.[1,26] Several injectable CPC and CS systems have compressive moduli ranging from 1 to 165 MPa.[26,33] There are also other moldable systems that use either a polymer or a microsphere to create a more workable putty or paste for placement into irregularly shaped defects.[13,20] These materials had diametrical tensile strengths ranging from 6 to 10 MPa.[13,20] The moldable bone filler material developed in this study had compressive moduli ranging from 10 to 350 MPa and UCS ranging from 5 to 20 MPa, depending on the formulation and setting conditions. The mechanical strength of the composite material is significantly less than that of cortical bone but near that of cancellous bone.

Using HY instead of CMC in the composite material resulted in a stronger material and a faster setting time. This was likely due to the increased number of hydroxyl groups present on the HY, allowing it to imbibe large quantities of water, much like it does in cartilage.[34] The MW of the CMC used was 2.5×10^5 Da, which is slightly larger

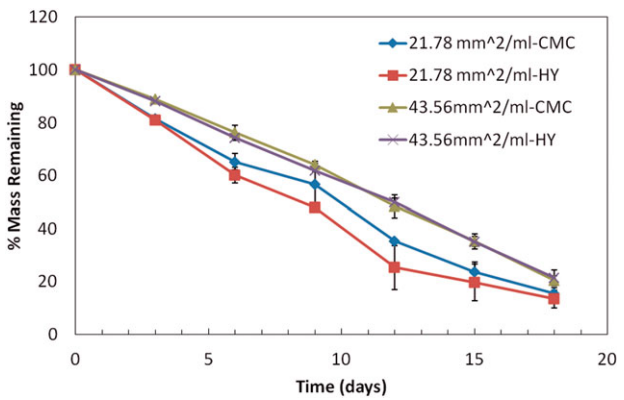

FIGURE 6. Effect of SA/Vol. ratio on degradation of composites containing either 5 wt % of CMC or HY (1.323×10^5 Da). Samples in 3 and 1.5 mL PBS had SA/vol. ratios of 21.8 m and 43.6 mm^2/mL, respectively; no significant difference was seen between the two SA/vol. ratios. (Data are mean ± SD, $n = 3$). [Color figure can be viewed in the online issue, which is available at wileyonlinelibrary.com.]

than that of the 1.3×10^5 Da HY that was chosen for continued use. Because the MW of these two polymers is similar, it was likely not much of a factor in their water-retention properties. The CMC used had fewer hydroxyl groups available to bind with water in part due to substitution with carboxymethyl groups during its synthesis. By retaining more water than CMC, and thereby decreasing the amount of free water for CS dissolution, the HY biopolymer makes it easier for solution supersaturation and conversion to CS dihydrate, which resulted in faster setting. Because the present material is intended to be implanted in a moldable (i.e., not set/hardened) state, the working time available to the surgeon after mixing is clinically important. A setting time of 20 min was used as a characterization bench mark, because setting times less than this may not provide enough time to implant the material properly. Similarly, setting times exceeding 20 min will likely plastically deform *in situ* and degrade more quickly in the wound site.

The strength of the bone filler material was directly related to the amount of CS. More CS present within a fixed volume of water allowed the conversion from hemihydrate to dihydrate to happen more quickly because the solution can more readily become supersaturated with dihydrate. This increased amount of dihydrate form of CS caused the resulting material to possess superior mechanical properties. All three compositions became stronger over the first couple of days when stored in the cell culture incubator at 100% humidity. This is likely due to the CS setting process being slowed down by the large amount of water in the air. Because the major structural component of the composites was not fully set during the first several testing points, the bone filler samples would be weaker than fully set samples. The average compressive modulus of the 90-5-2.5-2.5 samples stored in the incubator at day 7 is approximately 360 MPa, similar to the air dried 90-5-2.5-2.5 samples that had an average compressive modulus around 400 MPa. It is likely that after 7 days, the samples were fully set and the reason for the decrease in mechanical strength at day 14 was due to the excess humidity in the air weakening the CS matrix.[35] The amount of water added to the dry components to make the filler ranged from 300 to 600 μL/g and was chosen based on the handling properties of the resulting putty. A lower content of microspheres or plasticizer caused an increase in the mechanical properties of the composite filler because of the decreased water retention, increased amount of CS, and in the case of microspheres, a decreased number of stress concentrators. The gelatin microspheres are hydrophilic as are the plasticizers used to create a moldable material; this added water retention would slow down the conversion of CS hemihydrate to CS dihydrate in a similar manner as described above for the setting conditions. CAPPms would not contribute much to water retention because they are surface eroding and do not absorb much water as they degrade.

Setting conditions

The conditions in which the CS bone filler was set had a significant effect on the mechanical properties of the composite, which were directly related to the amount of water in the system. The additional water that the samples were exposed to in the humidified cell culture incubator or when immersed in PBS did not allow the material to ever fully set. The α-hemihydrate form of CS normally forms a stronger, denser, dihydrate material when dried.[36] During this reaction, the hemihydrate form of CS is converted into a dihydrate form; this reaction is driven by the solution becoming supersaturated with the dihydrate form followed by nucleation and crystal growth.[16] Once the solution is no longer saturated, more of the hemihydrate form can dissolve and supersaturate the solution again. With excess amounts of water in the system, it is difficult for the solution to become supersaturated and begin nucleation and crystal growth. It has also been shown that the addition of polymers or presence of biological molecules, such as proteins, can slow down the setting time and make it difficult for the material to set *in vivo*.[37] If the material is unable to fully set *in vivo* as intended, the mechanical integrity and therapeutic effects may be compromised.

In clinical applications, the actual setting environment will be likely somewhere between full immersion in solution and the cell culture incubator. Immersion in a fluid is the most common environment for investigating a bone grafting substitute's drug release and degradation profiles.[26,28,29,38,39] *In vivo* conditions would be difficult to replicate *in vitro* because many different factors must be considered. The bone filler composite will be loosely confined within the wound site and subjected to a small but continuously exchanged fluid flow from the body along with wound healing cells and bacteria. Immediately upon implantation within the body, proteins will begin to adsorb onto the surface of the material.[40] These adsorbed proteins can become entangled in the crystal structure and slow down the set time or weaken the mechanical strength of the material.[26,33] All of these factors will contribute to the degradation and function of the bone filler and should be considered carefully when planning *in vitro* experiments.

The degradation profiles showed the small filler samples degrading over the course of around 18 days. Although the ideal time for a grafting material to be present in a defect site is unknown, larger samples appropriate for (pre)clinical applications would take longer to degrade. Interestingly, the percentage mass remaining did not go all the way to zero. One reason for this observation was that at later time points in the experiment, the samples began to break apart considerably and accurate mass measurements could not be taken; therefore, the samples were considered completely degraded. Furthermore, Mamidwar et al.[41] showed that a calcium phosphate lattice forms as CS degrades, and this insoluble mineral phase will prevent the mass from reaching zero. The degradation profiles varied with the surface area to volume ratio of the sample and the amount of solution they were immersed in; this was likely due to saturation/solubility effects of the PBS. Once the solution containing the sample became saturated, dissolution of the components would slow considerably. The sample surface area to supernatant volume ratio should affect the degradation rate by

determining how quickly the solution becomes saturated, and generally, the solution should be at high enough volumes and changed frequently enough to remain at sink conditions to best understand the degradation and release mechanisms of a biomaterial.

Moldable systems

Moldable bone graft substitutes have the advantages of being easier to handle during implantation than pastes as well as having the ability to conform to any irregularly shaped defect, thereby minimizing the space between the native tissue and implanted material. These systems also remove the need for a preset material and allow for a better fit of the implanted graft and host tissue. Various types of biocompatible polymers have been used to create moldable bone graft substitute systems, such as CMC, sodium alginate, and poly(lactide-*co*-glycolide) (PLGA) microspheres.[13,15,16,20] When a moldable putty was created instead of a more viscous paste in these other systems, the degradation rate was comparable, whereas the mechanical properties were lower. In a study by Habraken et al.,[21] an injectable CPC was created using gelatin microspheres to create a workable paste and to create macropores for the in-growth of tissue. Simon et al.[13] created a composite bone graft paste by combining PLGA microspheres with a CPC, which resulted in a material that was mechanically weaker than CPC alone but contained up to 18% micropores that could allow in-growth of tissue. This paste still suffers from the slow degradation rate of CPCs; the material showed little signs of degradation after 3 months, even after the outermost PLGA particles had degraded leaving micropores.[13] In a manner similar to the moldable bone filler material presented here, it would be possible to tune the degradation and mechanical properties of these moldable systems by changing the base components and ratio of components.

CONCLUSION

A moldable, biocompatible, and biodegradable bone grafting substitute was developed using CS, microspheres, and a plasticizer. The mechanical strength and setting time of the filler material can be tailored by altering the ratio of various components or the type of plasticizer used. Adding any components to the CS, such as biopolymer or eventually antibiotics or biomolecules, increases its functionality but decreases its mechanical strength and ability to set in harsh environments. The plasticizer HY was shown to create a stronger composite material than those using CMC while still retaining its moldability and biocompatible nature. The samples degraded in a linear fashion over the course of 18–20 days in PBS, and samples containing HY instead of CMC showed a slightly slower initial degradation. In addition to possessing many of the desired mechanical properties of bone graft substitutes, the material can be loaded with bioactive molecules. The present composite filler will be further explored as an alternative to traditional bone grafting treatments.

REFERENCES

1. Brydone AS, Meek D, Maclaine S. Bone grafting, orthopaedic biomaterials, and the clinical need for bone engineering. Proc Inst Mech Eng H 2010;224:1329–1343.
2. Moghaddam A, Elleser C, Biglari B, Wentzensen A, Zimmermann G. Clinical application of BMP 7 in long bone non-unions. Arch Orthop Trauma Surg 2010;130:71–76.
3. Hak DJ. The use of osteoconductive bone graft substitutes in orthopaedic trauma. J Am Acad Orthop Surg 2007;15:525–536.
4. Motsitsi NS. Management of infected nonunion of long bones: The last decade (1996–2006). Injury-Int J Care Injured 2008;39:155–160.
5. Kanakaris NK, Lasanianos N, Calori GM, Verdonk R, Blokhuis TJ, Cherubino P, De Biase P, Giannoudis PV. Application of bone morphogenetic proteins to femoral non-unions: A 4-year multicentre experience. Injury 2009;40:54–61.
6. Thomas R, McManus JG, Johnson A, Mayer P, Wade C, Holcomb JB. Ocular injury reduction from ocular protection use in current combat operations. J Trauma 2009;66:S99–S103.
7. Yun HC, Branstetter JG, Murray CK. Osteomyelitis in military personnel wounded in Iraq and Afghanistan. J Trauma 2008;64:S163–S168.
8. Petersen K, Riddle MS, Danko JR, Blazes DL, Hayden R, Tasker SA, Dunne JR. Trauma-related infections in battlefield casualties from Iraq. Ann Surg 2007;245:803–811.
9. Athanasiou VT, Papachristou DJ, Panagopoulos A, Saridis A, Scopa CD, Megas P. Histological comparison of autograft, allograft-DBM, xenograft, and synthetic grafts in a trabecular bone defect: An experimental study in rabbits. Med Sci Monit 2010;16: BR24–BR31.
10. Mourino V, Boccaccini AR. Bone tissue engineering therapeutics: Controlled drug delivery in three-dimensional scaffolds. J R Soc Interface 2010;7:209–227.
11. McKee MD, Li-Bland EA, Wild LM, Schemitsch EH. A prospective, randomized clinical trial comparing an antibiotic-impregnated bioabsorbable bone substitute with standard antibiotic-impregnated cement beads in the treatment of chronic osteomyelitis and infected nonunion. J Orthop Trauma 2010;24:483–490.
12. Li B, Brown KV, Wenke JC, Guelcher SA. Sustained release of vancomycin from polyurethane scaffolds inhibits infection of bone wounds in a rat femoral segmental defect model. J Control Release 2010;145:221–230.
13. Simon CG, Khatri CA, Wight SA, Wang FW. Preliminary report on the biocompatibility of a moldable, resorbable, composite bone graft consisting of calcium phosphate cement and poly(lactide-co-glycolide) microspheres. J Orthop Res 2002;20:473–482.
14. Hasegawa M, Sudo A, Komlev VS, Barinov SM, Uchida A. High release of antibiotic from a novel hydroxyapatite with bimodal pore size distribution. J Biomed Mater Res B Appl Biomater 2004; 70B:332–339.
15. Reynolds MA, Aichelmann-Reidy ME, Kassolis JD, Prasad HS, Rohrer MD. Calcium sulfate-carboxymethylcellulose bone graft binder: Histologic and morphometric evaluation in a critical size defect. J Biomed Mater Res B Appl Biomater 2007;83B:451–458.
16. Thomas MV, Puleo DA. Calcium sulfate: Properties and clinical applications. J Biomed Mater Res B Appl Biomater 2009;88B:597–610.
17. Kelly CM, Wilkins RM, Gitelis S, Hartjen C, Watson JT, Kim PT. The use of a surgical grade calcium sulfate as a bone graft substitute—Results of a multicenter trial. Clin Orthop 2001:42–50.
18. Park YB, Mohan K, Al-Sanousi A, Almaghrabi B, Genco RJ, Swihart MT, Dziak R. Synthesis and characterization of nanocrystalline calcium sulfate for use in osseous regeneration. Biomed Mater 2011;6:11.
19. Aberg J, Eriksson O, Spens E, Nordblom J, Mattsson P, Sjodahl J, Svensson M, Engqvist H. Calcium sulfate spinal cord scaffold: A study on degradation and fibroblast growth factor 1 loading and release. J Biomater Appl 2012;26:667–685.
20. Ishikawa K, Miyamoto Y, Takechi M, Toh T, Kon M, Nagayama M, Asaoka K. Non-decay type fast-setting calcium phosphate cement: Hydroxyapatite putty containing an increased amount of sodium alginate. J Biomed Mater Res 1997;36:393–399.
21. Habraken W, Boerman OC, Wolke JGC, Mikos AG, Jansen JA. In vitro growth factor release from injectable calcium phosphate cements containing gelatin microspheres. J Biomed Mater Res A 2009;91A:614–622.

22. Zhu XH, Tabata Y, Wang CH, Tong YW. Delivery of basic fibroblast growth factor from gelatin microsphere scaffold for the growth of human umbilical vein endothelial cells. Tissue Eng A 2008;14:1939–1947.
23. Zou Y, Brooks JL, Talwalkar V, Milbrandt TA, Puleo DA. Development of an injectable two-phase drug delivery system for sequential release of antiresorptive and osteogenic drugs. J Biomed Mater Res B Appl Biomater. Forthcoming.
24. Jeon JH, Thomas MV, Puleo DA. Bioerodible devices for intermittent release of simvastatin acid. Int J Pharm 2007;340:6–12.
25. Jeon JH, Piepgrass WT, Lin YL, Thornas MV, Puleo DA. Localized intermittent delivery of simvastatin hydroxyacid stimulates bone formation in rats. J Periodontol 2008;79:1457–1464.
26. He YQ, Gao JP, Li XL, Ma ZQ, Zhang Y, Li M, Zhang YL, Wang XD, Qiu HX, Liu Y. Fabrication of injectable calcium sulfate bone graft material. J Biomater Sci Polym Ed 2010;21:1313–1330.
27. Parker AC, Smith JK, Courtney HS, Haggard WO. Evaluation of two sources of calcium sulfate for a local drug delivery system: A pilot study. Clin Orthop 2011;469:3008–3015.
28. Lewis KN, Thomas MV, Puleo DA. Mechanical and degradation behavior of polymer-calcium sulfate composites. J Mater Sci Mater Med 2006;17:531–537.
29. Tuzuner T, Uygur I, Sencan I, Haklar U, Oktas B, Ozdemir D. Elution characteristics and mechanical properties of calcium sulfate-loaded bone cement containing teicoplanin. J Orthop Sci 2007;12:170–177.
30. Tang H, Xu YQ, Zheng T, Li G, You YG, Jiang MY, Li J, Ding J. Treatment of osteomyelitis by liposomal gentamicin-impregnated calcium sulfate. Arch Orthop Trauma Surg 2009;129:1301–1308.
31. Nyan M, Sato D, Oda M, Machida T, Kobayashi H, Nakamura T, Kasugai S. Bone formation with the combination of simvastatin and calcium sulfate in critical-sized rat calvarial defect. J Pharmacol Sci 2007;104:384–386.
32. Lewis G, Brooks JL, Courtney HS, Li Y, Haggard WO. An approach for determining antibiotic loading for a physician-directed antibiotic-loaded PMMA bone cement formulation. Clin Orthop 2010;468:2092–2100.
33. Rajzer I, Castano O, Engel E, Planell JA. Injectable and fast resorbable calcium phosphate cement for body-setting bone grafts. J Mater Sci Mater Med 2010;21:2049–2056.
34. Hardingham TE, Fosang AJ. Proteoglycans—Many forms and many functions. FASEB J 1992;6:861–870.
35. Badens E, Veesler S, Boistelle R, Chatain D. Relation between Young's modulus of set plaster and complete wetting of grain boundaries by water. Colloids Surf A 1999;156:373–379.
36. Anusavice KJ. Gypsum products. In: Anusavice KJ, editor. Phhillips' Science of Dental Materials. St. Louis, MO: Saunders; 2003. p 255–281.
37. Ricci J, Alexander H, Nadkarni P, Hawkins M, Turner J, Rosenblum S, Brezenoff L, D DeLeonardis, Pecora G. Biological mechanisms of calcium-sulfate replacement by bone. In: Davies J, editor. Bone Engineering. Toronto: Em Squared Inc.; 2000. p 332–344.
38. Woo KM, Yu B, Jung HM, Lee YK. Comparative evaluation of different crystal-structured calcium sulfates as bone-filling materials. J Biomed Mater Res B Appl Biomater 2009;91B:545–554.
39. Guo H, Wei J, Liu CS. Development of a degradable cement of calcium phosphate and calcium sulfate composite for bone reconstruction. Biomed Mater 2006;1:193–197.
40. Hing KA. Bioceramic bone graft substitutes: Influence of porosity and chemistry. Int J Appl Ceram Technol 2005;2:184–199.
41. Mamidwar SS, Arena C, Kelly S, Alexander H, Ricci J. In vitro characterization of a calcium sulfate/PLLA composite for use as a bone graft material. J Biomed Mater Res B Appl Biomater 2007; 81B:57–65.